Università degli Studi di Trento

DIPARTIMENTO DI MATEMATICA
Corso di Dottorato di Ricerca in Matematica

Tesi di Dottorato di Ricerca

Robust control strategies for mean-field collective dynamics

CICLO XXXIV
Settore Scientifico Disciplinare MAT/08

Candidato:
Chiara Segala
Matricola 206166

Relatore:
Prof. Giacomo Albi

Anni 2018–2021

A Nicole, Diego e Nicolò

Contents

1 Introduction

"What is mathematics?
It is only a systematic effort
of solving puzzles posed by nature."

Shakuntala Devi

In nature it is quite common to see particular species of animals forming groups and moving together in an organized way; this phenomenon is particularly evident in flocks of birds, or schools of fish. Every individual that takes part of a community acquires a behaviour that depends on the whole group, not only on the single decision: the shift of an agent affects on an other agent that is "close" to the previous one in a certain sense. This fact occurs also in the society without realizing it, humans frequently influence each others. This is the case of opinion dynamics, when for example consumers are influenced towards a given good, or voters persuaded during political elections, or also the influence of opinions over social networks. This kind of event can be seen in a mathematical way by considering all the individuals with common characteristics as a unique set and the behaviours as the interactions between elements of that set. With his quote "The laws of nature are but the mathematical thoughts of God", the famous mathematician Euclid underlines the idea that mathematical relationships reflect real aspects of the physical world, that science relies on the assumption that we live in an ordered Universe that is subject to precise mathematical laws.

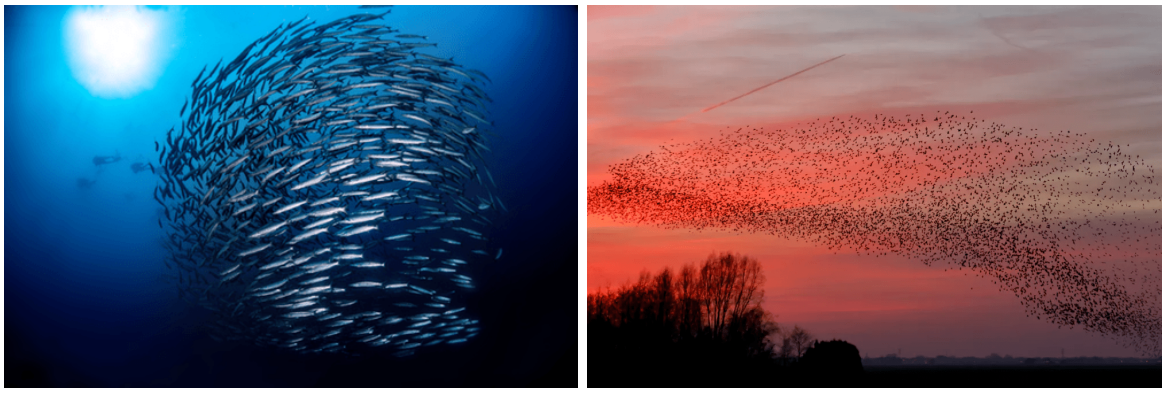

Figure 1.1: On the left, a school of fishes. On the right, starlings of birds.

The beauty of these phenomena in nature and the development of several application may justified the increased level of activity over the last years of the study of collective behaviour phenomena from a multiscale modelling perspective. Classical examples in socio-economy, biology and robotics are given by self-propelled particles, such animals and robots, see e.g. (4, 32, 61, 74, 113, 90). Those particles interact according to a nonlinear model encoding various social rules as for example attraction, repulsion and alignment. A particular feature of such models is their rich dynamical structure, which include different types of emerging patterns, including consensus, flocking, and milling (102, 147, 69, 88, 138).

Understanding the impact of control inputs in such complex systems is of great relevance for applications. Results in this direction allow to design optimized actions such as collision-avoidance protocols for swarm robotics (57, 140, 144, 100), pedestrian evacuation in crowd dynamics (6, 66, 87, 45), supply chain policies (117, 72), the quantification of interventions in traffic management (148, 108, 146) or in opinion dynamics (13, 101). From a mathematical point of view, a description of self-organized models is provided by complex system theory, where the overall dynamic is depicted by an ODEs system. Here, we will consider the control of high-dimensional nonlinear dynamics accounting the evolution of N agents with state $v_i(t) \in \mathbb{R}^d$,

$$\dot{v}_i = \frac{1}{N}\sum_{j=1}^{N} P(v_i, v_j)(v_j - v_i) + u_i\,, \qquad v_i(0) = v_i^0\,, \qquad i = 1, \dots, N, \tag{1.1}$$

where the control $u = u(t)$ is given by the minimization of the cost functional

$$u^* = \arg\min_u J(u; v^0) := \int_0^T \frac{1}{N}\sum_{j=1}^{N}(|v_j - \tilde{v}|^2 + \nu|u_j|^2)\,dt\,, \qquad \text{subject to (1.1)}\,. \tag{1.2}$$

The optimization horizon T expresses the time scale along which we minimize the running cost, encodes our objective as a function of the state and control variables. The parameter $\nu > 0$ is a penalization for the control energy, and $\tilde{v}$ is a prescribed consensus point, since in the context of this work, we are interested in consensus equilibrium, namely, reaching a consensus velocity $\tilde{v} \in \mathbb{R}^d$ such that $v_1 = \ldots = v_N = \tilde{v}$.
The original formulation of the interacting particle system (1.1) is at microscopic level through a system of ODEs, but a direct evaluation of such sums involve a $\mathcal{O}(N^2)$ cost, therefore study of microscopic model for a large system of individuals implies a considerable effort in numerical simulations, as models on real data may take into account very large number of interacting individuals. To reduce the computational complexity we can consider a more general level of description, that is the derivation of a mesoscopic approximation of the original dynamic. The basic idea is to analyse the density of particles, instead of focusing on the evolution of every single particle. Hence we will consider continuous models in order to simulate the collective behaviour in case of analysing systems with a large number of agents $N \gg 1$. By passing to the mean-field limit $N \to \infty$ of the ODE system (1.1), we obtain a PDE problem which describes how the density of the particles $g = g(t, v)$ changes in time

$$\partial_t g = -\nabla_v \cdot \Big[g\Big(\mathcal{P}[g] + u(t, g)\Big)\Big], \qquad g(v, 0) = g^0(v), \tag{1.3}$$

where $\mathcal{P}[g]$ denotes a nonlocal integral operator. The study of large particle limit has also in many cases allowed to analyse emerging patterns or identifying relevant parameters. The derivation of a model hierarchy starting from dynamical systems to kinetic equations and fluid dynamic models has been studied intensively in the literature, for example in (75, 93, 105, 73, 52).
Of particular interest for control design purposes is the study of mean-field control approaches where the control law obtain formal independence on the number of interacting agents (97, 94, 95, 43). The construction of computational methods for mean-field optimal control is a challenging problem due to the nonlocality and nonlinearity arising

from the interaction kernel (8, 2, 131). Furthermore, depending on the associated cost, non-smooth and/or non-convex optimization problems might also arise (51, 24).
We want to circumvent these difficulties proposing new approaches with a main focus on deriving robust numerical methods in the case of incomplete information, limited access or disturbances in the state of the system.
The introduction of uncertainty in the mathematical modelling of real world phenomena seems to be unavoidable for applications. In fact we can often have at most statistical information of the modelling parameters, which must be estimated from experiments or derived from heuristic observations (28, 36, 125). Therefore, to produce effective predictions and to better understand physical phenomena, we can incorporate in (1.1) a parameter reflecting the uncertainty in the interaction rules

$$\sum_{k=1}^{Z} \theta_k \,, \qquad \theta \in \Omega \subseteq \mathbb{R}^Z, \qquad \text{with a given distribution } \rho. \tag{1.4}$$

Figure 1.2: On the left, a dog herding sheep. On the right, crowd of people inside Arena in Verona.

The aim of this thesis is the construction of robust computational methods for mean-field control problems dealing with difficulties caused by nonlocal and nonlinear dynamic, or non-smooth and non-convex minimization functional, with particular attention to the case of limited or disturbed access to the state of the model. Each chapter is self consistent and refers to a research article, already published or almost ready to be submitted in a journal.
In order to circumvent the mentioned difficulties we propose an approach where we synthesize sub-optimal feedback-type controls through the linearization of the interaction kernel and by solving the resulting linear-quadratic optimal control problem through a Riccati equation, all based on the corresponding mean-field equations, similarly as in (114, 112). This approach also avoids the limitations associated to the synthesis of optimal feedback laws for high-dimensional nonlinear dynamics via the Hamilton-Jacobi-Bellman PDE (81, 21). The proposed methodology yields a control law for the linear model, which is later embedded into the non-linear dynamics (1.1). A sketch of this control concept is given in Figure 1 where we show the microscopic formulation of our approach. The main advantage of the proposed design is that unlike the classical control

loop (1, left), we do not require a continuous measurement/estimation of the nonlinear state, nor the synthesis of a nonlinear optimal feedback law. Instead, we only require periodic measurements of the nonlinear state to update our linearized system.
However, using the linear optimal control within the nonlinear model does not necessarily yield a stabilizing control law, since over time the nonlinear dynamics may be far from the linearization point. Because of the latter, we aim at quantifying the impact of this control and the number of linearization updates needed to stabilize the nonlinear system. Hence, we propose different controls, distinguishing between closed-loop and open-loop strategies: in the first case the control acts having access to the full information of the non-linear system at each time. In the second case, the control only requires information available at initial time. We quantify the performances of these control approaches by estimating the decay of macroscopic quantities associated to (1.1) such as the first and second moments of the particle ensemble.
In order to enhance open-loop strategies we introduce a novel Moment-driven Predictive Control (MdPC) framework. Based on dynamic estimates of the moments decay, we are able to perform a forward error analysis to estimate the next point in time where we need to update the dynamics and its feedback law. This strategy can be seen as model predictive control (MPC) technique (135, 47, 103, 22), where an open-loop control signal is applied only up to a subsequent point in time, after which the optimization is repeated. Moreover, the proposed control strategy is capable of treating efficiently high-dimensional control problems, and is robust in the case of limited access to the state and can be implemented with a small number of updates.

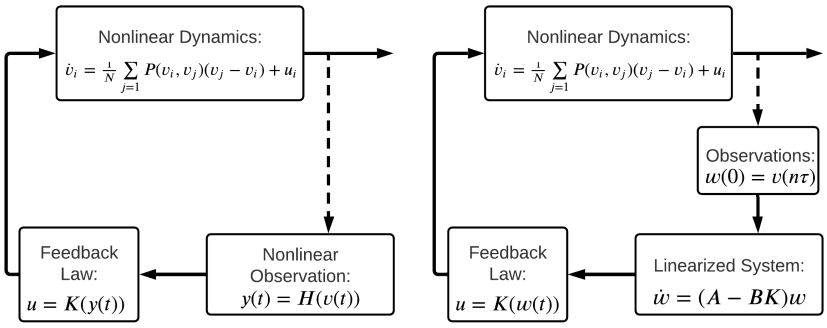

Figure 1.3: Left: the classical control loop for nonlinear dynamics. An often incomplete measurement of the state is recovered through a nonlinear observation. This observed state is inserted into a feedback law which requires the solution of a high-dimensional HJB PDE. This task is often unaffordable, and this block is replaced by a sub-optimal control law which is fed into the dynamics. Right: the Moment-driven predictive control methodology (MdPC) we propose simplifies the control loop on the left by requiring fewer measurements of the nonlinear state (every τ seconds), feeding this information into a linearized system for which the optimal feedback law can be easily computed.

We will focus then on the case where uncertainty (1.4) acts in the dynamic (1.1) as an additive random parameter constant in time. We will compare two different controls, one obtained from the usual minimization (1.2) and the other minimizing the expectation of J. With this last approach we will obtain a control independent from the noise and

we will evaluate the controls robustness using the H_∞ theory. H_∞ control methods that can effectively suppress the negative effects of disturbance have been proposed and have been successfully applied. So far, a lot of results have been published on this issue, works focused on first-order and higher-order multiagent systems with robustness for the H_∞ consensus problem under external disturbances (133, 129, 136, 130, 132). By reformulating the consensus control problem as a robust H_∞ control problem, we will derive sufficient conditions in terms of linear matrix inequalities (LMIs) to ensure the consensus performance and meanwhile the unknown feedback matrix of the proposed protocol is also determined.
In general, at the numerical level, techniques for uncertainty quantification can be classified in non-intrusive and intrusive methods. In an non-intrusive approach, the underlying model is solved for fixed samples with deterministic schemes and statistics of interest are determined by numerical quadrature, typical examples are Monte-Carlo and stochastic collocation methods (80, 139, 155). While in the intrusive case, the dependency of the solution on the stochastic input is described as a truncated series expansion in terms of orthogonal functions. Then, a new system is deduced that describes the unknown coefficients in the expansion. One of the most popular techniques of this type is based on stochastic Galerkin (SG) methods. In particular, generalized polynomial chaos (gPC) gained increasing popularity in UQ, for which spectral convergence on the random field is observed under suitable regularity assumptions (80, 120, 121, 154, 139).
The methods here developed makes use of the generalized polynomial chaos (gPC) expansion for the microscopic dynamic while in the mean-field case we combine a gPC expansion in the random space with a Monte Carlo method in the physical variables.

Figure 1.4: On the left, a traffic jam. On the right, swarmbots performing a task.

In optimal control for multiagent systems, the question of a more parsimonious control design remains open. Efficient controls strategies should target only few individuals of the population, instead of wasting resources on the entire group at once. Taking advantage of the mutual dependencies between the agents, they could use an effect that would spread their influence to the whole system, thus indirectly controlling the rest of agents. The property of control strategies to target only a small fraction of the total population is known in the mathematical literature as sparsity (48, 82, 56, 59). For example, in alignment models, the sparse control targeting at each instant only the agent farthest away from the mean velocity was shown to possess this property, see (51).

As an extension of the proposed methodology, we address the finite horizon optimal control problem with a non-smooth, sparsity-promoting control penalisation, the sparse control can indeed be obtained when the control cost is the ℓ_1-norm (51). This control synthesis is sparse, acting on a few agents over a finite time frame, however its numerical realisation is far more demanding due to the lack of smoothness in the cost functional. To circumvent this difficulty, we propose a numerical realisation of the control synthesis via proximal gradient method (31).
The final part of the thesis is devoted to applications, in particular we discuss the mathematical modelling of egressing pedestrians in an unknown environment with multiple exits. Control methodologies for crowd motion are of paramount importance in real-life applications for the design of safety measures and risk mitigation. The creation of virtual models of a large ensemble of pedestrians is a first step for reliable predictions, otherwise not easily reproducible with real-life experiments. We investigate different control problems to enhance the evacuation time of a crowd of agents, by few informed individuals, named leaders. Leaders are not recognizable as such and consist of two groups: a set of unaware leaders moving selfishly toward a fixed target, whereas the rest is coordinated to improve the evacuation time introducing different performance measures. Pedestrians have been properly modeled by means of different agent-based dynamics such as lattice models (58, 104), social force models (111, 142), or cellular automata models (1, 151).
We initially describe follower-leader dynamics microscopically by an agent-based model, subsequently a mean-field type model is introduced to approximate the large crowd of followers. In the literature we can find different level of description, using mesoscopic models (3, 7, 92) where the quantities of study are densities of agents; at a larger scale macroscopic models (54, 78, 60) describe the evolution of moments such as mass and momentum. Multiscale models have been also considered, to account for situations where different scales coexist, we refer in particular to (65, 67).
In this thesis the mesoscopic scale is efficiently solved by a class of numerical schemes based on direct simulation Monte-Carlo methods. Optimization of leader strategies is performed by a modified compass search method in the spirit of metaheuristic approaches. Finally, several virtual experiments are studied for various control settings and environments.

2 Moments driven predictive control

2.1 Introduction

The study of collective behaviour phenomena from a multiscale modelling perspective has seen an increased level of activity over the last years. Classical examples in socio-economy, biology and robotics are given by self-propelled particles, such animals and robots, see e.g. (4, 32, 61, 74, 116, 113, 90). Those particles interact according to a nonlinear model encoding various social rules as for example attraction, repulsion and alignment. A particular feature of such models is their rich dynamical structure, which include different types of emerging patterns, including consensus, flocking, and milling (102, 147, 69, 88, 138). Understanding the impact of control inputs in such complex systems is of great relevance for applications. Results in this direction allow to design optimized actions such as collision-avoidance protocols for swarm robotics (57, 140, 144, 100), pedestrian evacuation in crowd dynamics (6, 66, 87, 45), supply chain policies (117, 72), the quantification of interventions in traffic management (148, 108, 146) or in opinion dynamics (13, 17, 101). Here, we are concerned with the control of high-dimensional nonlinear systems of interacting particles which can describe self-organization patterns. We will consider dynamics accounting the evolution of N agents with state $v_i(t) \in \mathbb{R}^d$, undergoing a binary exchange of information weighted by a kernel $P : \mathbb{R}^d \times \mathbb{R}^d \to \mathbb{R}$ and forced by a control signal $u_i(t) \in \mathbb{R}^n$, represented as

$$\dot{v}_i = \frac{1}{N} \sum_{j=1}^{N} P(v_i, v_j)(v_j - v_i) + u_i \,, \qquad v_i(0) = v_i^0 \,, \qquad i = 1, \dots, N. \tag{2.5}$$

While the original formulation the interacting particle system (2.5) is at microscopic level through a system of ODEs, the study of large particle limit has in many cases allowed to analyse emerging patterns or identifying relevant parameters. The derivation of a model hierarchy starting from dynamical systems to kinetic equations and fluid dynamic models has been studied intensively in the literature, for example in (40, 75, 93, 105, 73, 52). Of particular interest for control design purposes is the study of mean-field control approaches where the control law obtain formal independence on the number of interacting agents (97, 94, 95, 43). The construction of computational methods for mean-field optimal control is a challenging problem due to the nonlocality and nonlinearity arising from the interaction kernel (8, 2, 131). Furthermore, depending on the associated cost, non-smooth and/or non-convex optimization problems might also arise (51, 24).
In order to circumvent these difficulties we propose an approach where we synthesize sub-optimal feedback-type controls through the linearization of the interaction kernel and by solving the resulting linear-quadratic optimal control problem through a Riccati equation , all based on the corresponding mean-field equations, similarly as in (114, 112). This approach also avoids the limitations associated to the synthesis of optimal feedback laws for high-dimensional nonlinear dynamics via the Hamilton-Jacobi-Bellman PDE (81, 21). The proposed methodology yields a control law for the linear model, which is later embedded into the non-linear dynamics (2.5). The main advantage of the proposed design is that we do not require a continuous measurement/estimation of the nonlinear state, nor the synthesis of a nonlinear optimal feedback law. Instead, we only require periodic measurements of the nonlinear state to update our linearized system.

However, using the linear optimal control within the nonlinear model does not necessarily yield a stabilizing control law, since over time the nonlinear dynamics may be far from the linearization point. Because of the latter, we aim at quantifying the impact of this control and the number of linearization updates needed to stabilize the nonlinear system. Hence, we propose different controls, distinguishing between closed-loop and open-loop strategies: in the first case the control acts having access to the full information of the non-linear system at each time. In the second case, the control only requires information available at initial time. We quantify the performances of these control approaches by estimating the decay of macroscopic quantities associated to (2.5) such as the first and second moments of the particle ensemble.
In order to enhance open-loop strategies we introduce a novel Moment-driven Predictive Control (MdPC) framework. Based on dynamic estimates of the moments decay, we are able to perform a forward error analysis to estimate the next point in time where we need to update the dynamics and its feedback law. This strategy can be seen as model predictive control (MPC) technique (135, 47, 103, 22), where an open-loop control signal is applied only up to a subsequent point in time, after which the optimization is repeated. Moreover, the proposed control strategy is capable of treating efficiently high-dimensional control problems, and is robust in the case of limited access to the state and can be implemented with a small number of updates.
The rest of the paper is organized as follows. In Section 2.2 we derive different control systems based on the linearization of the dynamics and the solution of the Riccati equation associated to the linear-quadratic optimal control problem. Section 2.3 is devoted to the mean-field approximation of the microscopic dynamics and presents bounds for the moments decay. In Section 2.4 the Moment-driven Predictive Control framework is described and two different implementations are presented. Finally, in Section 2.5 we assess the proposed design via numerical experiments, showing different applications in the context of opinion formation and alignment dynamics.

2.2 Control of an interacting multi-agent system

In this section we present a linearization-based approach for the control of large-scale interacting particle systems. We are concerned with the evolution of N interacting agents, whose states $v_i(t) \in \mathbb{R}^d$ evolve according to the following nonlinear model (2.5). Further assumptions regarding the interaction kernel $P(u, v)$ governing these interactions will be discussed in the forthcoming sections. The term $u_i \in \mathbb{R}^d$ represents an external control variable acting over the $i-$th agent of the system. The complete set of control variables is denoted by $u = (u_1, \dots, u_N) \in \mathbb{R}^{N\times d}$. In order to synthesize this control variable, we assume that u is the minimizer of a cost function $J(u; v(0))$, that is

$$u^* = \arg\min_u J(u; v^0) := \int_0^T \ell(v(t), u(t))\, dt\,, \qquad \text{subject to (2.5)}\,. \tag{2.6}$$

The optimization horizon T expresses the time scale along which we minimize the running cost $\ell(v, u)$, encodes our objective as a function of the state and control variables. In the context of this work, we are interested in *consensus equilibrium*, namely, reaching a consensus velocity $\tilde{v} \in \mathbb{R}^d$ such that $v_1 = \ldots = v_N = \tilde{v}$. With a slight abuse of notation, we shall denote indistinctively by $\tilde{v}$ the consensus state and the swarm configuration

$\tilde{v} \in \mathbb{R}^{N\times d}$ where all the agents share the same velocity. In order to promote consensus emergence, we solve the optimal control problem (2.6) to determine a control law u driving the system towards $\tilde{v}$ using the running cost

$$\ell(v,u) = \frac{1}{N}\sum_{j=1}^{N}(|v_j - \tilde{v}|^2 + \nu|u_j|^2) \tag{2.7}$$

where $\nu > 0$ is a penalization parameter for the control energy, and $\tilde{v}$ is a prescribed consensus point. The norm $|\cdot|$ is the usual Euclidean norm in $\mathbb{R}^d$.

2.2.1 Linearization and LQR approach for collective dynamics

We are interested in the synthesis of a feedback control law for the control of the nonlinear dynamics (2.5). We begin by defining the vector-valued function $F(v) : \mathbb{R}^{N\times d} \to \mathbb{R}^{N\times d}$ such that

$$F_i(v) = \frac{1}{N}\sum_{j=1}^{N} P(v_i, v_j)(v_j - v_i), \qquad i = 1, \dots, N.$$

We linearize the dynamics around $v_i = \bar{v}$ for every agent, which corresponds to an arbitrary equilibrium for the nonlinear dynamics (2.5), i.e. $F(\bar{v}) = 0$, and which can be different from the consensus state $\tilde{v}$. We further assume that the communication function $P(v_i, v_j)$ is such that $P(\bar{v}, \bar{v}) \equiv \bar{p}$, with $\bar{p}$ a bounded value. Computing the first order approximation of $F(v)$ around $\bar{v}$, we have $\nabla_v F(\bar{v})(v - \bar{v}) = A(v - \bar{v})$, where $A \in \mathbb{R}^{N\times N}$ is the Laplacian matrix defined as follows

$$(A)_{ij} = \begin{cases} a_d = \frac{\bar{p}(1-N)}{N}, & i = j, \\ a_o = \frac{\bar{p}}{N}, & i \neq j. \end{cases} \tag{2.8}$$

We observe that the structure of matrix A is such that $A(v - \bar{v}) = Av$ since $\bar{v}$ is a consensus point. To write the linearized system associated to (2.5) we further consider the change of variables $w_i(t) := v_i(t) - \bar{v}$, and we have

$$\dot{w}_i = \frac{1}{N}\sum_{j=1}^{N} \bar{p}(w_j - w_i) + u_i, \qquad w_i(0) = v_i^0 - \bar{v}. \tag{2.9}$$

For the linearized dynamics we cast as the *Linear Quadratic Regulator* (LQR) control problem, where the functional (2.6) reads as follows

$$J(u, w(0)) = \int_0^T w^\top Q w + \nu u^\top R u \, dt \tag{2.10}$$

in the matrix-vector notation with $w = (w_1, \dots, w_N)$ and matrices $Q \equiv R = \frac{1}{N}\mathrm{Id} \in \mathbb{R}^{N\times N}$. The linear dynamics (2.9) are equivalent to

$$\dot{w} = Aw + Bu, \qquad w(0) = v^0 - \bar{v}\,, \tag{2.11}$$

where $B = \mathrm{Id} \in \mathbb{R}^{N\times N}$ is the identity matrix, impliying that the pair (A, B) is controllable for any consensus state $\bar{v}$. Thus, in a neighbourhood of any constant state $\bar{v}$ the non linear system (2.5) admits a continuous stabilizing feedback, see e.g. (42). In order to synthesize a stabilizing control law we solve the optimal control problem (2.10)–(2.11), whose exact solution is given in feedback form by

$$u(t) = -\frac{N}{\nu} K(t) w(t) \tag{2.12}$$

with $K(t) \in \mathbb{R}^{N\times N}$ fulfilling the Differential Riccati matrix-equation

$$-\dot{K} = KA + A^\top K - \frac{N}{\nu} KK + Q, \quad K(T) = 0 \in \mathbb{R}^{N\times N}, \tag{2.13}$$

coupled to the evolution of the controlled system (2.11). For a general linear system we need to solve the $N \times N$ differential system (2.13), which can be costly for large-scale agent-based dynamics. However, in this case we can exploit the symmetric structure of the Laplacian matrix A to reduce the Riccati equation.

Proposition 2.1 (Properties of the Differential Riccati Equation (DRE))**.** *For the linear dynamics* (2.9)*, the solution of the Riccati equation* (2.13) *reduces to the solution of*

$$\begin{aligned}
-\dot{k_d} &= 2k_d a_d + 2(N-1)k_o a_o - \frac{N}{\nu}\left(k_d^2 + (N-1)k_o^2\right) + \frac{1}{N}, \\
-\dot{k_o} &= 2(N-2)k_o a_o + 2k_o a_d + 2k_d a_o - \frac{N}{\nu}\left(2k_d k_o + (N-2)k_o^2\right),
\end{aligned}$$

with terminal conditions $k_d(T) = k_o(T) = 0$. The solution K of the differential Riccati equation (2.13) *corresponds to $(K)_{ij} = \delta_{ij} k_d + (1-\delta_{ij}) k_o$.*

Proof. Given the structure of the matrices K, A and Q, solving the Riccati equation (2.13) componentwise leads to the following identities:

$$\begin{aligned}
\text{Diagonal entries } k_{ii}: &\qquad \frac{N}{\nu}(K^2)_{ii} = \frac{N}{\nu}\left(k_d^2 + (N-1)k_o^2\right). \\
\text{Off-diagonal entries } k_{ij}: &\qquad \frac{N}{\nu}(K^2)_{ij} = \frac{N}{\nu}\left(2k_d k_o + (N-2)k_o^2\right).
\end{aligned}$$

□

We can further simplify the Riccati-matrix system (2.14) using the dependency of coefficients a_d, a_o (2.8) and the parameter $\bar{p}$. This leads to

$$-\dot{k}_d = -\frac{2\bar{p}(N-1)}{N}(k_d - k_o) - \frac{N}{\nu}\left(k_d^2 + (N-1)k_o^2\right) + \frac{1}{N}, \qquad k_d(T) = 0\,, \tag{2.15}$$

$$-\dot{k}_o = \frac{2\bar{p}}{N}(k_d - k_o) - \frac{N}{\nu}\left(2k_d k_o + (N-2)k_o^2\right), \qquad k_o(T) = 0. \tag{2.16}$$

Since we are interested in the dynamics for large number of agents, we introduce the following scalings

$$k_d \leftarrow N k_d, \quad k_o \leftarrow N^2 k_o, \quad \alpha(N) = \frac{N-1}{N}.$$

For the sake of simplicity, we keep the same notation also for the scaled variables k_d, k_o. Under this scaling the system (2.15)–(2.16) reads

$$-\dot{k_d} = -2\bar{p}\alpha(N)\left(k_d - \frac{k_o}{N}\right) - \frac{1}{\nu}\left(k_d^2 + \frac{\alpha(N)}{N}k_o^2\right) + 1, \qquad k_d(T) = 0, \tag{2.17}$$

$$-\dot{k_o} = 2\bar{p}\left(k_d - \frac{k_o}{N}\right) - \frac{1}{\nu}\left(2k_dk_o + \alpha(N)k_o^2 - \frac{1}{N}k_o^2\right), \qquad k_o(T) = 0\,, \tag{2.18}$$

and the Riccati feedback law (2.12) is given by

$$u_i = -\frac{1}{\nu}\left(\left(k_d - \frac{k_o}{N}\right)w_i(t) + \frac{k_o}{N}\sum_{j=1}^{N} w_j(t)\right). \tag{2.19}$$

Plugging the control into the linear dynamics (2.9) and rearranging the terms we have

$$\dot{w_i} = \left(\bar{p} - \frac{k_o}{\nu}\right)\frac{1}{N}\sum_{j=1}^{N} w_j - \left(\bar{p} + \frac{k_d}{\nu} - \frac{k_o}{\nu N}\right)w_i, \qquad w_i(0) = v_i^0 - \bar{v}. \tag{2.20}$$

The controlled dynamics (2.20) are non-autonomous as the coefficients $k_d(t), k_o(t)$, have to be determined offline by solving (2.17)–(2.18) backwards in time.
In order to analyse the large-scale behaviour of the system we introduce the average of the agent states, and a weighted combination of the Riccati coefficients, respectively

$$m_w^N(t) := \frac{1}{N}\sum_{j=1}^{N} w_j(t), \quad s(t) := k_d(t) + \alpha(N)k_o(t).$$

From (2.20), (2.17) and (2.18), these quantities are governed by

$$\dot{m}_w^N(t) = -\frac{1}{\nu}s(t)m_w^N(t), \qquad m_w^N(0) = m_v^N(0) - \bar{v},$$
$$-\dot{s}(t) = 1 - \frac{1}{\nu}s(t)^2, \qquad s(T) = 0.$$

The second equation has an explicit solution $s(t) = \sqrt{\nu}\tanh((T-t)/\sqrt{\nu})$, always non-negative for $t \in [0, T]$ (114). The average $m_v^N(t)$ follows a relaxation towards $\bar{v}$

$$\dot{m}_v^N(t) = -\frac{1}{\sqrt{\nu}}\tanh\left(\frac{T-t}{\sqrt{\nu}}\right)(m_v^N(t) - \bar{v}).$$

Remark 1 (Second order dynamics)**.** *This approach can be extended to second order models (69, 88, 138). Here, the state space of a swarm of N agents is characterized by position and velocities $(x_i(t), v_i(t))_i \in \mathbb{R}^{2\times d}$, evolving according to*

$$\dot{x}_i = v_i, \qquad \dot{v}_i = \frac{1}{N}\sum_{j=1}^{N} P(x_i, x_j)(v_j - v_i) + u_i, \qquad i = 1, \dots, N\,. \tag{2.22}$$

where $u \in \mathbb{R}^{N\times d}$. We consider again a functional of type (2.7)*, where we enforce a consensus point $v_i = v_j = \tilde{v}$ for every i, j. Linearizing around this point and introducing the shift $y_i = x_i - \bar{v}t, \quad w_i = v_i - \bar{v}$, the system is transformed into*

$$\begin{bmatrix} \dot{y} \\ \dot{w} \end{bmatrix} = \begin{bmatrix} 0 & Id \\ 0 & A \end{bmatrix} \begin{bmatrix} y \\ w \end{bmatrix} + \begin{bmatrix} 0 \\ Id \end{bmatrix} u\,.$$

This second-order system system is controllable (112), and the associated DRE reads

$$\begin{bmatrix} \dot{K}_{11} & \dot{K}_{12} \\ \dot{K}_{21} & \dot{K}_{22} \end{bmatrix} = \begin{bmatrix} 0 & 0 \\ 0 & K_{21} + K_{22}A \end{bmatrix} + \begin{bmatrix} 0 & 0 \\ K_{11} + AK_{21} & K_{12} + AK_{22} \end{bmatrix} - \frac{N}{\nu} \begin{bmatrix} K_{12}K_{21} & K_{12}K_{22} \\ K_{22}K_{21} & (K_{22})^2 \end{bmatrix} + \begin{bmatrix} 0 & 0 \\ 0 & Id \end{bmatrix},$$

with terminal conditions $K_{ij}(T) = 0$, for $i, j = 1, 2$. This system is easily solved with $K_{11} = K_{12} = K_{21} = 0$ and K_{22} satisfying a Riccati equation equivalent to (2.13)*. Hence, the results we obtain for the first order system can be extended to second order systems. We will further discuss this extension in the numerical section.*

2.2.2 Riccati-based control laws for the non-linear system

In order to approximate the synthesis of feedback laws for the original nonlinear optimal control problem (2.6), we study sub-optimal stabilizing strategies induced by the Riccati control (2.12). Without loss of generality, we will consider the stabilization problem towards $\tilde{v} = 0$. We will focus on different ways to synthesize a control law based on the information retrieved in the linearized case: a closed-loop control, an open-loop strategy, and a simplified inexact open-loop control.

Closed-loop control A well-known local strategy for the control of nonlinear dynamics is to use the optimal feedback control obtained from the linearized dynamics. In this case, the controlled system reads

$$\dot{v}_i = \frac{1}{N} \sum_{j=1}^{N} P(v_i, v_j)(v_j - v_i) + R_i[v](t), \qquad v_i(0) = v_i^0, \tag{2.23}$$

where the operator $R_i[\cdot]$ is the feedback (2.12) applied directly to the state of the nonlinear system $v(t) = (v_i(t))_{i=1}^N$, namely

$$R_i[v](t) = -\frac{1}{\nu} \left(\left(k_d(t) - \frac{k_o(t)}{N} \right) v_i(t) + \frac{k_o(t)}{N} \sum_{j=1}^{N} v_j(t) \right),$$

where $k_d(t), k_o(t)$ are still obtained by solving the system (2.17)–(2.18). In general, such a control law is expected to work only for initial states sufficiently close to the state around which the dynamics have been linearised. We shall investigate in detail the properties of the closed-loop in the following section.

Open-loop control The open-loop strategy we propose applies the control signal obtained from the linear synthesis $u_i(t; v^0)$ directly into the the non-linear dynamics as follows

$$\dot{v}_i = \frac{1}{N}\sum_{j=1}^{N} P(v_i, v_j)(v_j - v_i) + R_i[w](t), \qquad v_i(0) = v_i^0,$$
$$\dot{w}_i = \frac{1}{N}\sum_{j=1}^{N} \bar{p}(w_j - w_i) + R_i[w](t), \qquad w_i(0) = v_i^0,$$

where the control $R_i[w](t)$ is computed according to (2.12). This approach is open-loop, since all the information on the state of the non-linear system reduces to the initial state of linearized system, assuming $w_i^0 = v_i^0$. While this approach is clearly outperformed by the closed-loop feedback law in terms of robustness, it has the advantage that it can be implemented without requiring a continuous measurement of the full nonlinear state $v(t)$, making it appealing for systems where recovering the true state of the dynamics can be expensive or time-consuming.

Inexact open-loop control An inexact, but simpler, implementation of the open-loop approach (2.24) obtained when the control $R_i[\cdot]$ is evaluated only with respect to the initial data v_i^0, that is $R_i[v^0](t)$, where the dependence on t is limited to $k_o(t)$ and $k_d(t)$. This setting avoids the evaluation of system in (2.24), and only requires the computation of

$$\dot{v}_i = \frac{1}{N}\sum_{j=1}^{N} P(v_i, v_j)(v_j - v_i) + R_i[v^0](t), \qquad v_i(0) = v_i^0. \tag{2.25}$$

The open-loop control laws are meant to be embedded in a Model Predictive Control framework, ensuring a sufficiently frequent update of the state of the nonlinear system ensuring stability of the resulting control system. This shall be further analysed in Section 2.4. In the following section we will study the performance of these control strategies when stabilizing the non-linear dynamics in the case $N \gg 1$.

2.3 Mean-field limits and moments estimates

The stabilization strategies (2.23) and (2.24) are clearly suboptimal with respect to the original optimal control problem, and in general will not guarantee the stabilization of the non-linear dynamics (2.5). In this section we quantify the discrepancy between the desired target state and the final state obtained by the stabilization strategies (2.23) and (2.24). In order to estimate these performances in the case where a large number of agents is present, i.e. $N \gg 1$, we discuss our approaches in the *mean-field limit*. Here, we consider the empirical density distribution of agents in order to describe the collective behavior of a large ensemble of particles, and we retrieve upper and lower bounds for the decay of the mean-field density towards the desired configuration. For further details on mean-field derivation of particles systems we refer to (53, 52, 49).

Remark 2. *Mean field limits of controlled interacting agent systems have been studied from different perspectives. For example, mean field control models are obtainable in the*

large particle limit by means of quasi-invariant limit of binary interactions, as shown in (8, 13), or via a BBGKY hierarchy on the corresponding optimality systems, as studied in (118). We also refer to (97, 94) for rigorous results on the convergence and existence of minimizers for mean field optimal control problems.

2.3.1 Open-loop Riccati control

We introduce the empirical joint probability distribution of particles for the system (2.5) and (2.9) is given by

$$\lambda^N(t,v,w) = \frac{1}{N}\sum_{i=1}^{N}\delta(v-v_i(t))\delta(w-w_i(t)),$$

where $\delta(\cdot)$ is a Dirac measure. We assume enough regularity on the interaction kernel, assuming that particles remain in a fixed compact domain for all N and in the whole time interval $[0,T]$. We refer to (49, 52) for a rigorous treatment of the mean-field limit of interacting particle systems. Hence, we introduce the test function $\phi(v,w) \in C_0^1(\mathbb{R}^{2d})$ and by Liouville's theorem we compute the time variation of the inner-product $\langle \lambda^N(t), \phi\rangle$, given by

$$\frac{d}{dt}\langle \lambda^N(t),\phi\rangle = \frac{1}{N}\sum_{i=1}^{N}(\nabla_v\phi(v_i,w_i)\cdot\dot{v}_i(t) + \nabla_w\phi(v_i,w_i)\cdot\dot{w}_i(t)).$$

Denoting by $\lambda^N(t) := \lambda^N(t,v,w)$, we define the marginal densities f^N, g^N, the average $m_1[f^N]$ and the second moment $m_2[f^N]$ as follows

$$\begin{aligned} f^N(t,w) &:= \int_{\mathbb{R}^d}\lambda^N(t,v,w)dv, \qquad g^N(t,v) := \int_{\mathbb{R}^d}\lambda^N(t,v,w)dw; \\ m_1[f^N](t) &:= \int_{\mathbb{R}^d} w f^N(t,w)dw\,, \quad m_2[f^N](t) := \int_{\mathbb{R}^d}|w|^2 f^N(t,w)dw\,. \end{aligned} \tag{2.26}$$

With the standard derivation of the mean-field limit, we obtain in the strong form the evolution equation for $\lambda^N(t,v,w)$ as follows

$$\begin{aligned} \partial_t\lambda^N = &-\nabla_v\cdot\left[\lambda^N\left(\mathcal{P}[g^N] - a^N(t)w - b^N(t)m_1[f^N]\right)\right] \\ &-\nabla_w\cdot\left[\lambda^N\left(\bar{p}(m_1[f^N]-w) - a^N(t)w - b^N(t)m_1[f^N]\right)\right], \end{aligned}$$

where $\mathcal{P}[g]$ denotes the nonlocal integral operator

$$\mathcal{P}[g](v,t) = \int_{\mathbb{R}^d} P(v,v_*)(v_*-v)g(v_*,t)dv_*,$$

and $a^N(t)$ and $b^N(t)$ are obtained from the scaled Riccati system (2.17)-(2.18). Since we are interested in the limit of a large number of agents, for $N\to\infty$ we have

$$\lim_{N\to\infty} a^N(t) = \frac{k_d(t)}{\nu}, \qquad \lim_{N\to\infty} b^N(t) = \frac{k_o(t)}{\nu},$$

where k_d and k_o fulfill

$$-\dot{k_d} = -2\bar{p}k_d - \frac{k_d^2}{\nu} + 1, \qquad -\dot{k_o} = 2\bar{p}k_d - \frac{k_o}{\nu}\left(2k_d + k_o\right) . \tag{2.27}$$

Then, the joint mean-field model can be conveniently written as

$$\begin{aligned}\partial_t \lambda = &-\nabla_v \cdot \left[\lambda\left(\mathcal{P}[g] - \frac{k_d}{\nu}w - \frac{k_o}{\nu}m_1[f]\right)\right] \\ &- \nabla_w \cdot \left[\lambda\left(\bar{p}\left(m_1[f] - w\right) - \frac{k_d}{\nu}w - \frac{k_o}{\nu}m_1[f]\right)\right],\end{aligned} \tag{2.28}$$

with intial data $\lambda(v, w, 0) = \lambda^0(v, w)$. Integrating the mean-field equation (2.28) with respect to v and w, the evolution of the marginals $f(w, t)$ and $g(v, t)$ is given by

$$\partial_t g = -\nabla_v \cdot \left[g\left(\mathcal{P}[g] - \frac{k_d}{\nu}m_1[h] - \frac{k_o}{\nu}m_1[f]\right)\right], \qquad g(v, 0) = g^0(v) \tag{2.29a}$$

$$\partial_t f = -\nabla_w \cdot \left[f\left(\left(\bar{p} - \frac{k_o}{\nu}\right)m_1[f] - \left(\bar{p} + \frac{k_d}{\nu}\right)w\right)\right], \qquad f(w, 0) = g^0(w) \tag{2.29b}$$

with $m_1[h](v, t)$ being the average of the conditional probabilty $h(w|v, t)$ defined as

$$\lambda(t, v, w) = h(t, w|v)g(t, v), \qquad m_1[h](t, v) = \int_{\mathbb{R}^d} wh(t, w|v)dw.$$

We observe that equation (2.29b) is the mean-field equation associated to the linear controlled model (2.20) (114). On the other hand, the equation for the non-linear model (2.29a) is coupled to the solution of the linear model through the control.

Remark 3 (Inexact mean-field open-loop control)**.** *If we consider the inexact open-loop control* (2.25)*, where the control acts only on the information measured at the initial time t_0, we derive a consistent mean-field limit following the procedure described in this section. The mean-field equation for $\lambda(v, w, t)$ reads*

$$\partial_t \lambda = -\nabla_v \cdot \left[\lambda\left(\mathcal{P}[g] - \frac{k_d}{\nu}w - \frac{k_o}{\nu}m_1[g^0]\right)\right], \qquad \lambda(v, w, 0) = \lambda^0(v, w).$$

The marginal distribution corresponds to the initial data $g^0(w)$ and $g(t, v)$ respectively, and the system (2.29) *reduces then to the equation*

$$\partial_t g = -\nabla_v \cdot \left[g\left(\mathcal{P}[g] - \frac{k_d}{\nu}m_1[h] - \frac{k_o}{\nu}m_1[g^0]\right)\right], \qquad g(v, 0) = g^0(v). \tag{2.30}$$

Bounds of decay moments We are interested in the evolution of the first moment and variance of the nonlinear mean-field density $g(t, v)$, denoted by $m_1[g](t)$ and $\sigma^2[g](t)$, respectively. Stabilizing the system towards target consensus point $\bar{v} = 0$ requires estimates on the decay of moments towards zero. We assume the kernel $P(\cdot, \cdot)$ to be a symmetric and bounded function, namely

$$P(v, v_*) = P(v_*, v), \qquad P(v, v_*) \in [-a, b], \qquad \forall v, v_* \in \mathbb{R}^d, \qquad a, b \geq 0. \tag{\textbf{A}}$$

Hence we have the following results

Lemma 2.2. *Let assumption* (**A**) *holds for the interaction kernel* $P(\cdot)$*, then the average of non-linear model* (2.29a) *decays as follows*

$$\frac{d}{dt}m_1[g] = -\frac{k_d + k_o}{\nu}m_1[g], \qquad m_1[g](0) = m_1[g^0], \tag{2.31}$$

and the average of the linear model $m_1[f](t)$ *coincides with* $m_1[g](t)$ *for* $t \geq 0$*.*
The variance variance $\sigma^2[g](t)$ *evolves according to*

$$\frac{d}{dt}\sigma^2[g] = -\int_{\mathbb{R}^{2d}}|v - v_*|^2 P(v, v_*)g(v)g(v_*)dvdv_* - 2\frac{k_d}{\nu}\varrho[f, g]\sqrt{\sigma^2[f]\sigma^2[g]}, \tag{2.32}$$

with intial data $\sigma^2[g](0) = \sigma^2[g^0]$*, where* $\varrho[f, g]$ *is the correlation coefficient. Moreover the variance of the linear model* $\sigma^2[f]$ *satisfies*

$$\frac{d}{dt}\sigma^2[f] = -2\Big(2\bar{p} + \frac{k_d}{\nu}\Big)\sigma^2[f], \qquad \sigma^2[f^0] = \sigma^2[g^0]. \tag{2.33}$$

Proof. By construction of model (2.29) the first moment at time zero coincides, i.e. $m_1[f^0] = m_1[g^0]$. The first moment of $g(t, v)$ satisfies

$$\begin{aligned}\frac{d}{dt}m_1[g] &= \int_{\mathbb{R}^{2d}} P(v, v_*)(v_* - v)gg_*dvdv_* - \frac{k_d}{\nu}\int_{\mathbb{R}^d} m_1[h](v)g\ dv - \frac{k_o}{\nu}m_1[f] \\ &= -\frac{k_d}{\nu}\int_{\mathbb{R}^{2d}} w\lambda(v, w)\ dvdw - \frac{k_o}{\nu}m_1[f] = -\frac{k_d + k_o}{\nu}m_1[f],\end{aligned}$$

where we omitted time dependencies and we denote by gg_* the product of $g(t, v)$ and $g(t, v_*)$. The last two equalities follow from the symmetry of $P(\cdot)$ and the definition of joint distribution.
The second moment of $g(t, v)$, $m_2[g](t)$ satisfies the following equation

$$\begin{aligned}\frac{d}{dt}m_2[g] =& -\int_{\mathbb{R}^{2d}}|v - v_*|^2 P(v, v_*)gg_*dvdv_* - 2\frac{k_o}{\nu}m_1[g]m_1[f] - 2\frac{k_d}{\nu}\int_{\mathbb{R}^{2d}} vw\lambda(v, w)dvdw, \\ =& -\int_{\mathbb{R}^{2d}}|v - v_*|^2 P(v, v_*)gg_*dvdv_* - 2\frac{k_d + k_o}{\nu}|m_1[g]|^2 - 2\frac{k_d}{\nu}\varrho[f, g]\sqrt{\sigma^2[f]\sigma^2[g]}\end{aligned}$$

where we used the equivalence of $m_1[g] \equiv m_1[f]$ and the relation between the correlation coeffiecient $\varrho[f, g]$ and the covariance between f and g, namely

$$\varrho[f, g]\sqrt{\sigma^2[f]\sigma^2[g]} = \int_{\mathbb{R}^{2d}} vw\lambda(v, w)dvdw - m_1[f]m_1[g].$$

By observing that

$$\frac{d}{dt}|m_1[g]|^2 = -2\frac{k_d + k_o}{\nu}|m_1[g]|^2$$

and using the definition $\sigma^2[g] = m_2[g] - |m_1[g]|^2$, we obtain the equation for the variance of the non-linear model (2.32). The variance for the linear model is obtained directly from (2.32), imposing $P(v, v_*) = \bar{p}$ and observing that the double integral becomes

$$\int_{\mathbb{R}^{2d}}|w - w_*|^2 ff_*dwdw_* = 2\sigma^2[f]. \tag{2.34}$$

□

From the evolution equation of the variance $\sigma[g](t)$ we retrieve the following estimates on the decay.

Proposition 2.3. *Under assumption* (**A**) *on the interaction kernel* $P(\cdot)$*, we have the following lower and upper bounds for the evolution of the variance* $\sigma^2[g]$*:*

$$\sigma^2[g^0]e^{-2bt}\left(1-B_b^+(0,t)\right)^2 \le \sigma^2[g](t) \le \sigma^2[g^0]e^{2at}\left(1+B_a^-(0,t)\right)^2, \quad \textit{where} \tag{2.35}$$

$$\begin{aligned} B_c^{\pm}(t_0,t) &= \frac{1}{\nu}\int_{t_0}^{t-t_0}\beta(s-t_0)k_d(s)e^{\pm c(s-t_0)}ds, \\ \beta(t-t_0) &= \exp\left\{-2\bar{p}(t-t_0)-\frac{1}{\nu}\int_{t_0}^{t-t_0}k_d(r)dr\right\}. \end{aligned} \tag{2.36}$$

Proof. Consider first the case $P(v,w) \ge -a$. We bound from below the interaction kernel in equation (2.32),

$$\begin{aligned} \frac{d}{dt}\sigma^2[g](t) &\le 2a\int_{\mathbb{R}^{2d}}|v-v_*|^2 g g_* dv dv_* - 2\frac{k_d}{\nu}\varrho[f,g]\sqrt{\sigma^2[f]\sigma^2[g]} \\ &\le 2a\sigma^2[g] - 2\frac{k_d}{\nu}\sqrt{\sigma^2[f]\sigma^2[g]}. \end{aligned}$$

where we first used the identity (2.34) and $|\varrho| \le 1$. In order to estimate the growth of the right hand side we note that because of (2.33), $\sigma[f](t)$ is given by

$$\sigma^2[f](t) = \sigma^2[g^0]\exp\left\{-4\bar{p}t - \frac{2}{\nu}\int_0^t k_d(s)ds\right\} =: \sigma^2[g^0]\beta(t)^2.$$

Substituting the estimate in the previous equation we obtain

$$\frac{d}{dt}\sigma^2[g](t) \le 2a\sigma^2[g](t) + \frac{2k_d}{\nu}\beta(t)\sqrt{\sigma^2[g^0]\sigma^2[g](t)}.$$

An estimate can be obtained using the change of coordinate $z = \sigma^2$, for $z \neq 0$:

$$\frac{d}{dt}z(t) = az(t) + \frac{k_d}{\nu}\beta(t)\sqrt{\sigma^2[g^0]}.$$

This first-order linear differential equation admit an exact solution as follows

$$z(t) = z(0)e^{at}\left(1+\frac{1}{\nu}\int_0^t e^{-as}k_d(s)\beta(s)ds\right). \tag{2.37}$$

Applying the Petrovitsch's theorem (145), we obtain the upper variance bound

$$\sigma^2[g](t) \le \sigma^2[g^0]e^{2at}\left(1+\frac{1}{\nu}\int_0^t e^{-as}k_d(s)\beta(s)ds\right)^2.$$

We continue with the case $P(v,w) \le b$. Bounding from above $P(\cdot,\cdot)$ in (2.32) we have

$$\frac{d}{dt}\sigma^2[g](t) \ge -2b\sigma^2[g](t) - 2\frac{k_d}{\nu}\sqrt{\sigma^2[f]\sigma^2[g]}.$$

Solving exactly (2.33), and substituting $\sigma[f](t)$ into the previous equation we obtain

$$\frac{d}{dt}\sigma^2[g](t) \geq -2b\sigma^2[g](t) - \frac{2k_d}{\nu}\beta(t)\sqrt{\sigma^2[g^0]\sigma^2[g](t)}.$$

Proceeding as in equation (2.37) leads to

$$\sigma^2[g](t) \geq \sigma^2[g^0]e^{-2bt}\left(1 - \frac{1}{\nu}\int_0^t e^{bs}k_d(s)\beta(s)ds\right)^2.$$

□

Figure 2.5 shows two examples for the decay of $\sigma^2[g]$ and the bounds for the kernel

$$P(v,w) = \alpha + \frac{K}{(\varsigma + |v-w|^2)^\gamma}, \qquad \alpha, \varsigma, \gamma \geq 0, \text{ and } K \in \mathbb{R}, \tag{2.38}$$

associated to Cucker-Smale consensus dynamics (69). On the left, we consider the attractive case where $P(\cdot)$ is positive and bounded in $[0,1]$, with $\alpha = 0, \varsigma = 1, K = 1$ and $\gamma = 2$. On the right, we show an attraction-repulsion dynamics with kernel $-1 \leq P(\cdot,\cdot) \leq 9$ where $\alpha = 9, \varsigma = 0.1, K = -1$ and $\gamma = 1$. The value of σ_g^2 is computed integrating numerically a mean-field approximation of the nonlinear dynamic equation. In both cases, the initial density of particle $g^0(v)$ is

$$g^0(v) = \frac{2}{3}\chi_{[1/4,7/4]}(v).$$

.

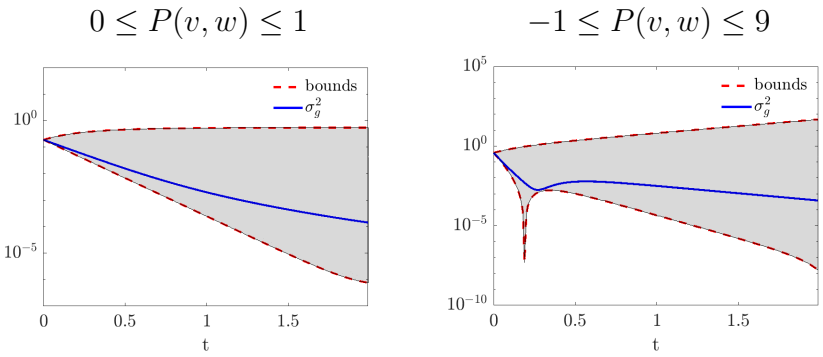

Figure 2.5: Variance decay and bounds for the open-loop approach (2.24). On the left we observe the decay for an attractive dynamics, on the right the attractive-repulsive case.

Remark 4 (Bounds for inexact open-loop Riccati control)**.** *For the inexact open-loop Riccati control we observe that bounds on moments can be computed in similar fashion. From* (2.30)*, the first moment is given by*

$$\frac{d}{dt}m_1[g](t) = -\frac{k_d(t) + k_o(t)}{\nu}m_1[g^0], \qquad m_1[g](0) = m_1[g^0]. \tag{2.39}$$

A substantial difference with respect to the exponential decay of the average (2.31) *is observed since the exact solution to* (2.39) *is*

$$m_1[g](t) = m_1[g^0]\left(1 - \frac{1}{\nu}\int_0^t (k_d(s) + k_o(s))\, ds\right). \tag{2.40}$$

Bounds of the variance of $g(v,t)$ *are retrieved as a particular case of Proposition 2.3. The time evolution of* $\sigma^2[g]$ *reads*

$$\frac{d}{dt}\sigma^2[g] = -\int_{\mathbb{R}^{2d}} |v - v_*|^2 P(v, v_*) g g_* dv dv_* - 2\frac{k_d}{\nu}\varrho[g^0, g]\sqrt{\sigma^2[g^0]\sigma^2[g]},$$

and the bounds for $\sigma^2[g](t)$ *correspond to the estimate in* (2.35) *with* $\beta(t) \equiv 1$,

$$\sigma^2[g^0]e^{-2bt}\left(1 - \frac{1}{\nu}\int_0^t e^{bs}k_d(s)\, ds\right)^2 \leq \sigma^2[g](t) \leq \sigma^2[g^0]e^{2at}\left(1 + \frac{1}{\nu}\int_0^t e^{-as}k_d(s)\, ds\right)^2 \tag{2.41}$$

The loss of the exponential decay of the average (2.31) *constitutes the main drawback of this approach, although we can still steer the density towards a reference solution.*

2.3.2 Closed-loop Riccati control

We perform the derivation of the mean-field limit and moment bounds for the system (2.23). Given the mean-field density $g(v,t)$, the mean-field limit of (2.23) is

$$\partial_t g = -\nabla_v \cdot \left(g\left(\mathcal{P}[g] - \frac{k_d}{\nu}v - \frac{k_o}{\nu}m_1[g]\right)\right), \qquad g(v,0) = g^0(v), \tag{2.42}$$

where $k_o(t), k_d(t)$ are obtained by a Riccati system (2.27).

Bounds of decay moments The first moment and variance equations are given in the following Lemma.

Lemma 2.4. *Under the assumption* (**A**) *the first moment of* (2.42) *evolves according* (2.31)*. The evolution of the variance* $\sigma^2[g]$ *satisfies the equation*

$$\frac{d}{dt}\sigma^2[g] = -\iint |v - v_*|^2 P(v, v_*) g(v) g(v_*) dv dv_* - \frac{2k_d}{\nu}\sigma^2[g]. \tag{2.43}$$

We omit the computations of the proof, since they follow the same line of Lemma 2.2. In particular, it is enough to observe that the variance equation of the open-loop Riccati (2.32) collapses to (2.43) taking $f(t,v) = g(t,v)$. The following estimates on the decay of the variance hold.

Proposition 2.5. *Under assumption* (**A**) *on the interaction kernel* $P(\cdot)$*, there exist lower and upper bounds for the variance of* g *given by*

$$\sigma^2[g^0]e^{-2bt}C_\nu(0,t) \leq \sigma^2[g](t) \leq \sigma^2[g^0]e^{2at}C_\nu(0,t), \tag{2.44}$$

where

$$C_\nu(0,t) = \exp\left\{-\frac{2}{\nu}\int_0^t k_d(s)ds\right\}.$$

Proof. Since the interaction kernel is bounded and using the identity (2.34) for $\sigma^2[g]$, it follows that

$$-2\Big(b+\frac{k_d}{\nu}\Big)\sigma^2[g] \leq \frac{d}{dt}\sigma^2[g] \leq 2\Big(a-\frac{k_d}{\nu}\Big)\sigma^2[g]. \tag{2.45}$$

□

In Figure 2.6 the decay of the variance $\sigma^2[g]$ and the bounds associated to kernel (2.38) are shown. We choose the same parameters as reported in Figure 2.5. We observe that bounds of the closed-loop control (2.23) are closer compared to equation (2.24). Moreover, a stronger decay is observed. Hence, we expect a better performance of the closed-loop control over the open-loop approaches. However, the open-loop approach (2.24) is useful when dealing with incomplete information or limited access to the non-linear dynamics.
We devote the next section to the development of a synthesis method based on predictive horizons estimated a-priori through the bounds of the open-loop strategy (2.24).

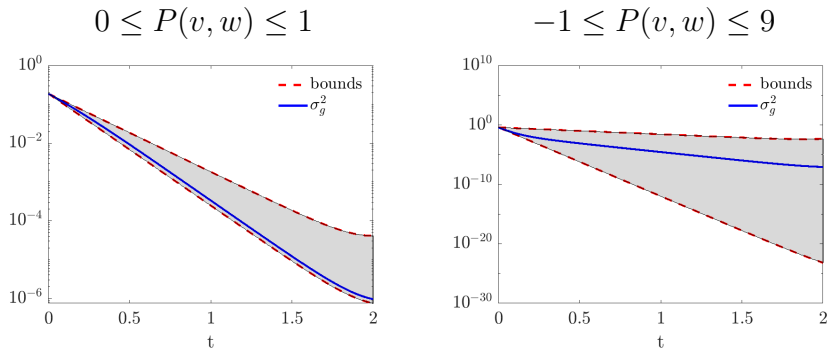

Figure 2.6: Variance decay and bounds for the open-loop approach (2.23). On the left we observe the decay for an attractive dynamics, on the right the attractive-repulsive case.

2.4 Moments driven predictive control (MdPC)

In order to utilize the stabilization properties of the control loops proposed in the previous sections, we discuss their implementation in a receding horizon framework. Here, we prescribe a control horizon where the control signal is applied, after which there is an update procedure including a re-calculation of the control law based on the current state of the system. There exists a vast literature addressing the design of nonlinear model predictive control (MPC) algorithms, we refer the reader to (119, 103) and references therein.
In the general nonlinear MPC control algorithm, an open-loop optimal control signal is synthesized over a prediction horizon $[0, T_p]$, by solving a problem of the form (2.6). Having prescribed the system dynamics and the running cost, this optimization problem depends on the initial state $v(0)$ and the horizon T_p only. The optimal signal u^*, which is obtained for the whole horizon $[0, T_p]$, is implemented over a shorter control horizon $[0, T_c]$. At $t = T_c$ the initial state of the system is re-calibrated to $v(0) = v(T_c)$ and the optimization is repeated. Relevant issues in the MPC literature are the selection of

suitable horizons T_p and T_c which can ensure asymptotic stability of the closed-loop, as well as the design of effective optimization methods to make this implementation suitable for real-time control.
Here instead, we propose a novel class of MPC-type algorithms where instead of fixing a prediction horizon, the re-calibration of the control laws (2.24)-(2.25) is triggered adaptively in time based on a direct estimate of the moments decay. This is similar in spirit to the literature on event-based MPC methods, see for example (89) where an event-based framework for the control of a team of cooperating distributed agents and (149) for networked systems is proposed.

Variance driven Predictive Control MdPC(σ^2) Starting from the open-loop control (2.29) we consider densities at initial time given by $g(v,0) = g^0(v)$, $f^0(w) \equiv g^0(w)$ and the joint distribution $\lambda^0(v,w) \equiv \lambda(v,w,t_0)$. To shorten the notation we introduce the general semi-discretization of the mean-field dynamics (2.28) as follows

$$\lambda^{n+1}(v,w) = \Phi_{\Delta t}[\lambda^n; u^n[f^n]](v,w), \qquad \lambda^0(v,w) = \lambda(v,w,0), \quad n \geq 0, \tag{2.46}$$

coupled with the solution of the Riccati system (2.27). Here, $\Phi_{\Delta t}$ defines the time discretization, and $u^n[f^n]$ encodes the control dependency on the density, given by

$$u^n[f^n](w,t_n) = \frac{1}{\nu}\left(k_d(t_n)w + k_o(t_n)m_1[f^n](t_n)\right).$$

Our goal is to predict the error in the variance decay $\sigma^2[g](t)$ directly from (2.35) by computing the difference between the upper and lower bounds

$$\Delta_\sigma(t_0,t) = \sigma^2[g(v,t_0)]\left[(e^{2a(t-t_0)}\left(1 + B_a^-(t_0,t)\right)^2 - e^{-2b(t-t_0)}\left(1 - B_b^+(t_0,t)\right)^2\right], \tag{2.47}$$

where $B_c^\pm(t_0,t)$ are the quantities defined in (2.36). Then we can use $\Delta_\sigma(t_0,t)$ to control the decay of the variance $\sigma^2[g](t)$ in order to keep the variance of $g(v,t)$ below a fixed threshold $\delta > 0$. In this way, we can find time $t_1 > t_0$ such that $\Delta_\sigma(t_0,t_1) > \delta$ and evolve the dynamics in the time interval $[t_0,t_1]$. The procedure is reinitialized updating the state of the linearized dynamics at time t_1 by setting $f(t_1,v) \equiv g(t_1,v)$. We formalize this procedure in Algorithm 1.

Algorithm 1 [MdPC(σ^2)]

0. Set $k \leftarrow 0$, $t_k = 0$, $g^k(v) = g(v,0)$, $f^k(v) = g(v,0)$ and tolerance δ
1. Solve the Riccati equation to obtain k_d, k_o on the time interval $[0,T]$
2. Find the time t_{k+1} such that $t_{k+1} := \min\{t | t_k < t \leq T, \Delta_\sigma(t_k,t) > \delta\}$

while $t_{k+1} \leq T$ **do**

i. Evolve the dynamics (2.46) up to t_{k+1}
ii. Set $g_{k+1}(v) = g(v,t_{k+1})$, $f_{k+1}(v) = g(v,t_{k+1})$
iii. $k \leftarrow k+1$
iv. Compute t_{k+1} from step 2.

end while

Mean and variance driven Predictive Control, MdPC(m_1, σ^2) For the inexact open-loop control approach (2.30) it is necessary to modify the previous algorithm controlling also the decay of the first moment of $g = g(v,t)$. For this, we introduce the semidiscretized mean-field model of (2.30)

$$\lambda^{n+1}(v,w) = \Phi_{\Delta t}[\lambda^n; u^n[g^0]](v,w), \qquad \lambda^0(v,w) = \lambda(v,w,0), \quad n \geq 0\,, \tag{2.48}$$

where the control is given by

$$u^n[g^0](w,t_n) = \frac{1}{\nu}\left(k_d(t_n)w + k_o(t_n)m_1[g^0]\right).$$

According to the bounds (2.41), the decay of the variance is controlled by $\Delta_\sigma(t_0,t)$ as in (2.47) with

$$B_c^{\pm}(t_0,t) = \frac{1}{\nu}\int_{t_0}^{t-t_0} k_d(s)e^{\pm c(s-t_0)}ds.$$

However, in this case the convergence towards the desired state is not guaranteed since the decay of the first moment (2.40) does not match the moment of the linearized model (2.29b). To guarantee consensus convergence we require (2.40) to be contractive. For this, we introduce the control quantity

$$\Delta_m(t_0,t) = \left|1 - \frac{1}{\nu}\int_{t_0}^{t-t_0}\left(k_d(s) + k_o(s)\right)\,ds\right|,$$

which we use to determine updates in Algorithm 2.

Algorithm 2 [MdPC(m_1, σ^2)]

---

0. Set $k \leftarrow 0$, $t_k = 0$, $g^k(v) = g(v,0)$ and tolerances $\delta, \tau > 0$
1. Solve the Riccati equation to obtain k_d, k_o on the time interval $[0,T]$.
2. Find the times t_δ, t_τ such that

$$\begin{aligned} t_\delta &:= \min\{t | t_k < t \leq T, \Delta_\sigma(t_k,t) > \delta\},\\ t_\tau &:= \min\{t | t_k < t \leq T, \Delta_m(t_k,t) > \tau\},\\ t_{k+1} &:= \min\{t_\delta, t_\tau\} \end{aligned} \tag{2.49}$$

while $t_{k+1} \leq T$ **do**
  i. Evolve the dynamics (2.48) up to t_{k+1}
  ii. Set $g^{k+1}(v) = g(v,t_{k+1})$ and $g^0(v) = g(v,t_{k+1})$
  iii. $k \leftarrow k+1$
  iv. Compute t_{k+1} from (2.49);
end while

Remark 5. *We observe that when an update is performed at each time step, that is for values of δ small enough, the MdPC approaches is equivalent to a discretization of the closed-loop control* (2.42)*. Indeed, since for every $n \geq 0$, we have $f^n \equiv g^n$, the mean-field model* (2.46) *reduces to*

$$g^{n+1}(v) = \Phi_{\Delta t}[g^n; u[g^n]](v), \qquad n \geq 0, \qquad g^0(v) = g(v,t_0), \tag{2.50}$$

where the control is given by $u[g^n](v,t_n) = \frac{1}{\nu}\left(k_d(t_n)v + k_o(t_n)m_1[g^n](t_n)\right)$.

2.5 Numerical Experiments

In this section we present different numerical tests on microscopic and mean-field dynamics. We analyze three different cases: a first-order opinion dynamics, a second-order alignment model, and first-order aggregation model. For the numerical solution of the mean-field model (2.29) we employ mean-field Monte-Carlo methods (MFMCs) developed in (14). These methods fall in the class of fast algorithms developed for interacting particle systems such as direct simulation Monte-Carlo methods (DSMCs) (34, 79, 23), or most recently Random Batch Methods (RBMs) (122).
We consider N_s particles $v^0 \equiv \{v_i^0\}_i$ sampled from the initial distribution $g^0(v)$, and we duplicate the sample defining $w^0 \equiv v^0$ for the linearized dynamics. We introduce the following approximation for the mean-field dynamics

$$\begin{aligned} v_i^{n+1} &= (1 - \Delta t \hat{P}_i^n) v_i^n + \Delta t \hat{P}_i^n \hat{V}_i^n - \Delta t u_i^n, \\ w_i^{n+1} &= (1 - \Delta t \bar{p}) w_i^n + \Delta t \bar{p} \hat{m}_1^n - \Delta t u_i^n, \end{aligned} \tag{2.51}$$

for $n \geq 0$ and where the quantities $\hat{P}_i^n$ and $\hat{V}_i^n$ are computed from a sub-sample of M particles randomly selected from the whole ensemble of N_s particles as follows

$$\hat{P}_i^n = \frac{1}{M} \sum_{k=1}^{M} P(v_i^n, v_{i_k}^n), \qquad \hat{V}_i^n = \frac{1}{M} \sum_{k=1}^{M} \frac{P(v_i^n, v_{i_k}^n)}{\hat{P}_i^n} v_{i_k}^n, \qquad i = 1, \dots, N_s.$$

For the open-loop mean-field dynamics (2.46) the control u_i^n is defined as

$$u_i^n = -\frac{1}{\nu} \left(k_d^n w_i^n + k_o^n \hat{m}_1^n \right), \qquad \hat{m}_1^n = \frac{1}{N_s} \sum_{j=1}^{N_s} w_i^n.$$

The scheme (2.51) reduces to a set of equations for the mean-field dynamics for the closed-loop (2.50) and inexact open-loop (2.48), respectively. In the closed-loop setting (2.50) the control term is computed as

$$u_i^n = -\frac{1}{\nu} \left(k_d^n v_i^n + k_o^n \hat{m}_1^n \right), \qquad \hat{m}_1^n = \frac{1}{N_s} \sum_{j=1}^{N_s} v_i^n,$$

and in the inexact open-loop approach (2.48) we have

$$u_i^n = -\frac{1}{\nu} \left(k_d^n v_i^0 + k_o^n \hat{m}_1^0 \right), \qquad \hat{m}_1^0 = \frac{1}{N_s} \sum_{j=1}^{N_s} v_i^0.$$

We report in Table 2.1 the different choices of parameters used for the numerical discretization of the mean-field dynamics and for each control approach, respectively. We compare the performance of the control laws through the discretized cost

$$J_{\Delta t, N_s}(u, g^0) := \frac{\Delta t}{N_s} \sum_{n=0}^{N_T} \sum_{j=1}^{N_s} (|v_j^n|^2 + \nu |u_j^n|^2), \tag{2.52}$$

with time step Δt and N_s Monte Carlo samples.

	N_s	M	Δt	ν	T	δ	τ
Test 1: Opinion formation	1e4	100	1e-2	1e-2	1	1e-1	1
Test 2: Cucker-Smale dynamics	1e5	100	5e-2	1e-1	3	1	–
Test 3: Aggregation dynamics	1e5	10	1e-2	1	7	1e-1	–

Table 2.1: Simulation and optimization parameters for each test case.

2.5.1 Test 1: Opinion formation

We show an example in the context of opinion formation by Hegselmann and Krause (110). We consider the positive interaction kernel defined as $P(v, w) = C \cdot \chi(|w - v| < \eta)$, where $\eta = 0.25$ represents the confidence level and with a constant $C = 10$, and χ is an indicator function. The initial density of particle $g^0(v)$ is chosen such that consensus towards the target $\bar{v} = 0$ would not be reached without control action, e.g. $g^0(v) = \frac{2}{3}\chi_{[1/4,7/4]}(v)$. We use the forward scheme (2.51) with fixed time step $\Delta t = 0.01$, sampling size $N_s = 10000$ of the initial distribution $g^0(v)$ and fixed $M = 100$ for the approximation of the non-local interactions. To compare the mean-field dynamics with the microscopic we simulate $N = 50$ agents uniformly sampled from g^0.
In the top row of Figure 2.7 the uncontrolled dynamics are shown, where clusters of opinions emerge due to structure of the interaction kernel P. The second and third rows of Figure 2.7 depict the controlled dynamics for the microscopic and the mean-field dynamics. The left column of Figure 2.7 illustrates the convergence to the target when the MdPC(m_1, σ^2) is applied. Algorithm 2 is used with δ and τ chosen according to Table (2.1). The vertical lines in the plots represent the times of the update. We have a different situation with the MdPC(σ^2) approach 1, depicted in the middle column of Figure 2.7. In this case the control is applied by directly embedding the linear synthesis into the the non-linear dynamics. As a consequence, we also require the evolution of the linear state that we plot in a dashed green line for the microscopic case. The right column of Figure 2.7 reports the closed-loop control results. To better interpret these results, we perform a numerical analysis to study the decay of the variance $\sigma^2[g]$ using different values of δ in Algorithm 1 and Algorithm 2. Figure 2.8 compares the variance of the system as the values of the tolerance δ changes. It can be seen that as δ decreases, the MdPC(σ^2) approaches the closed-loop control. This numerical evidence is further confirmed by Table 2.2. With decreasing values of δ we have an increasing number of updates and the values of the functional $J_{\Delta t,N_s}$ computed in (2.52) is similar for the three control approaches. We observe that the closed-loop control corresponds to a limit case of the moment-driven MPC methods.

2.5.2 Test 2: Cucker-Smale dynamics

We study alignment in a second-order, 1D model with Cucker-Smale type interactions (69). We consider a state characterized by $(x_i, v_i) \in \mathbb{R}^2$. The interaction kernel is given by $P(x, y) = \frac{1}{(1+|y-x|^2)^\gamma}$, with $\gamma \geq 0$, which is a decreasing function of the relative distance, bounded to $[0, 1]$. Under the condition $\gamma \geq 1/2$, the convergence to consensus of the free dynamics depends on the initial state (69). We set $\gamma = 2$ and a suitable initial state, such that the flocking state is not achieved without control action. To perform

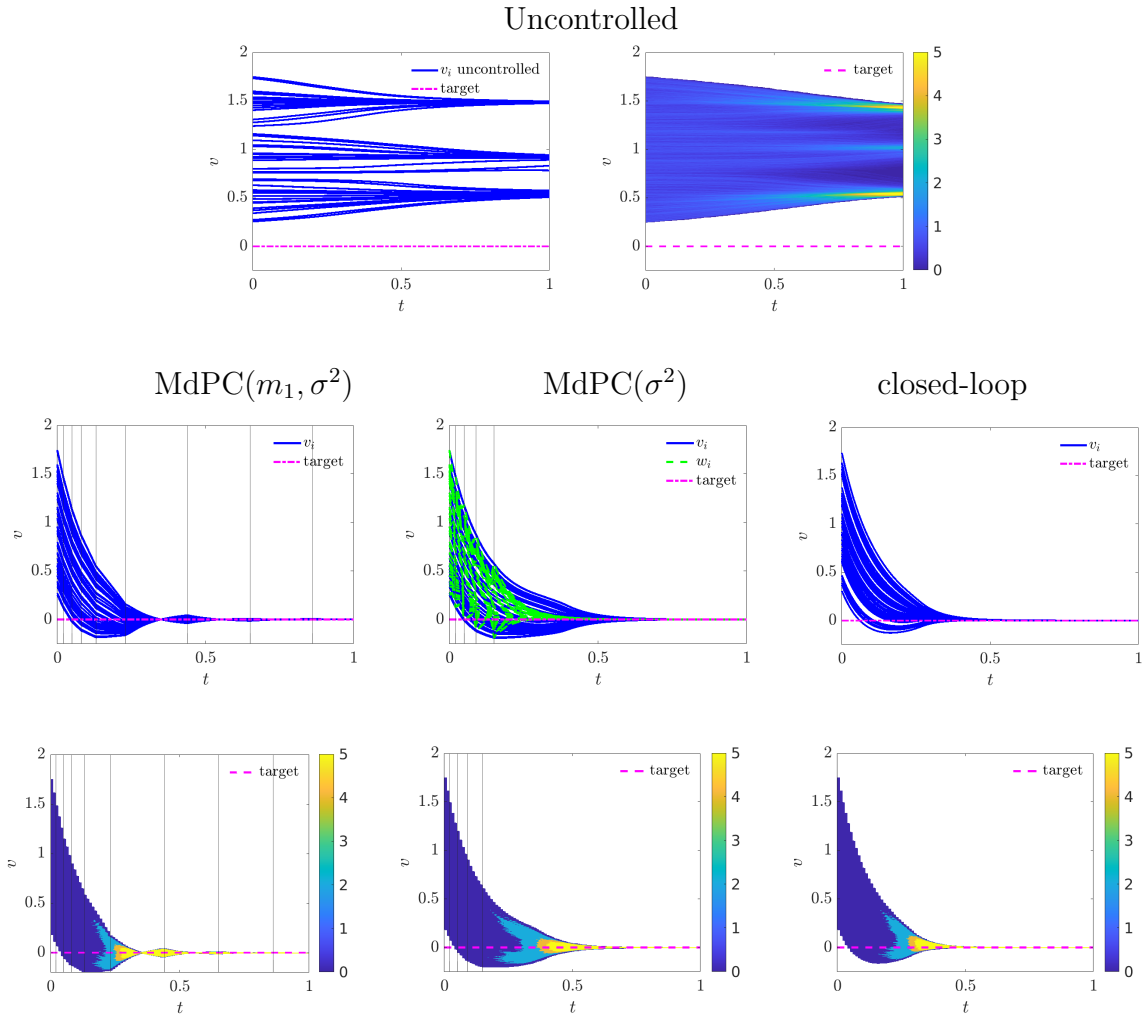

Figure 2.7: *Test 1.* Top: uncontrolled discrete and mean-field evolution of the model. Middle: the controlled discrete case. Bottom: the controlled mean-field dynamics.

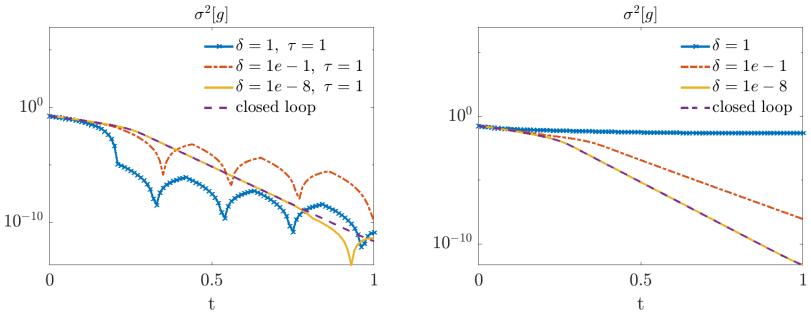

Figure 2.8: *Test 1.* Semi-log plot with a comparison between variance decay with different values of the tolerance δ. Left: variance decays for MdPC(m_1, σ^2). Right: decays for MdPC(σ^2) compared with respect to the closed-loop control.

	MdPC(m_1, σ^2)			MdPC(σ^2)		
δ	1	0.1	1e-8	1	0.1	1e-8
`update` (%)	4 %	8%	71 %	0 %	4 %	72 %
$\sigma^2[g](T)$	1.28e-11	1.26e-10	3.80e-12	5.04e-2	8.94e-9	2.22e-12
$J_{\Delta t,N_s}$	1.8131	0.1306	0.1281	0.1777	0.1309	0.1281

Table 2.2: *Test 1.* We compare the different MdPC approaches with respect to the closed-loop control. For MdPC(m_1, σ^2) the tolerance for the mean is set $\tau = 1$. The number of updates indicates the percentage of control updates over the total number of time steps $N_T = 100$ (for reference, the closed-loop control would require a 100%). The final value of the variance is denoted by $\sigma^2(T)$, and $J_{\Delta t,N_s}$ corresponds to the value of the cost functional (2.52). For the closed-loop control $\sigma^2(T) = 3.80e-12$ and $J_{\Delta t,N_s} = 0.1281$.

our analysis we refer to the second-order dynamics (2.22) and use Remark 1 to obtain the Riccati equations. Unlike the first-order dynamics, the constrained mean-field has a transport term

$$\partial_t g + v \cdot \nabla_x g = -\nabla_v \cdot \left(g \left(\mathcal{P}[g] + u(t)\right)\right), \qquad g(x, v, 0) = g^0(x, v),$$

and the nonlocal operator $\mathcal{P}$ is defined as

$$\mathcal{P}[g](x, v, t) = \int_{\mathbb{R}^d \times \mathbb{R}^d} P(x, y)(w - v) g(y, w, t)\, dy\, dw.$$

We discretize the mean-field model employing the forward scheme (2.51) with fixed time step $\Delta t = 0.05$, sampling size of $N_s = 100000$ particles and fixed $M = 100$. In order to treat the additional transport term in the dynamics, we use a splitting method to perform the free transport step. The control is computed by means of MdPC(σ^2). We refer to Table (2.1) for the choice of parameters.
Figure 2.9 presents the initial data at the top, which is a bivariate distribution unimodal in space and bimodal in velocity defined as follows:

$$g^0(x, v) = \frac{1}{4\pi\sigma_x\sigma_v} \exp\left(-\frac{x^2}{2\sigma_x^2}\right)\left[\exp\left(-\frac{(v + v_-)^2}{2\sigma_v^2}\right) + \exp\left(-\frac{(v + v_+)^2}{2\sigma_v^2}\right)\right],$$

with $\sigma_x = 0.2, \sigma_v = 0.4$ and $v_- = -1, v_+ = 4$. We compare the evolution of the density distribution in the phase space (x, v), jointly with a set of $N = 30$ microscopic points $(x_i(t), v_i(t))$ sampled from the initial distribution. The middle row depicts two time frames of the uncontrolled dynamics, where alignment is not reached. In the bottom row we report the constrained dynamics, where the alignment is reached at time $T = 3$ and the density $g(x, v, t)$ concentrates at the target state $\bar{v} = 0$, whereas its support is bounded in space.
We perform a numerical study for the variance decay $\sigma^2[g]$ using different tolerances δ in Algorithm 1 for MdPC(σ^2). Figure 2.10 compares the decay of the variance of the system as the values of the tolerance δ changes. On the left we observe the decay for $\delta = 1$ jointly with the update and the evolution of the variance bounds. On the right, it can be seen that as δ decreases MdPC(σ^2) is similar to the closed-loop control dynamics. Table 2.3 quantifies the performances of the MdPC(σ^2) reporting the percentage of control

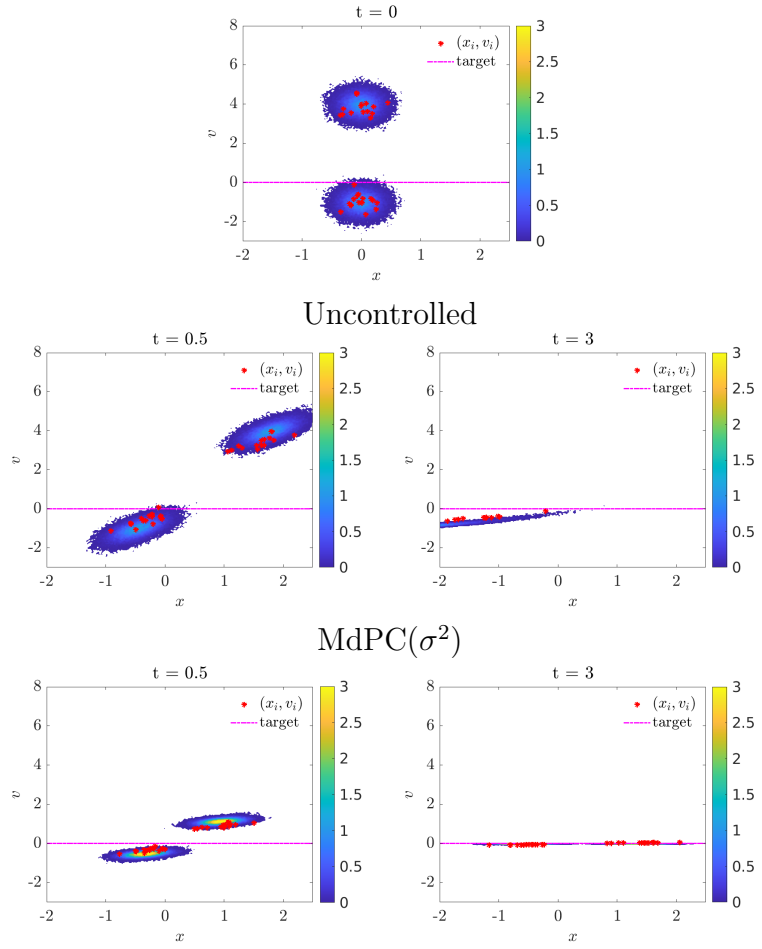

Figure 2.9: *Test 2.* Comparison between the uncontrolled and controlled mean-field evolution of the Cucker-Smale dynamics with MdPC(σ^2) and $\delta = 1$. Without control intervention the alignment state is not reached.

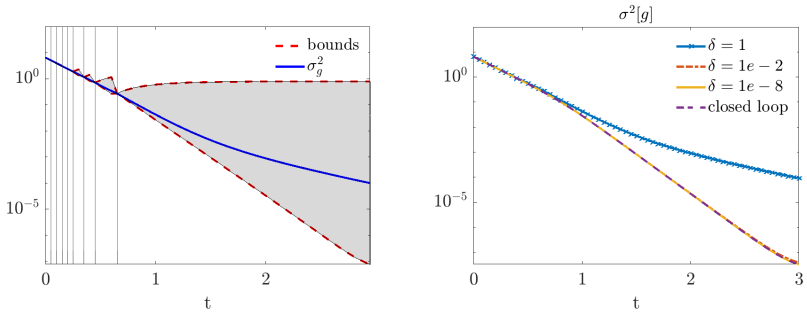

Figure 2.10: *Test 2.*Left: variance and bounds for the second order attractive one-dimensional mean-field dynamics with tolerance $\delta = 1$. Right: variance decays with different values of δ.

updates performed over $N_T = 60$ steps, the variance $\sigma^2[g]$ at time $T = 3$, and the value of the cost functional (2.52).

	MdPC(σ^2)			closed-loop
δ	1	1e-2	1e-8	- -
update (%)	13 %	40 %	99 %	100%
$\sigma^2[g](T)$	9.1393e-05	3.9247e-08	3.3374e-08	3.3371e-08
$J_{\Delta t,N_s}$	3.0059	2.9976	2.9951	2.9951

Table 2.3: *Test 2.* Number of updates and final values of the variance using different values of δ. We compare the different control approaches. The update percentage is computed over $N_T = 60$.

Remark 6. *The synthesis of a control through the Riccati equation provides an optimal control for L^2-tracking type cost functionals with linear dynamics. However, for the general non-linear case such control is sub-optimal, e.g. (8, 116). The MdPC approaches furnish an adaptive synthesis of sub-optimal feedback controls for large-scale non-linear dynamics. For the microscopic Cucker-Smale model with $N = 30$ agents, we compare the performance of the sub-optimal control, computed with the MdPC(σ^2) algorithm with $\delta > 0$, and the optimal control, computed solving the microscopic optimality system arising from Pontryagin's Maximum principle, as in (24). Hence, we consider the optimal and suboptimal trajectories towards consensus, measured as*

$$\mathcal{V}(u(t)) := \frac{1}{N}\sum_{i=1}^{N} |v_i(u_i(t))|^2 \tag{2.53}$$

We report in Figure 2.11, on the left, the evolution in time of $\mathcal{V}(u(t))$, observing faster decay for decreasing values of δ, and faster decay for the optimal control.

Remark 7. *In real applications, the number of agents is finite, and the mesoscopic feedback control can be seen as an approximation to the finite-dimensional control law. We quantify the discrepancy between two different feedback controls, when they are both applied to the microscopic linear dynamics* (2.9)*. In particular, we consider two controls $u_{i,micro}, u_{i,meso}$ defined as in* (2.19)*, for $i = 1, \dots, N$*

$$u_{i,\mathtt{s}} = -\frac{1}{\nu}\left(\left(k_{d,\mathtt{s}} - \frac{k_{o,\mathtt{s}}}{N}\right) w_i(t) + \frac{k_{o,\mathtt{s}}}{N}\sum_{j=1}^{N} w_j(t)\right), \qquad \mathtt{s} = \{micro, meso\},$$

where $k_{d,micro}, k_{o,micro}$ satisfy the microscopic system (2.17)–(2.18)*, while $k_{d,meso}$, $k_{o,meso}$ satisfy the mean-field equations in* (2.27)*. We report in Table 2.4 the values of the cost functional J in 2.10, using the controls u_{micro}, u_{meso} for different numbers of agents, while in Figure 2.11, on the right, we present the evolution of the error $|J^N_{micro} - J^N_{meso}|$ as a function of N. We can observe that as the number of agent increases, the mean-field control becomes closer to the optimal microscopic control.*

2.5.3 Test 3: Aggregation dynamics

The last example is a first-order aggregation model in 2D, where agents interact according to an attraction-repulsion kernel. We consider the following interaction kernel $P(v, w) =$

Agents N	5	25	50	75	100	500
J^N_{micro}	0.927	0.637	0.724	0.715	0.739	0.776
J^N_{meso}	0.987	0.646	0.729	0.719	0.741	0.777

Table 2.4: Values of functional J using the microscopic and mean-field control for different values of the number of agents N.

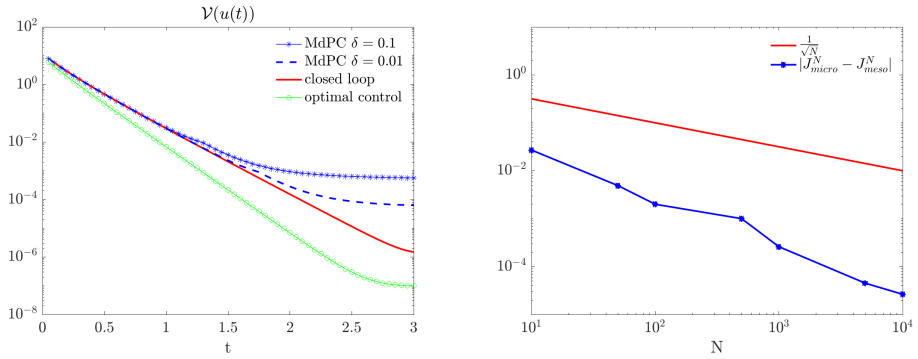

Figure 2.11: On the left, semilog plot of $\mathcal{V}(u(t))$ in (2.53) for three suboptimal approaches: MdPC(σ^2) with $\delta = 0.1$, $\delta = 0.01$ and $\delta \to 0$ (closed loop), and for the optimal control case. On the right loglog plot of the decreasing quantity $|J^N_{micro} - J^N_{meso}|$ as the number of agents N increases.

$|w - v|^{\alpha-2} - |w - v|^{\beta-2}$, where $\alpha = 4$ and $\beta = 2$. For these specific values of the parameters it can be shown that the equilibrium configuration is an uniform distribution on an annulus of radius $R = \frac{1}{\sqrt{3}}$, and same center of mass as the initial distribution. For analytical and numerical characterizations of the equilbrium of these models we refer to (27). We consider an initial density of particles uniformly distributed on the 2D disc of radius $R_0 = \frac{2}{\sqrt{3}}$ centered in $(-1, 1)$, that is

$$g^0(v) = \frac{1}{|\mathcal{C}|}\chi_{\mathcal{C}}(v)\,, \qquad \mathcal{C} := \{v \in \mathbb{R}^2 : |v - (-1, 1)^\top| \leq R_0\}\,,$$

and $|\mathcal{C}|$ denoting its volume. In order to simulate the dynamics we consider $N_s = 100000$ particles sampled from $g^0(v)$ and we implement the forward scheme (2.51) with fixed time step $\Delta t = 0.01$. We select $M = 10$ particles for the approximation of the non-local interactions. We use the MdPC(σ^2) approach with a penalization factor $\nu = 1$ and a stopping tolerance $\delta = 0.1$. In Figure 2.12 we report the evolution of the mean-field and the microscopic dynamics. The latter is sampled with $N = 30$ particles from g^0. The second row of Figure 2.12 shows the uncontrolled dynamics, where mass concentrates towards a 2D annulus of radius $R = 1/\sqrt{3}$. While the third row depicts the open-loop control case where MdPC(σ^2) is applied. At time $T = 7$ the distribution is converged to a concentration at $\bar{v} = (\bar{v}_1, \bar{v}_2) = (0, 0)$.
As in previous tests we illustrates a comparison between different open-loop controls varying tolerance δ in algorithms 1. Figure 2.13 and Table 2.5 highlight that with a very small value of δ, the MdPC approach coincides with the closed-loop approach.

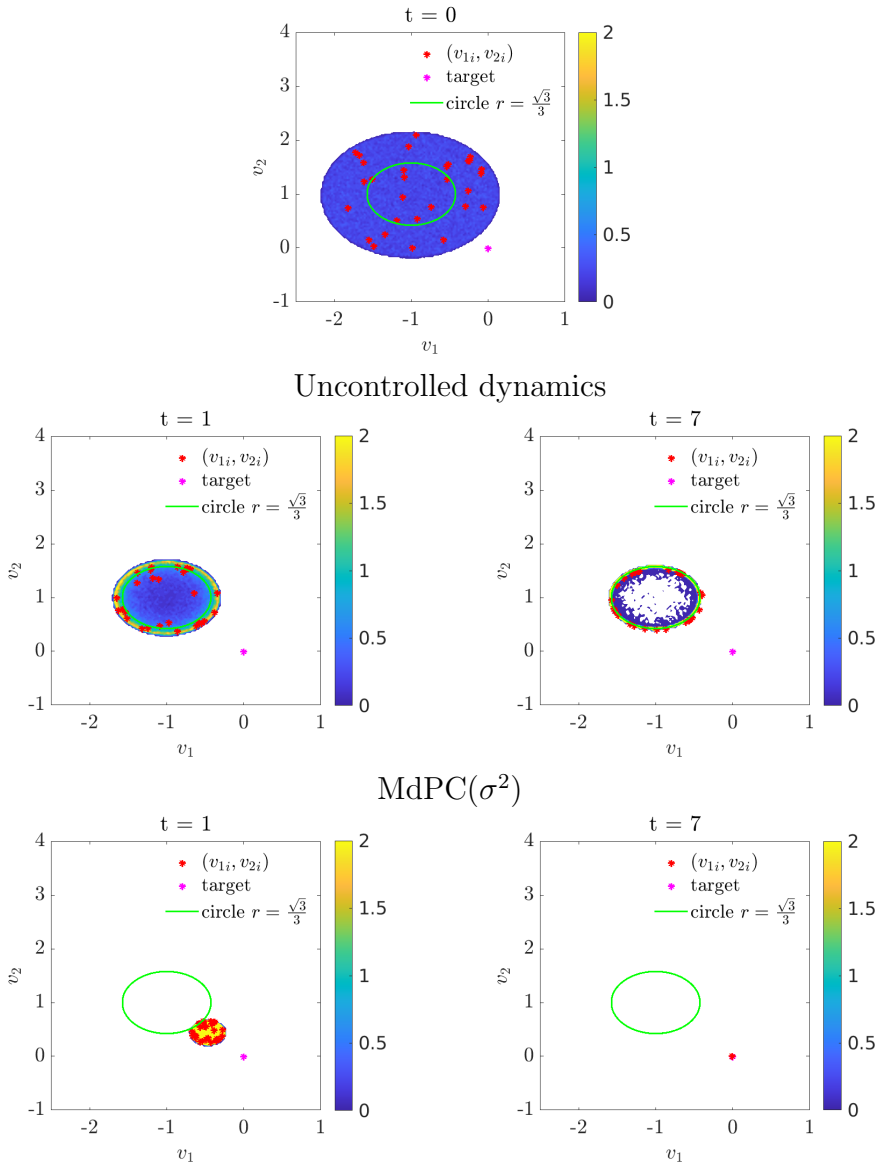

Figure 2.12: *Test 3.* Comparison between the uncontrolled and controlled mean-field evolution of the aggregation dynamics with MdPC(σ^2) and $\delta = 0.1$. Without control intervention the alignment state is not reached.

	MdPC(σ^2)			closed-loop
δ	1	1e-1	1e-9	- -
`update` (%)	1 %	4 %	99 %	100%
$\sigma^2[g](T)$	1.6875e-09	2.1253e-08	2.6151e-08	2.6187e-08
$J_{\Delta t, N_s}$	3.0459	2.9751	2.9750	2.9750

Table 2.5: *Test 3: Aggregation dynamics.* Number of updates and final values of the variance using different values of δ. The update percentage is computed over $N_T = 700$.

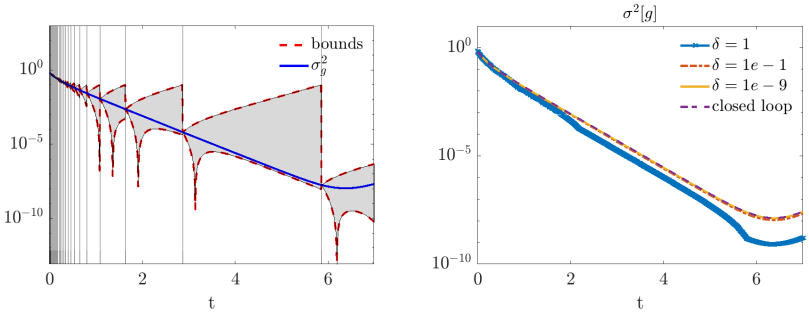

Figure 2.13: *Test 3.* Left: variance evolution and bounds for the first order attractive-repulsive one-dimensional mean-field dynamics with tolerance $\delta = 0.1$. Right: variance decays with different values of δ.

2.5.4 CPU time analysis

We present a computational cost analysis of the proposed methods based on the setting of Test 1 (opinion formation) in section 2.5.1. The main advantage of the control methods presented in this paper is that they do not rely on a continuous measurement of the true state of the system unlike classical feedback laws. Instead, we derive indicators which trigger once a system measurement (and control signal update) is required, drastically reducing the amount of instances in which a state estimation is necessary. Therefore, to make a fair comparison of the various approaches in a realistic context, we include an estimation time, X, which is the amount of time a black-box requires to recover a one-step estimate of the true state of the system given a measurement. The estimation time is independent from the feedback law. In this setting, the closed-loop approach will estimate the state of the true dynamics n_t times, with n_t the total number of time steps. For the MdPC approaches, the estimation time X contributes only for the number of time steps required for the control update, $\bar{p}n_t$ for $0 < \bar{p} \leq 1$. However, in these cases, the CPU time spent flagging whether an update is required or not, i.e. $\bar{q}$. Moreover, for the specific case of MdPC(σ^2) algorithm we also account the cost of evaluating the linearized dynamics at each time-step, i.e. $n_t\bar{Z}$. Hence, we can estimate the total CPU time for each of the proposed methods as follows:

$$Y_{cl} = n_t X, \quad Y_{ex} = \bar{p}_{ex} n_t X + n_t \bar{Z} + \bar{q}_{ex}, \quad Y_{in} = \bar{p}_{in} n_t X + \bar{q}_{in}, \tag{2.54}$$

where Y_{cl} is associated to the closed loop approach, Y_{ex} to MdPC(σ^2), and Y_{in} to MdPC(m_1, σ^2). In Figure 2.14, on the left, we report the CPU times (2.54) as a function of the number of agents N, for a fixed value of the estimation time $X = 0.2$. In Table 2.6 we show different numerical values for reference, note that the percentages of update for the MdPC approach are insensitive to the number of agents and we have $\bar{p}_{ex} = 0.04$, $\bar{p}_{in} = 0.08$. For this CPU analysis we consider the setting of Test 1, where we fixed for MdPC(σ^2) $\delta = 0.1$, and for the MdPC(m_1, σ^2) $\tau = 1$ and $\delta = 0.1$. In the right plot, we report the CPU time for fixed $N = 5000$. In this regime, the cost of the linear dynamics is $\bar{Z} = 0.1$ seconds per time step, computed as the time average over the evolution of $N = 5000$ agents. While the cost to look whether an update is required is $\bar{q}_{ex} = \bar{q}_{in} = 0.01$ seconds for the whole time interval. We observe that there exists a critical value above which the MdPC approaches become more efficient than a closed-loop

feedback. In particular for very cheap estimates of the real dynamics, before the critical point A, the closed-loop approach is faster than the open-loop ones. After the critical value B, close to $X = 0.1$, the closed-loop becomes considerably more expensive than the MdPC approaches.

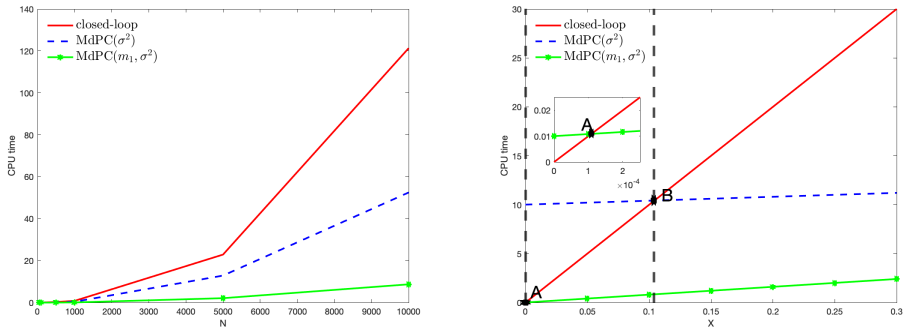

Figure 2.14: CPU time in seconds for the three approaches. On the left as a function of the number of agents N with fixed $X = 0.2$ seconds, on the right as a function of the time X, which is the amount of time a black-box requires to recover a one-step estimate of the non-linear model, with fixed $N = 5000$.

N–agents	50	100	500	1000	5000	10000	update (%)
closed loop	0.01	0.02	0.26	0.81	22.89	121.32	100%
MdPC(σ^2)	0.004	0.006	0.098	0.392	12.873	52.501	4%
MdPC(m_1, σ^2)	0.001	0.002	0.018	0.063	2.094	8.694	8%

Table 2.6: CPU time in seconds for N agents in the three control approaches with $X = 0.2$. The last column shows the percentage of updates over the time range.

2.6 Conclusions

We have studied the design of control laws for interacting particle system based on the solution of the optimal control problem associated to linearized dynamics. We have assessed the impact of different sub-optimal control laws into the original non-linear dynamics deriving mean-field limits of the microscopic constrained systems and estimating analytically and numerically the decay of the first and second moments. We proposed a novel numerical technique based on the moments decay (MdPC). In particular, we obtain a hierarchy of approximations from open-loop to closed-loop control by scaling the tolerance level. These strategies have shown to be robust even with considerably fewer updates of the control law for the non-linear dynamics. The proposed methodology expands the existing NMPC literature by developing a new paradigm in which the control laws are updated based on dynamic information of the system. Here, the use of moments information is a particular example suitable in the context of mean-field

dynamics. Further extensions and analysis will include the study of other dynamic indicators for control update, in particular those that could be linked to a physical observable of the system, and the incorporation of nonlinear state estimation in the control loop.

3 Robust feedback stabilization of interacting multi-agent systems with uncertainties

3.1 Introduction

In this manuscript we consider the mathematical modelling and control of phenomena of collective dynamics under uncertainties. These phenomena have been studied in several field such as socio-economy, biology and robotics where system of interacting particles are given by self-propelled particles, such animals and robots, see e.g. (4, 32, 61, 74, 113, 90). Those particles interact according to a possibly nonlinear model, encoding various social rules as for example attraction, repulsion and alignment. A particular feature of such models is their rich dynamical structure, which include different types of emerging patterns, including consensus, flocking, and milling (102, 147, 69, 88, 138).

Understanding the impact of control inputs in such complex systems is of great relevance for applications. Results in this direction allow to design optimized actions such as collision-avoidance protocols for swarm robotics (57, 140, 144, 100), pedestrian evacuation in crowd dynamics (6, 66, 87, 45), supply chain policies (117, 72), the quantification of interventions in traffic management (148, 108, 146) or in opinion dynamics (13, 101).

The introduction of uncertainty in the mathematical modelling of real world phenomena seems to be unavoidable for applications, since often at most statistical information of the modelling parameters is available. The later has typically been estimated from experiments or derived from heuristic observations (28, 36, 125). To produce effective predictions and to describe understand physical phenomena, we may incorporate parameters reflecting the uncertainty in the interaction rules, and/or external disturbances (55).

Here, we are concerned with the robustness of controls influencing the evolution of a collective motion of interacting agent system. The controls we are considering are aimed to stabilize the system's dynamic under external uncertainty. From a mathematical point of view, a description of self-organized models is provided by complex system theory, where the overall dynamics is depicted by a large scale system of ordinary differential equations (ODEs).

More precisely, we consider the control of high-dimensional dynamics accounting N agents with state $v_i(t,\theta) \in \mathbb{R}^d$, $i = 1, \dots, N$, evolving according to

$$\frac{d}{dt} v_i(t,\theta) = \sum_{j=1}^{N} a_{ij}(v_j(t,\theta) - v_i(t,\theta)) + u_i(t,\theta) + \sum_{k=1}^{Z} \theta_k \,, \qquad v_i(0) = v_i^0, \tag{3.55}$$

where $A = [a_{ij}] \in \mathbb{R}^{N\times N}$ defines the nature of binary interaction among agents, and $\theta = (\theta_1, \dots, \theta_Z)^\top \in \mathbb{R}^{Z\times d}$ is a random input vector with a given probability density distribution on Z as $\rho \equiv \rho_1 \otimes \dots \otimes \rho_Z$. The control signal $u_i(t,\theta) \in \mathbb{R}^d$ is designed to stabilize the state toward a target state $\bar{v} \in \mathbb{R}^{N\times d}$, and its action is influenced by the random parameter θ. This is also due to the fact, that later we will be interested in closed–loop or feedback controls on the state $(v_1 \dots, v_N)$ that in turn dependent on the unknown parameter θ.

Of particular interest will be controls designed via minimization of linear quadratic

(parametric) regulator functional such as

$$\min_{u(\cdot,\theta)} J(u;v^0) := \int_0^{+\infty} \left[v^\top Q v + \nu u^\top R u\right]\, d\tau, \tag{3.56}$$

with Q positive semi-definite matrix of order N, R positive definite matrix of order N. In this case, the linear quadratic dynamics allows for an optimal control u^* stabilising the desired state $v_d = 0$, expressed in feedback form, and obtained by solving the associated matrix Riccati -equations. Those aspects will be also addressed in more detail below.

In order to assess the performances of controls, and quantify their robustness we propose estimates using the concept of $\mathcal{H}_\infty$ control. In the $\mathcal{H}_\infty$ consensus problem under external disturbances, control methods have already been proposed and applied to first-order and higher-order multiagent systems, see e.g. (133, 129, 136, 130, 132). Further, we refer to (30) for a different approach for $\mathcal{H}_\infty$ control problem interpreted as dynamic games.

We formulate the consensus problem as $\mathcal{H}_\infty$ control problem, we derive sufficient conditions in terms of linear matrix inequalities (LMIs) to ensure the consensus robustness, and determine a feedback formulation for the control action. Additionally, we consider the large–agent limit and show that the robustness is guaranteed independent of the number of agents. Furthermore, we will discuss the efficient simulations of system (3.55) by means of uncertainty quantification techniques. In general, at the numerical level, techniques for uncertainty quantification can be classified in non-intrusive and intrusive methods. In an non-intrusive approach, the underlying model is solved for fixed samples with deterministic schemes and statistics of interest are determined by numerical quadrature, typical examples are Monte-Carlo and stochastic collocation methods (80, 139, 155). While in the intrusive case, the dependency of the solution on the stochastic input is described as a truncated series expansion in terms of orthogonal functions. Then, a new system is deduced that describes the unknown coefficients in the expansion. One of the most popular techniques of this type is based on stochastic Galerkin (SG) methods. In particular, generalized polynomial chaos (gPC) gained increasing popularity in uncertainty quantification (UQ), for which spectral convergence on the random field is observed under suitable regularity assumptions (80, 120, 121, 154, 139).

The methods here developed makes use of the generalized polynomial chaos (gPC) expansion for the microscopic dynamics while in the mean-field case we combine a gPC expansion in the random space with a Monte Carlo method in the physical variables.

The manuscript is organized as follows, in Section 3.2 we introduce the problem setting and propose different feedback control laws; in Section 3.3 we reformulate the problem in the setting of $\mathcal{H}_\infty$ control and provide conditions for the robustness of the controls in the microscopic and mean-field case. Section 3.4 is devoted to the description of numerical strategies for the simulation of the agent systems, and to different numerical experiments, which assess the performances and compare different methods.

3.2 Control of interacting agent system with uncertainties

We are concerned with the control of high-dimensional systems of interacting agents with random inputs. We consider the evolution of N agents with state $v(t,\theta) \in \mathbb{R}^{N\times d}$

as follows

$$\frac{d}{dt}v_i(t,\theta) = \frac{1}{N}\sum_{j=1}^{N}\bar{p}(v_j(t,\theta) - v_i(t,\theta)) + u_i(t,\theta) + \sum_{k=1}^{Z}\theta_k \tag{3.57}$$

with deterministic initial data $v_i(0) = v_i^0$ for $i = 1,\dots,N$, and where $\theta_k \in \Omega_k \subseteq \mathbb{R}^d$ for $k = 1,\dots,Z$ are random inputs, distributed according to a compactly supported probability density $\rho \equiv \rho_1 \otimes \cdots \otimes \rho_Z$, i.e., $\rho_k(\theta) \geq 0$ a.e., $\mathrm{supp}(\rho_k) \subseteq \Omega_k$ and $\int_{\Omega_k}\rho_k(\theta)\,d\theta = 1$. For simplicity we also assume that the random inputs have zero average $\mathbb{E}[\theta_k] = 0$. The control signal $u(t,\theta) \in \mathbb{R}^{N\times d}$ is designed minimizing the (parameterized) objective

$$u^*(\cdot,\theta) = \arg\min_{u(\cdot,\theta)} J(u;v^0) := \int_0^{+\infty}\exp(-r\tau)\left(\frac{1}{2N}\sum_{j=1}^{N}(|v_j(\tau,\theta)-\bar{v}|^2 + \nu|u_j(\tau,\theta)|^2)\right)d\tau, \tag{3.58}$$

with $\nu > 0$ being a penalization parameter for the control energy, the norm $|\cdot|$ being the usual Euclidean norm in $\mathbb{R}^d$. The discount factor $\exp(-r\tau)$ is introduced to have a well–posed integral, however, for simplicity of the presentation we will consider the case $r = 0$, see also the remarks below.

We assume that $\bar{v}$ is a prescribed consensus point, namely, in the context of this work we are interested in reaching a consensus velocity $\bar{v} \in \mathbb{R}^d$ such that $v_1 = \ldots = v_N = \bar{v}$, and w.l.o.g. we can assume $\bar{v} = 0$. Note that $\bar{v} = 0$ is also the steady state of the dynamics in absence of disturbances. Hence, we may view $u(\cdot,\theta)$ as a stabilizing control of the zero steady state of the system. Furthermore, we will be interested in feedback controls u.

Recall that the (deterministic) linear model (3.57), without uncertainties, allows a feedback stabilization by solving the resulting optimal control problem through a Riccati equations (115, 12). In this case the controlled dynamics (3.57) is reformulated in a matrix-vector notation as follows

$$\frac{d}{dt}v(t) = Av(t) + Bu(t), \qquad u(t) = -\frac{1}{\nu}Kv(t) \tag{3.59}$$

where $B = \mathrm{Id}_N$ is the identity matrix of order N, and

$$(A)_{ij} = \begin{cases} a_d = \frac{\bar{p}(1-N)}{N}, & i = j, \\ a_o = \frac{\bar{p}}{N}, & i \neq j, \end{cases} \qquad (K)_{ij} = \begin{cases} k_d, & i = j, \\ k_o, & i \neq j, \end{cases} \tag{3.60}$$

are the matrices associated to the linear dynamics, and where $k_d(t), k_o(t)$ are solutions to the Algebraic Riccati Equations (ARE) for $\alpha(N) = \frac{N-1}{N}$:

$$\begin{aligned} 0 &= -2\bar{p}\alpha(N)\left(k_d - \frac{k_o}{N}\right) - \frac{1}{\nu}\left(k_d^2 + \frac{\alpha(N)}{N}k_o^2\right) + 1, \\ 0 &= 2\bar{p}\left(k_d - \frac{k_o}{N}\right) - \frac{1}{\nu}\left(2k_dk_o + \alpha(N)k_o^2 - \frac{1}{N}k_o^2\right). \end{aligned} \tag{3.61}$$

Note that the previous set of equations also allows to consider the limit of infinitely many agents $N \to \infty$ leading to a corresponding mean field control.

The previous considerations motivate to extend formula (3.59) to the parameteric case (3.57). Hence, in the presence of parameteric noise the feedback control is written explicitly as follows

$$u_i(t,\theta) = -\frac{1}{\nu}\left(Kv(t,\theta)\right)_i = -\frac{1}{\nu}\left(\left(k_d - \frac{k_o}{N}\right)v_i(t,\theta) + \frac{k_o}{N}\sum_{j=1}^{N} v_j(t,\theta)\right). \tag{3.62}$$

The question now arise if the given feedback is robust with respect to the uncertainties θ. In the following, we will provide a measure for the robustness of control (3.62) in the framework of $\mathcal{H}_\infty$ control. Some additional remarks are in order that allow to generalize formula (3.62).

Remark 8 (Non-zero average)**.** *In presence of general uncertainties with known expectation, we modify the control* (3.62) *for model* (3.57) *including a correction factor given by the the expected values of the random inputs,*

$$u_i(t,\theta) = -\frac{1}{\nu}\left(\left(k_d - \frac{k_o}{N}\right)v_i(t,\theta) + \frac{k_o}{N}\sum_{j=1}^{N} v_j(t,\theta)\right) - \sum_{k=1}^{Z}\mu_k, \tag{3.63}$$

for $\mu_k = \mathbb{E}[\theta_k]$ *for* $k = 1,\dots,Z$.

Remark 9 (Noise-independent control)**.** *In case of a deterministic feedback control we may consider the expectation of the objective* (3.58) *subject to the noisy model* (3.57)

$$\bar{u}^*(\cdot) = \arg\min_{u(\cdot)} \mathbb{E}\left[\int_0^{+\infty} \frac{1}{2}(v^\top Q v + \nu u^\top R u)\, dt\right],$$

where we introduce the matrices $Q = R = \frac{1}{N}Id_N$. *In this case we have the following deterministic optimal feedback control is deduced*

$$\bar{u}_i(t) = -\frac{1}{\nu}\left(k_d\mathbb{E}\left[v_i(t,\theta)\right] + \frac{k_o}{N}\sum_{j\neq i}^{N}\mathbb{E}\left[v_j(t,\theta)\right]\right) - \sum_{k=1}^{Z}\mu_k, \tag{3.64}$$

where $\mu_k = \mathbb{E}[\theta_k]$ *for* $k = 1,\dots,Z$, k_d, k_o *satisfy equations* (3.61). *We refer to Appendix 3.6 for detail computations for the synthesis of* (3.64).

Remark 10 (Unbounded objective)**.** *The objective* (3.58) *may be unbounded in the case* $r = 0$. *Clearly, adding the exponential discount factor for the cost will be a remedy to this problem, however, for the forthcoming presentation we excluded the discount factor as simplification.*

3.3 Robustness in the $\mathcal{H}_\infty$ setting

In the context of $\mathcal{H}_\infty$ theory, controllers are synthesized to achieve stabilization with guaranteed performance. In this section we exploit the theory of Linear Matrix Inequality (LMI) in order to figure out the robustness of the control we take into account. The introduction of LMI methods in control has dramatically expanded the types and

complexity of the systems we can control, it is possible to use LMI solvers to synthesize optimal or suboptimal controllers and estimators for multiple classes of state-space systems. We refer to (143, 126, 41, 83) as references for LMI methods in control. We consider the linear system (3.57) with control (3.62) under the following reformulation

$$\frac{d}{dt}v = \widehat{A}v + \widehat{B}\theta, \tag{3.65}$$

where we consider the random input vector $\theta = (\theta_1, \dots, \theta_Z)^\top \in \mathbb{R}^{Z\times d}$, and the matrices

$$\widehat{A} = A - \frac{1}{\nu}K, \qquad \widehat{B} = \mathbb{1}_{N\times Z}.$$

with $\mathbb{1}$ a matrix of ones of dimension $N \times Z$. We introduce the frequency transfer function $\hat{G}(s) := (s\mathrm{Id}_N - \widehat{A})^{-1}\widehat{B}$, such that $\hat{G} \in R\mathcal{H}_\infty$, the set of proper rational functions with no poles in the closed complex right half-plane, and the signal norm $\|\cdot\|_{\mathcal{H}_\infty}$ measuring the size of the transfer function in the following sense

$$\|\hat{G}\|_{\mathcal{H}_\infty} = \operatorname{ess\,sup}_{\omega\in\mathbb{R}} \bar{\sigma}(\hat{G}(i\omega)), \tag{3.66}$$

where given P, $\bar{\sigma}(P)$ is the largest singular value of P. The general $\mathcal{H}_\infty$-optimal control problem consists of finding a stabilizing feedback controller u which minimizes the cost function (3.66), we refer to Appendix 3.7 for a more general context, and to (85, 99) for a more theoretical treatment and introduction to control state-space theory. However, the direct minimization of the cost $\|\hat{G}\|_{\mathcal{H}_\infty}$ is in general a very hard task, and unfeasible with direct methods. To reduce such complexity, a possibility consists in finding conditions for the stabilizing controller that achieves a norm bound for a given threshold $\gamma > 0$,

$$\|\hat{G}\|_{\mathcal{H}_\infty} \leq \gamma. \tag{3.67}$$

Hence, robustness of a given control u is measured in terms of the smallest γ satisfying (3.67). In order to provide a quantitative result we can rely on the following equivalency result

Lemma 3.1. *Given the frequency transfer function $\hat{G}$, associated to* (3.65)*, a necessary and sufficient condition to guarantee the $\mathcal{H}_\infty$ bound* (3.67) *is to prove that it exists a positive definite square matrix of order N, $X > 0$, such that the following algebraic Riccati equation holds*

$$A^\top X + XA - \frac{1}{\nu}K^\top X - \frac{1}{\nu}XK + \frac{Z}{\gamma}XX + \frac{1}{\gamma}Id_N = 0. \tag{3.68}$$

with minimal value of $\gamma > 0$.

For the proof of this result we refer to the more general case reported in the Appendix 3.7.

Theorem 3.2. *Consider system* (3.65) *with structure induced by* (3.57)*, and consider a square matrix X with the following structure*

$$(X)_{ij} = \begin{cases} x_d, & i = j, \\ x_o, & i \neq j. \end{cases}$$

Then for N sufficiently large and finite, control u (3.62) is $\mathcal{H}_\infty$-robust, with $c_N > 0$ and $\gamma > \frac{1}{c_N}$, where

$$c_N = \bar{p} + \frac{1}{\nu}(k_d - \frac{k_o}{N}).$$

Proof. Under the hypothesis of the theorem, (3.68) reduces to the following system

$$\begin{aligned} 0 = {} & \frac{2\bar{p}(1-N)}{N}x_d + \frac{2\bar{p}(N-1)}{N}x_o - \frac{2}{\nu}k_d x_d - \frac{2(N-1)}{\nu N}k_o x_o \\ & + \frac{1}{\gamma}x_d^2 + \frac{N-1}{\gamma}x_o^2 + \frac{1}{\gamma}, \end{aligned} \tag{3.69}$$

$$\begin{aligned} 0 = {} & \frac{2\bar{p}(1-N)}{N}x_o + \frac{2\bar{p}}{N}x_d + \frac{2\bar{p}(N-2)}{N}x_o - \frac{2}{\nu}k_d x_o - \frac{2}{\nu N}k_o x_d \\ & - \frac{2(N-2)}{\nu N}k_o x_o + \frac{2}{\gamma}x_d x_o + \frac{N-2}{\gamma}x_o^2. \end{aligned} \tag{3.70}$$

Since we are interested in the dynamics for a large number of agents, and to capture correctly a consistent description we scale the off-diagonal elements x_o of X according to

$$\tilde{x}_o = \sqrt{N}x_o.$$

Under this scaling the previous system reads

$$\begin{aligned} 0 = {} & \frac{2\bar{p}(1-N)}{N}x_d + \frac{2\bar{p}(N-1)}{N\sqrt{N}}\tilde{x}_o - \frac{2}{\nu}k_d x_d - \frac{2(N-1)}{\nu N\sqrt{N}}k_o\tilde{x}_o + \frac{1}{\gamma}x_d^2 + \frac{N-1}{\gamma N}\tilde{x}_o^2 + \frac{1}{\gamma}, \\ 0 = {} & \frac{2\bar{p}(1-N)}{N\sqrt{N}}\tilde{x}_o + \frac{2\bar{p}}{N}x_d + \frac{2\bar{p}(N-2)}{N\sqrt{N}}\tilde{x}_o - \frac{2}{\nu\sqrt{N}}k_d\tilde{x}_o - \frac{2}{\nu N}k_o x_d - \frac{2(N-2)}{\nu N\sqrt{N}}k_o\tilde{x}_o \\ & + \frac{2}{\gamma\sqrt{N}}x_d\tilde{x}_o + \frac{N-2}{\gamma N}\tilde{x}_o^2. \end{aligned} \tag{3.71}$$

From the two equations of system (3.71), and setting

$$c = \bar{p} + \frac{k_d}{\nu}, \tag{3.72}$$

we obtain two second order equations for x_d and $\tilde{x}_o$

$$\begin{aligned} 0 &= x_d^2 - 2\gamma c x_d + \tilde{x}_o^2 + 2\gamma\alpha\mathcal{O}\Big(\frac{1}{\sqrt{N}}\Big)\tilde{x}_o + 1, \\ 0 &= \tilde{x}_o^2 - 2\gamma\Big(\beta - \frac{x_d}{\gamma}\Big)\mathcal{O}\Big(\frac{1}{\sqrt{N}}\Big)\tilde{x}_o + 2\gamma\alpha\mathcal{O}\Big(\frac{1}{\sqrt{N}}\Big)x_d, \end{aligned} \tag{3.73}$$

with solutions

$$\begin{aligned} x_d^{\pm} &= \gamma c \pm \sqrt{\gamma^2 c^2 - 1 - \tilde{x}_o^2 - 2\gamma\alpha\mathcal{O}\Big(\frac{1}{\sqrt{N}}\Big)\tilde{x}_o}, \\ \tilde{x}_o^{\pm} &= \mathcal{O}\Big(\frac{1}{\sqrt{N}}\Big)\left(\gamma\Big(\beta - \frac{x_d}{\gamma}\Big) \pm \sqrt{\gamma^2\Big(\beta - \frac{x_d}{\gamma}\Big)^2 - 2\gamma\alpha x_d}\right), \end{aligned}$$

where

$$\alpha = \bar{p} - \frac{k_o}{\nu} \quad \text{and} \quad \beta = \frac{k_d + k_o}{\nu}.$$

We can write the matrix X as

$$X = \frac{\tilde{x}_o}{\sqrt{N}}\, \mathbb{1}_N + (x_d - \frac{\tilde{x}_o}{\sqrt{N}})\, I_N,$$

and the eigenvalues of X are

$$\lambda_i = \lambda = x_d - \frac{\tilde{x}_o}{\sqrt{N}} \quad \text{for} \quad i = 1, \ldots, N-1 \quad \text{and} \quad \lambda_N = x_d + (N-1)\frac{\tilde{x}_o}{\sqrt{N}}.$$

If we subtract equations in (3.71) we find the following second order equation in the variable $\lambda = (x_d - \frac{\tilde{x}_o}{\sqrt{N}})$

$$\lambda^2 - 2\gamma\Big(\bar{p} + \frac{1}{\nu}(k_d - \frac{k_o}{N})\Big)\lambda + 1 = 0,$$

with solutions

$$\lambda^{\pm} = (x_d - \frac{\tilde{x}_o}{\sqrt{N}})^{\pm} = \gamma c_N \pm \sqrt{\gamma^2 c_N^2 - 1},$$

with

$$c_N = \bar{p} + \frac{1}{\nu}\left(k_d - \frac{k_o}{N}\right). \tag{3.74}$$

The diagonal elements of the matrix X are

$$x_d = \frac{\tilde{x}_o}{\sqrt{N}} + \lambda^{\pm}.$$

With the help of a symbolic calculus software, we can now compute $\tilde{x}_o^{\pm}$ from (3.73)

$$\tilde{x}_o^{\pm} = \pm\sqrt{\widetilde{z}^{\pm}\Big(2\gamma(\frac{k_d}{\nu} - \bar{p}) - \widetilde{z}^{\pm}\Big) - 1} \cdot \mathcal{O}\Big(\frac{1}{\sqrt{N}}\Big),$$

with

$$\widetilde{z}^{\pm} = \gamma c \pm \sqrt{\gamma^2 c^2 - 1},$$

and c as in Eq. (3.72). Therefore we have

$$\lambda_i = x_d - \frac{\tilde{x}_o^{\pm}}{\sqrt{N}} = \lambda^{\pm} \quad \text{for} \quad i = 1, \ldots, N-1$$
$$\lambda_N = x_d + (N-1)\frac{\tilde{x}_o^{\pm}}{\sqrt{N}} = \lambda^{\pm} + N\frac{\tilde{x}_o^{\pm}}{\sqrt{N}} \in \mathcal{O}\Big(1\Big).$$

We first study the positivity of the eigenvalue $\lambda^{\pm} = \gamma c_N \pm \sqrt{\gamma^2 c_N^2 - 1}$ in terms of the parameters γ and c_N. First of all, we need $\gamma \geq \frac{1}{c_N}$ to ensure existence of the square root. In addition, if $c_N > 0$

$$\lambda^+ > 0 \quad \text{if} \quad \gamma c_N > -\sqrt{\gamma^2 c_N^2 - 1} \quad \text{which is always true,}$$
$$\lambda^- > 0 \quad \text{if} \quad \gamma c_N > \sqrt{\gamma^2 c_N^2 - 1} \quad \text{which is also always true.}$$

On the contrary, if $c_N \leq 0$, $\lambda^{\pm}$ is never positive. Under the same assumptions $\gamma \geq \frac{1}{c_N}$, and $c_N > 0$ we have the last eigenvalue λ_N always positive too.

□

3.3.1 Mean-field estimates for $\mathcal{H}_\infty$ control

In order to estimate these results when a large number of agents is present, i.e. $N \gg 1$, we discuss our approaches in the *mean-field limit*, where the uncertainty is accounted as . Here, we consider the density distribution of agents in order to describe the collective behavior of the ensemble of particles. We introduce the empirical joint probability distribution of particles for the system (3.57), it is given by

$$f^N(t, v, \theta) = \frac{1}{N} \sum_{i=1}^{N} \delta(v - v_i(t, \theta)),$$

where $\delta(\cdot)$ is a Dirac measure over the trajectories $v_i(t, \theta)$ with $\theta = (\theta_1, \ldots, \theta_Z)$. We consider enough regularity assuming that particles remain in a fixed compact domain for all N and in the whole time interval $[0, T]$. Computing the mean-field limit of dynamics (3.57) we obtain

$$\partial_t f(t, v, \theta) = -\nabla_v \cdot \left(f(t, v, \theta) \left(\left(\bar{p} - \frac{k_o}{\nu} \right) m_1[f](t, \theta) - \left(\bar{p} + \frac{k_d}{\nu} \right) v + \sum_{k=1}^{Z} \theta_k \right) \right),$$

with initial data $f(0, v, \theta) = f^0(v, \theta)$, where $m_1[f]$ denotes the average density

$$m_1[f](t, \theta) = \int_{\mathbb{R}^d} v f(t, v, \theta) dv.$$

For the many particle limit, we can recover a mean-field estimate of the $\mathcal{H}_\infty$ condition similarly as in 3.2. Indeed, for $N \to \infty$ the nonlinear system (3.71) reads

$$0 = -2\bar{p} x_d - \frac{2}{\nu} k_d x_d + \frac{1}{\gamma} x_d^2 + \frac{1}{\gamma} x_o^2 + \frac{1}{\gamma},$$
$$0 = \frac{1}{\gamma} x_o^2.$$

Hence, we observe that the structure of matrix X in (3.68), becomes diagonal with values

$$x_d^{\pm} = \gamma \left(\bar{p} + \frac{k_d}{\nu} \right) \pm \sqrt{\gamma^2 \left(\bar{p} + \frac{k_d}{\nu} \right)^2 - 1}, \qquad x_o^{\pm} = 0,$$

and to ensure positivity of the eigenvalues is enough to require that

$$\gamma > \frac{1}{c},$$

where γ is the bound of the $\mathcal{H}_\infty$ norm, and $c = \bar{p} + k_d/\nu$ corresponds to the limiting value of c_N, defined in (3.74).

Remark 11. *We recall that we can choose a control where k_d and k_o satisfy system* (3.61)*. In particular if we let $N \to \infty$ and we choose the infinite horizone case,* (3.61) *reduces to*

$$0 = \frac{k_d^2}{\nu} + 2\bar{p}k_d - 1,$$
$$0 = \frac{k_o^2}{\nu} + \frac{2}{\nu}k_d k_o - 2\bar{p}k_d,$$

hence

$$k_d^{\pm} = -\nu\bar{p} \pm \nu\sqrt{\bar{p}^2 + \frac{1}{\nu}}, \qquad k_o^{\pm} = k_d \pm \nu\sqrt{\frac{k_d^2}{\nu^2} + \frac{2\bar{p}k_d}{\nu}}.$$

In this particular case, and using k_d^+, the condition becomes $\gamma > \sqrt{\frac{\nu}{\bar{p}^2\nu+1}}$. Figure 11 shows the quantity

$$\gamma(\nu, \bar{p}) = \sqrt{\frac{\nu}{\bar{p}^2\nu + 1}},$$

for different values of ν and $\bar{p}$. As expected, we have a smaller value of γ, hence more robustness, when the penalization factor ν is smaller and when $\bar{p}$ is bigger, this means more attraction between particles.

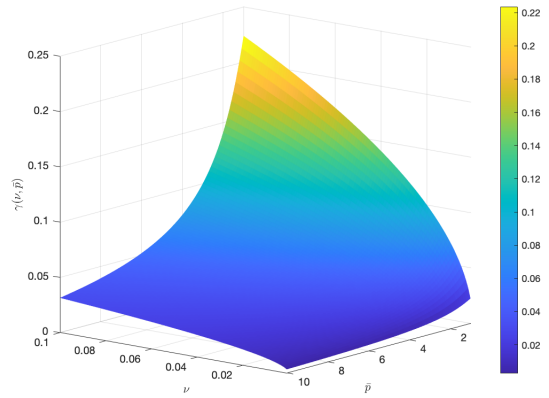

Figure 3.15: Value of γ as a function of ν and $\bar{p}$.

3.4 Numerical approximation of the noisy dynamics

In this section we present numerical tests based on linear noisy microscopic and mean-field equations. In particular, we give numerical evidence of the robustness of the control

Probability law of θ	Expansion polynomials	Support
Gaussian	Hermite	$(-\infty, +\infty)$
Uniform	Legendre	$[a, b]$
Beta	Jacobi	$[a, b]$
Gamma	Laguerre	$[0, +\infty)$
Poisson	Charlier	$\mathbb{N}$

Table 3.7: The different gPC choices for the polynomial expansions.

in (3.62) and we show a comparison with the noise independent control in (3.83). For the numerical approximation of the noisy dynamics we use the Stochastic Galerkin (SG) belonging to the class of generalized polynomial chaos (gPC) ((123, 128, 154)). In all tests the time integration has been performed through a 4th order Runge-Kutta method.

3.4.1 gPC approximation for robust constrained interacting agent systems

We approximate the dynamics using a generalized polynomial chaos approach applied to the interacting particle system with uncertainties (19, 55). Polynomial chaos expansion provides a way to represent a random variable with finite variance as a function of an M-dimensional random vector using a polynomial basis that is orthogonal to the distribution of this random vector. Depending on the distribution, different expansion types are distinguished, as shown in Table 3.7. We recall first some basic notions on gPC approximation techniques and for the sake of simplicity we consider a one dimensional setting $d = 1$. Let $(\Omega, \mathcal{F}, P)$ be a probability space where Ω is an abstract sample space, $\mathcal{F}$ a $\sigma-$algebra of subsets of Ω and P a probability measure on $\mathcal{F}$. Let us define a random variable

$$\theta : (\Omega, \mathcal{F}) \to (I_\Theta, \mathcal{B}(\mathbb{R}^Z)) \tag{3.75}$$

where $I_\Theta \in \mathbb{R}^Z$ is the range of θ and $\mathcal{B}(\mathbb{R}^Z)$ is the Borel σ-algebra of subsets of $\mathbb{R}^Z$, we recall that Z is the dimension of the random input $\theta = (\theta_1, \dots, \theta_Z)$ and where we assume that each component is independent. We consider the linear spaces generated by orthogonal polynomials of θ_j with degree up to M: $\{\Phi_{k_j}^{(j)}(\theta)\}_{k_j=0}^M$, with $j = 1, \dots, Z$. Assuming that the probability law for the function $v_i(\theta, t)$ has finite second order moment, the complete polynomial chaos expansion of v_i is given by

$$v_i(\theta, t) = \sum_{k_1, \dots, k_Z \in \mathbb{N}} \hat{v}_{i,k_1 \dots k_Z}(t) \prod_{j=1}^{Z} \Phi_{k_j}^{(j)}(\theta_j),$$

where the coefficients $\hat{v}_{i,k_1 \dots k_Z}(t)$ are defined as

$$\hat{v}_{i,k_1 \dots k_Z}(t) = \mathbb{E}_\theta \left[v_i(\theta, t) \prod_{j=1}^{Z} \Phi_{k_j}^{(j)}(\theta_j) \right]$$

where the expectation operator $\mathbb{E}_\theta$ is computed with respect to the joint distribution $\rho = \rho_1 \otimes \dots \otimes \rho_Z$, and where $\{\Phi_k^{(j)}(\theta_j)\}_k$ is a set of polynomials which constitute the optimal basis with respect to the known distribution $\rho(\theta_j)$ of the random variable θ_j, such that

$$\mathbb{E}_{\theta_j} \left[\Phi_k^{(j)}(\theta_1) \Phi_h^{(j)}(\theta_j) \right] = \mathbb{E}_{\theta_j} \left[\Phi_h^{(j)}(\theta_j)^2 \right] \delta_{hk},$$

with δ_{hk} the Kronecker delta function. From the numerical point of view we have that through a gPC-type method it is possible to achieve an exponential order of convergence to the exact solution of the problem, unlike Monte Carlo techniques for which the order is $\mathcal{O}(1/\sqrt{M})$ where M is the number of samples. Considering the noisy model 3.57 with control $u_i(t)$ in 3.62, we have

$$\dot{v}_i(\theta,t) = \frac{\bar{p}}{N}\sum_{j=1}^{N}\Big(v_j(\theta,t)-v_i(\theta,t)\Big)-\frac{1}{N\nu}\sum_{j=1}^{N}\Big(k_o(t)v_j(\theta,t)+k_d(t)v_i(\theta,t)\Big)+\sum_{j=1}^{Z}\theta_j. \quad (3.76)$$

We apply the gPC decomposition to the solution of the differential equation $v_i(\theta,t)$ in (3.76) and to the stochastic variable θ_k, and for $i=1,\dots,N,\ l=1,\dots,Z$, we have

$$\begin{aligned} v_i^M(\theta,t) &= \sum_{k_1,\dots,k_Z=0}^{M}\hat{v}_{i,k_1\dots k_Z}(t)\prod_{j=1}^{Z}\Phi_{k_j}^{(j)}(\theta_j),\\ \theta_l^M(\theta) &= \sum_{k_1,\dots,k_Z=0}^{M}\hat{\theta}_{l,k_1\dots k_Z}(t)\prod_{j=1}^{Z}\Phi_{k_j}^{(j)}(\theta_j), \end{aligned} \quad (3.77)$$

with

$$\hat{\theta}_{l,k_1\dots k_Z} = \mathbb{E}_\theta\left[\theta_l\prod_{j=1}^{Z}\Phi_{k_j}^{(j)}(\theta_j)\right] = \mathbb{E}_{\theta_l}\left[\theta_l\Phi_{k_l}^{(l)}(\theta_l)\right]\prod_{j=1,j\neq l}^{Z}\mathbb{E}_{\theta_j}\left[\Phi_{k_j}^{(j)}(\theta_j)\right].$$

Then we obtain the following polynomial chaos expansion

$$\begin{aligned} &\frac{d}{dt}\sum_{k_1,\dots,k_Z=0}^{M}\hat{v}_{i,k_1\dots k_Z}\prod_{j=1}^{Z}\Phi_{k_j}^{(j)}(\theta_j) = \\ &= \frac{1}{N}\sum_{h=1}^{N}\sum_{k_1,\dots,k_Z=0}^{M}\left[\left(\bar{p}-\frac{k_o}{\nu}\right)\hat{v}_{h,k_1\dots k_Z}-\left(\bar{p}+\frac{k_d}{\nu}\right)\hat{v}_{i,k_1\dots k_Z}\right]\prod_{j=1}^{Z}\Phi_{k_j}^{(j)}(\theta_j) \\ &\quad+\sum_{l=1}^{Z}\sum_{k_1,\dots,k_Z=0}^{M}\hat{\theta}_{l,k_1\dots k_Z}(t)\prod_{j=1}^{Z}\Phi_{k_j}^{(j)}(\theta_j). \end{aligned} \quad (3.78)$$

Multiplying by $\prod_{j=1}^{Z}\Phi_{k_j}^{(j)}(\theta_j)$ and integrating with respect to the distribution $\rho(\theta)$, we end up with

$$\begin{aligned} \frac{d}{dt}\hat{v}_{i,k_1\dots k_Z} = \frac{1}{N}\sum_{h=1}^{N}&\left[\left(\bar{p}-\frac{k_o}{\nu}\right)\hat{v}_{h,k_1\dots k_Z}-\left(\bar{p}+\frac{k_d}{\nu}\right)\hat{v}_{i,k_1\dots k_Z}\right]\\ &+\sum_{l=1}^{Z}\mathbb{E}_{\theta_l}\left[\theta_l\Phi_{k_l}^{(l)}(\theta_l)\right]\prod_{j=1,j\neq l}^{Z}\mathbb{E}_{\theta_l}\left[\Phi_{k_j}^{(j)}(\theta_j)\right]. \end{aligned}$$

For the numerical tests we approximate the integrals using quadrature rules.

Remark 12. *For model 3.64, where the control is noise-independent, as follows*

$$u_i = -\frac{1}{\nu}\left(k_d\mathbb{E}_\theta\left[v_i\right]+\frac{k_o}{N}\sum_{h\neq i}^{N}\mathbb{E}_\theta\left[v_h\right]+s\sum_{j=1}^{Z}\mathbb{E}_\theta\left[\theta_j\right]\right),$$

the gPC approximation turns out to be

$$\begin{aligned}\frac{d}{dt}\hat{v}_{i,k_1\dots k_Z} &= \frac{\bar{p}}{N}\sum_{h=1}^{N}\left(\hat{v}_{h,k_1\dots k_Z}-\hat{v}_{i,k_1\dots k_Z}\right)\\ &-\frac{\prod_{j=1}^{Z}\mathbb{E}_{\theta_j}\left[\Phi_{k_j}^{(j)}(\theta_j)\right]}{\prod_{j=1}^{Z}\mathbb{E}_{\theta_j}\left[\left(\Phi_{k_j}^{(j)}(\theta_j)\right)^2\right]}\left(k_d\hat{v}_{i,00\dots0}+\frac{k_o}{N}\sum_{h\neq i}^{N}k_o\hat{v}_{h,00\dots0}+s\sum_{j=1}^{Z}\mu_j\right)\\ &+\sum_{l=1}^{Z}\mathbb{E}_{\theta_l}\left[\theta_l\Phi_{k_l}^{(l)}(\theta_l)\right]\prod_{j=1,j\neq l}^{Z}\mathbb{E}_{\theta_j}\left[\Phi_{k_j}^{(j)}(\theta_j)\right].\end{aligned} \tag{3.79}$$

We recover the mean and the variance of the random variable $v(\theta)$ as

$$\begin{aligned}\mathbb{E}_\theta[v_i(\theta)] &= \int_{\mathbb{R}^2} v_i(\theta)d\rho = \hat{v}_{i,00\dots0},\\ \mathbb{V}_\theta[v_i(\theta)] &= \int_{\mathbb{R}^2}(v_i(\theta)-\hat{v}_{i,00\dots0})^2 d\rho = \sum_{k_1,\dots,k_Z=0}^{M}\hat{v}^2_{i,k_1\dots k_Z}-\hat{v}^2_{i,00\dots0}.\end{aligned}$$

3.4.2 Numerical tests

In this section we present different numerical tests on microscopic and mean-field dynamics, to compare the robustness of controls described in sections 3.2. We analyze one- and two-dimensional dynamics, for every test we consider the attractive case with $\bar{p}=1$. The initial distribution of particles v_0 is chosen such that consensus towards the target $\bar{v}=0$ would not be reached without control action. We implement the gPC approximations in (3.78) and (3.79) and we use the forward Euler scheme with fixed time step $\Delta t = 0.01$ to integrate the resulting differential equations until the final time $T=1$. We are taking into account a dynamics with $Z=2$ additive noises, a Gaussian noise θ_1 with density distribution $\rho_1 \sim \mathcal{N}(\mu,\sigma^2)$, and a uniform noise θ_2 with $\rho_2 \sim \mathcal{U}(a,b)$. This assumption of normal and uniform distributions for the stochastic parameter corresponds to the case of an Hermite and Legendre polynomial chaos expansions, respectively, as shown in Table 3.7. For every test we have $M=10$ terms of the gPC decomposition.

Test 1: one-dimensional consensus dynamics In the one-dimensional microscopic case we take $N=100$ agents, and a uniform initial distribution of particles, $v_0 \sim \mathcal{U}(10,20)$. Figure 3.16 shows means, as continuous and dashed lines, and confidence regions of the two noisy dynamics for different distributions ρ_1, ρ_2. The confidence region is computed as the region between the values

$$\frac{1}{N}\sum_{i=1}^{N}\left(\mathbb{E}_\theta[v_i(\theta)]\right) \mp \max_{i=1,\dots,N}\left(\sqrt{\mathbb{V}_\theta[v_i(\theta)]}\right).$$

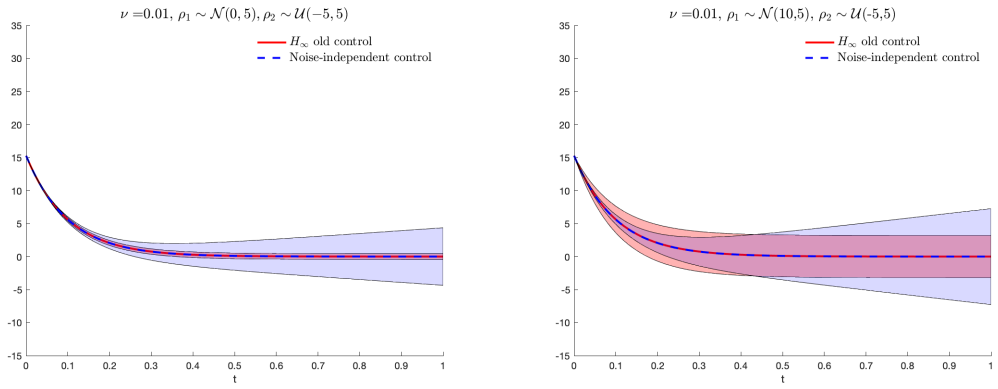

Figure 3.16: Test 1: comparison between the two controls in (3.62) and (3.83) applied to the noisy model, in terms of dynamics mean and variance for different ρ_1, ρ_2.

Numerical results show that both introduced controls are capable to drive the particles to a desired state even in case of a dynamic dependent by random inputs. Moreover we can observe that, with the $\mathcal{H}_\infty$ control, the variance of the noisy dynamics is stabilized over time, while in the case of a noise-independent control the variance keeps growing. This is due to the fact that the noise-independent control has information only on the mean of state and noise while the $\mathcal{H}_\infty$ feedback control directly depends on the state, and as a consequence on the noise of the dynamics.

Test 2: two-dimensional consensus dynamics In the two-dimensional microscopic case we take $N = 100$ agents, and an initial configuration of particles uniformly distributed on a 2D disc, as shown in Figure 3.17. 2D means and confidence regions of the two noisy dynamics can be seen in Figure 3.18, for different values of the penalization factor ν and different distributions $\rho_1,\ \rho_2$.

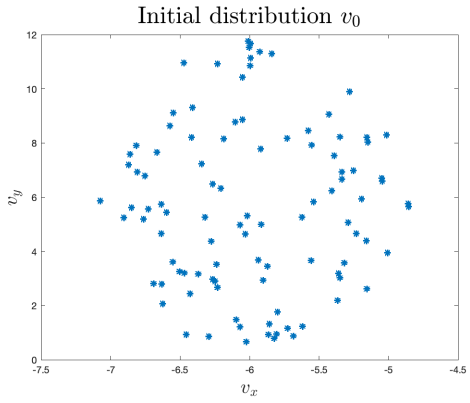

Figure 3.17: Test 2: Two-dimensional case. Initial distribution v_0.

We recall that, for the control u in Eq. (3.62), the size of the transfer function $\hat{G}$ related to the state-space system (3.65) in terms of the $\mathcal{H}_\infty$ signal norm is

$$\|\hat{G}\|_{\mathcal{H}_\infty} \leq \gamma.$$

From Theorem 3.2 we know that the $\mathcal{H}_\infty$ control u is robust with a constant $\gamma > \frac{1}{c_N}$, $c_N > 0$. We compute the value c_N for the two cases in Figure 3.18, and we have $c_N = 14.29$ for a penalization factor $\nu = 0.01$, while $c_N = 4.55$ for $\nu = 0.1$. As expected, we have more robustness for a smaller ν, interpreted as the control cost.

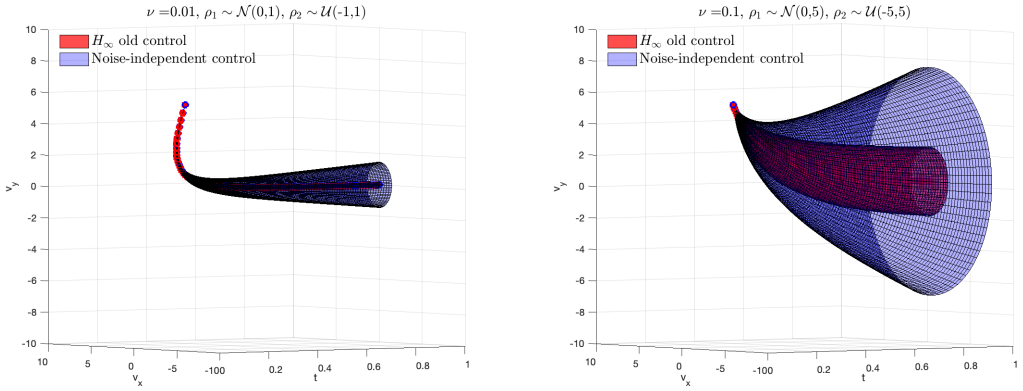

Figure 3.18: Two-dimensional case. Comparison between the two controls in (3.62) and (3.83) applied to the noisy model, in terms of dynamics mean and variance for different values of ν, ρ_1, ρ_2.

Test 3: mean-field consensus dynamics In the mean field limit, the Monte Carlo (MC) method is employed for the approximation of the distribution function $f(t, v, \theta)$ in the phase space whereas the random space at the particles level is approximated through the gPC technique.
Considering this MC-gPC scheme, we work on particles system thanks to Monte Carlo using a sample of $N_s = 10^4$ agents, then we consider the gPC scheme at the microscopic level and the density $f(t, v, \theta)$ is reconstructed as the histogram of $v(t, \theta)$. The reconstruction step of the mean density has been done with 50 gridpoints.
Mean and variance of the statistical quantity are computed as

$$\begin{aligned}
\mathbb{E}_\theta[f(t,v,\theta)] &= \int\int f(t,v,\theta) d\rho_1(\theta_1) d\rho_2(\theta_2) \\
&= \sum_{l,h=1}^{L} f(t,v,\theta^{lh}) \rho_1(\theta_1^l) \rho_2(\theta_2^h) \omega_1^l \omega_2^h, \\
\mathbb{V}_\theta[f(t,v,\theta)] &= \int\int f(t,v,\theta)^2 d\rho_1(\theta_1) d\rho_2(\theta_2) - \left(\mathbb{E}_\theta[f(t,v,\theta)]\right)^2 \\
&= \sum_{l,h=1}^{L} f(t,v,\theta^{lh})^2 \rho_1(\theta_1^l) \rho_2(\theta_2^h) \omega_1^l \omega_2^h - \left(\mathbb{E}_\theta[f(t,v,\theta)]\right)^2,
\end{aligned} \tag{3.80}$$

where for $l, h = 1, \dots, L$ and $\hat{v}_{k,j} \in \mathbb{R}^{N_s}$, $f(t, v, \theta^{lh})$ is computed as the histogram of

$$v(\theta^{lh}) = \sum_{k,j=0}^{M} \hat{v}_{k,j} \Phi_k(\theta_1^l) \Psi_j(\theta_2^h).$$

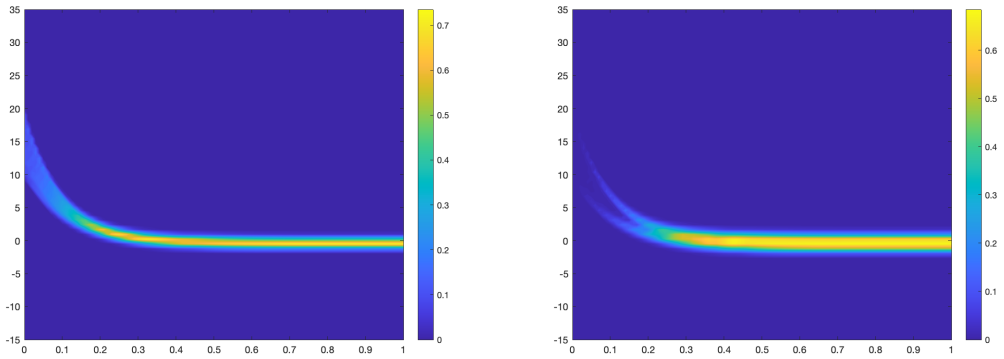

Figure 3.19: Meanfield one-dimensional case. Mean and standard deviation over time for the $\mathcal{H}_\infty$ control in (3.62), with parameters $\bar{p} = 1, \nu = 0.01, \rho_1 \sim \mathcal{N}(0,5), \rho_2 \sim \mathcal{U}(-5,5)$.

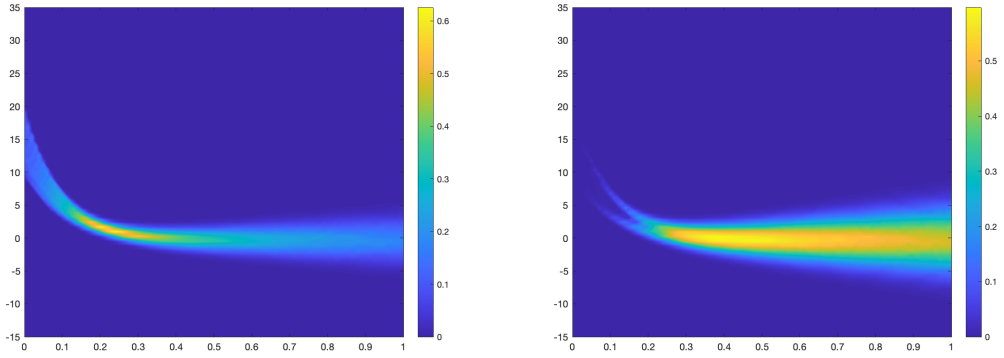

Figure 3.20: Meanfield one-dimensional case. Mean and standard deviation over time for the noise independent control in (3.83), with parameters $\bar{p} = 1, \nu = 0.01, \rho_1 \sim \mathcal{N}(0,5), \rho_2 \sim \mathcal{U}(-5,5)$.

We consider the same parameters as in the left plot of the one dimensional microscopic case in Figure 3.16, and since θ_1, θ_2 are a Gaussian and a uniform noise respectively, we approximate the integrals in (3.80) using a Gauss-Hermite and Legendre-Gauss quadrature rules with $L = 40$ quadrature points.
Figures 3.19 and 3.20 show the consistency with the microscopic case in Figure 3.16, on the left.

3.5 Conclusions

The introduction of uncertainties in multiagent systems is of paramount importance for description of realistic phenomena. We concentrated in this chapter with the mathematical modelling and control of collective dynamics with uncertainties and we investigated the robustness of controls proposing estimates based on $\mathcal{H}_\infty$ theory. We reformulated the control problem as a robust $\mathcal{H}_\infty$ control problem, and we derived sufficient conditions

in terms of linear matrix inequalities (LMIs) to ensure the control performance. We did the robustness analysis also in a meanfield framework obtaining a consistent result with the microscopic scale. Some numerical tests were proposed to compare the $\mathcal{H}_\infty$ control with another control found minimizing the expectation of a functional with respect to the noise. The numerical methods here developed makes use of the generalized polynomial chaos (gPC) expansion for the microscopic dynamics while in the mean-field case we combine a gPC expansion in the random space with a Monte Carlo method in the physical variables. Both controls are capable to drive the particles to a desired state even in case of a dynamic dependent by random inputs, but we generically observed that only the $\mathcal{H}_\infty$ control, is able to stabilize over time the variance of the noisy dynamics.

3.6 Appendix A. Noise-independent control

In this section we look for a new control, minimizing the expectation of the cost functional (3.58) subject to the noisy model (3.57). Hence, we consider the expected value of the quadratic cost

$$\bar{u}^*(\cdot) = \arg\min_{u(\cdot)} \mathbb{E}\left[\int_0^T \frac{1}{2}(v^\top Q v + \nu u^\top R u)\, dt\right],$$

where we introduce the matrices $Q = R = \frac{1}{N}\mathrm{Id}_N$. We claim that in this case an optimal feedback control is obtained as follows

$$\bar{u}(t) = -\frac{N}{\nu}\Big(K\ \mathbb{E}_\theta[v] + S\ \mathbb{E}_\theta[\theta]\Big), \tag{3.81}$$

where $K \in \mathbb{R}^{N\times N}$ and $S \in \mathbb{R}^{N\times Z}$ fulfill the Riccati matrix-equations

$$\begin{cases} -\dot{K} = KA + A^\top K - \frac{N}{\nu}K^2 + \frac{1}{N}I_N, \quad K(T) = 0_N, \\ \\ -\dot{S} = KB + A^\top S - \frac{N}{\nu}KS, \quad S(T) = 0_{N\times M}. \end{cases} \tag{3.82}$$

Theorem 3.3. *Assume matrices K and S have the following structures*

$$(K)_{ij} = \begin{cases} k_d, & i = j, \\ k_o, & i \neq j, \end{cases} \qquad (S)_{ij} = s \cdot \mathbb{1}_{N\times Z}.$$

Matrices K and S are denfined by 2 and 1 element respectively.
Then the $i-th$ component of the control u is given by

$$u_i = -\frac{1}{\nu}\left(k_d\mathbb{E}[v_i] + \frac{k_o}{N}\sum_{j\neq i}^{N}\mathbb{E}[v_j] + s\sum_{j=1}^{Z}\mathbb{E}[\theta_j]\right), \tag{3.83}$$

where k_d and k_o, after a scaling, turn out to be the same as in equations (3.61)*, while s satisfies*

$$-\dot{s} = k_d + \alpha(N)k_o - \frac{s}{\nu}\left(k_d + \alpha(N)k_o\right), \qquad s(T) = 0, \tag{3.84}$$

with $\alpha(N) = \frac{N-1}{N}$.

Proof. From Proposition 2.1 of (12), we can prove that k_d, k_o satisfy equations (3.61). Given the structure of the matrices S, K and B, and solving the second equation in (3.82) componentwise leads to the following identities:

$$\begin{aligned}(KB)_{ij} &= k_d + (N-1)k_o,\\ (A^\top S)_{ij} &= s\left(a_d + (N-1)a_o\right),\\ (KS)_{ij} &= s\left(k_d + (N-1)k_o\right).\end{aligned}$$

We can further simplify the Riccati-matrix system (3.82) using the dependency of coefficients a_d, a_o. And since we are interested in the dynamics for large number of agents, we introduce the following scalings

$$s \leftarrow Ns, \quad k_d \leftarrow Nk_d, \quad k_o \leftarrow N^2 k_o, \quad \alpha(N) = \frac{N-1}{N}. \tag{3.85}$$

For the sake of simplicity, we keep the same notation also for the scaled variables s, k_d, k_o. Under this scaling, the second equation in (3.82) reads

$$-\dot{s} = k_d + \alpha(N)k_o - \frac{s}{\nu}\left(k_d + \alpha(N)k_o\right), \qquad s(T) = 0\,,$$

and the Riccati feedback law (3.81) is given by Eq. (3.83) The coefficients $s(t), k_d(t), k_o(t)$, have to be determined integrating backwards in time. □

Remark 13. *Since the $\mathcal{H}_\infty$ theory is based on the infinite horizone case,* (3.84) *reduces to*

$$0 = k_d + \alpha(N)k_o - \frac{s}{\nu}\left(k_d + \alpha(N)k_o\right),$$

hence $s = \nu$.

3.7 Appendix B. $\mathcal{H}_\infty$ control setting

Define a state-space system $G : L^2 \to L^2$ by $y = G\theta$, with θ a random input as defined in (3.75), if

$$\begin{aligned}\frac{d}{dt}v(t) &= \widetilde{A}v(t) + \widetilde{B}\theta,\\ y(t) &= Cv(t) + D\theta,\end{aligned}$$

where $v(t)$ is the system state, and $y(t)$ is the observed output. It is proved (see e.g. (85, 41)) that for any stable state-space system, G, there exists a frequency transfer function $\hat{G} \in R\mathcal{H}_\infty$ such that

$$\hat{G}(s) = \left[\begin{array}{c|c}\widetilde{A} & \widetilde{B}\\ \hline C & D\end{array}\right] = D + C(sI_N - \widetilde{A})^{-1}\widetilde{B}. \tag{3.86}$$

where s is a complex number and $R\mathcal{H}_\infty$ is the set of proper rational functions with no poles in the closed right half-plane, in particular $R\mathcal{H}_\infty = R \cap \mathcal{H}_\infty$, where R is the

space of rational functions and $\mathcal{H}_\infty$ is a signal space of "transfer functions" for linear time-invariant systems, we refer to (41, 83, 99) for the theoretical details .
State space $\widetilde{A}, \widetilde{B}, C, D$ or the transfer function is a representation of a system and these formats uses matrices or complex-valued functions (a signal) to parameterize the representation. The signal norm $\|\cdot\|_{\mathcal{H}_\infty}$ measures the size of the transfer function in a certain sense and the $\mathcal{H}_\infty$-optimal control problem consists of finding a stabilizing controller $u = Ky$ which minimizes the cost function

$$\|\hat{G}\|_{\mathcal{H}_\infty} = \operatorname{ess\,sup}_{\omega\in\mathbb{R}} \bar{\sigma}(\hat{G}(i\omega)).$$

The direct minimization of the cost $\|\hat{G}\|_{\mathcal{H}_\infty}$ turns out to be a very hard problem, and it is therefore not feasible to tackle it directly. Instead, it is much easier to construct conditions which state whether there exists a stabilizing controller which achieves the norm bound

$$\|\hat{G}\|_{\mathcal{H}_\infty} \leq \gamma,$$

for a given $\gamma > 0$.
We want now to reduce a problem arising in system and control theory to a standard linear matrix inequalities.
The history of LMIs in the analysis of dynamical systems goes back more than 100 years. The story begins in about 1890, when Lyapunov published his seminal work introducing what we now call Lyapunov theory. Then, in the 1940's Lur'e, Postnikov, and others in the Soviet Union applied Lyapunov's methods to some specific practical problems in control engineering. The next major breakthrough came in the early 1960's, when Yakubovich, Popov, Kalman, and other researchers succeeded in reducing the solution of the LMIs that arose in the problem of Lur'e to simple graphical criteria, using what we now call the positive-real (PR) lemma, that shows how LMIs can be used to constrain the eigenvalues of a system:

Lemma 3.4. *Given the frequency transfer function $\hat{G}$, the following are equivalent:*

- $\|\hat{G}\|_{\mathcal{H}_\infty} \leq \gamma$.
- $\exists$ *a positive definite square matrix of order N, $X > 0$ s.t.* (3.87) *holds.*

$$\begin{bmatrix} \widetilde{A}^\top X + X\widetilde{A} & X\widetilde{B} \\ \widetilde{B}^\top X & -\gamma I_Z \end{bmatrix} + \frac{1}{\gamma} \begin{bmatrix} C^\top \\ D^\top \end{bmatrix} \begin{bmatrix} C & D \end{bmatrix} < 0. \tag{3.87}$$

By 1970, it was known that the LMI appearing in the PR lemma could be solved not only by graphical means, but also by solving a certain algebraic Riccati equation (ARE). In a 1971 paper ((152)) on quadratic optimal control, J. C. Willems is led to the following Lemma with equivalent characterization through a Riccati equation

Lemma 3.5. *The following are equivalent:*

- $\exists X > 0$ *s.t.* (3.87) *holds.*

- $\exists X > 0$ *s.t.* (3.88) *holds.*

$$\widetilde{A}^\top X + X\widetilde{A} - (X\widetilde{B} + C^\top D)(-\gamma I_Z + \frac{1}{\gamma} D^\top D)^{-1}(\widetilde{B}^\top X + D^\top C) + \frac{1}{\gamma} C^\top C = 0. \quad (3.88)$$

Proof. The structure of of Eq. (3.87) is

$$\begin{bmatrix} \hat{A} & \hat{B} \\ \hat{B}^\top & \hat{D} \end{bmatrix} \begin{bmatrix} x_1 \\ x_2 \end{bmatrix} = \begin{bmatrix} 0 \\ 0 \end{bmatrix},$$

this system can be solved using the Schur-complement theory. Provided that $\widehat{D}^{-1}$ exists, we have

$$\begin{cases} \hat{A}x_1 + \hat{B}x_2 = 0, \\ \hat{B}^\top x_1 + \hat{D}x_2 = 0, \end{cases}$$

$$\rightarrow \quad x_2 = -\hat{D}^{-1}\hat{B}^\top x_1 \quad \rightarrow \quad \left(\hat{A} - \hat{B}\hat{D}^{-1}\hat{B}^\top\right) x_1 = 0.$$

Hence, provided that exixts X such that (3.88) has a solution, then for all ξ

$$\xi^\top \left(\widetilde{A}^\top X + X\widetilde{A} - (X\widetilde{B} + C^\top D)(-\gamma I_Z + \frac{1}{\gamma} D^\top D)^{-1}(\widetilde{B}^\top X + D^\top C) + \frac{1}{\gamma} C^\top C \right) \xi = 0.$$

Further, (3.88) is the Schur-complement of

$$M_{sc} := \begin{bmatrix} \widetilde{A}^\top X + X\widetilde{A} + \frac{1}{\gamma} C^\top C & \widetilde{B}^\top X + D^\top C \\ X\widetilde{B} + C^\top D & \frac{1}{\gamma} D^\top D - \gamma I_Z \end{bmatrix}.$$

Hence for $\eta = -\hat{D}\hat{B}^\top \xi$ and $\forall \xi$, we have that

$$\begin{bmatrix} \xi & \eta \end{bmatrix} M_{sc} \begin{bmatrix} \xi \\ \eta \end{bmatrix} = 0.$$

For a general vector $\begin{bmatrix} \xi & \varrho \end{bmatrix}^\top$, we compute

$$\begin{bmatrix} \xi \\ \varrho \end{bmatrix} = \begin{bmatrix} \xi \\ \eta \end{bmatrix} + \begin{bmatrix} 0 \\ \varrho - \eta \end{bmatrix},$$

and then

$$\begin{bmatrix} \xi & \varrho \end{bmatrix} M_{sc} \begin{bmatrix} \xi \\ \varrho \end{bmatrix} = 0 + \begin{bmatrix} 0 & \varrho - \eta \end{bmatrix} M_{sc} \begin{bmatrix} 0 \\ \varrho - \eta \end{bmatrix} = \begin{bmatrix} \varrho - \eta \end{bmatrix}^\top \left[\tfrac{1}{\gamma} D^\top D - \gamma I_Z \right] \begin{bmatrix} \varrho - \eta \end{bmatrix} < 0$$

for γ sufficiently large. □

4 Proximal gradient approaches for optimal control of interacting agent systems

4.1 Introduction

This chapter addresses control problems for second-order, nonlinear, multi-agent systems. In such dynamics, the state of each agent is characterised by position and velocity, and these agents interact according to a nonlinear model that can encode various social rules as for example attraction, repulsion and alignment. From a mathematical point of view, a description of self-organized models is provided by complex system theory, where the overall dynamic is depicted by an ODEs system, and the control is given by the minimization of a cost functional. In this context, we focus on the design of control laws enforcing consensus emergence, we understand consensus as a travelling formation in which every agent has the same velocity. We show the use of such control strategy in the case of the Cucker-Smale model (71, 24).

In optimal control for multiagent systems, the question of a more parsimonious control design remains open. Efficient controls strategies should target only few individuals of the population, instead of wasting resources on the entire group at once. Taking advantage of the mutual dependencies between the agents, they could use an effect that would spread their influence to the whole system, thus indirectly controlling the rest of agents. The property of control strategies to target only a small fraction of the total population is known in the mathematical literature as sparsity (48, 82, 56, 59). For example, in alignment models, the sparse control targeting at each instant only the agent farthest away from the mean velocity was shown to possess this property, see (51). As an extension of the proposed classical control, we address the finite horizon optimal control problem with a non-smooth, sparsity-promoting control penalisation, the sparse control can indeed be obtained when the control cost is the ℓ_1-norm (51). This control synthesis is sparse, acting on a few agents over a finite time frame, however its numerical realisation is far more demanding due to the lack of smoothness in the cost functional. To circumvent this difficulty, we propose a numerical realisation of the control synthesis via proximal gradient method (31).

Since the study of microscopic model for a large system of individuals implies a considerable effort in numerical simulations, to reduce the computational complexity we consider also a more general level of description, that is the derivation of a mesoscopic approximation of the original dynamic. Hence we will consider continuous models in order to simulate the collective behaviour in case of analysing systems with a large number of agents. A numerical section will end the chapter, with tests on sparse control at microscopic and meanfield level, a CPU time analysis of the proposed algorithm, and finally a comparison between the sparse control and another type of sparsity realised using a leader-follower model.

4.2 Constrained interacting agents systems

We consider a set of N agents with states $(x_i(t), v_i(t)) \in \mathbb{R}^d \times \mathbb{R}^d$, where d is the dimension of the physical space, interacting under the second-order dynamics

$$\begin{aligned} \frac{\mathrm{d}x_i}{\mathrm{d}t} &= v_i, \quad i = 1, 2, \ldots, N \\ \frac{\mathrm{d}v_i}{\mathrm{d}t} &= \frac{1}{N} \sum_{j=1}^{N} P(x_i, x_j)(v_j - v_i) + u_i, \quad i = 1, 2, \ldots, N \end{aligned} \tag{4.89}$$

with initial conditions $x_i(0) = x_i^0$ and $v_i(0) = v_i^0$. $P(x_i, x_j) = P(\|x_i - x_j\|_2)$ is a radial interaction kernel that describes binary symmetric interactions between particles.
Now, suppose we have an interest in having the N particles composing our system to reach a certain state. The control is determined as the external forcing term $u(t) := (u_1(t), u_2(t), \ldots, u_N(t))^T$ whose components are

$$u_i : \mathbb{R}_+ \to U$$

with U compact subset of $\mathbb{R}^d$. In order to synthesize this control variable, we assume that u is the minimizer of a cost function $\mathcal{J}(u; x(0), v(0))$, that is

$$u^* = \arg\min_{u \in C} \mathcal{J}(u; x^0, v^0) := \int_0^T \ell(x(t), v(t), u(t))\, dt\,, \qquad \text{subject to (4.89)}\,. \tag{4.90}$$

The optimization horizon T expresses the time scale along which we minimize the running cost $\ell(x, v, u)$, encodes our objective as a function of the state and control variables. C is a nonempty closed and convex set. And in our case we take $C = [-M, M]^{N \times d},\ M \in \mathbb{R}^+$, i.e. for every agent i and component j we want $|u_{ij}| \leq M$.
In this context, we focus on the design of control laws enforcing consensus emergence, we are interested in having the particles composing our system to reach a consensus state, which is the state where all particles have the same velocity

$$\bar{v} := \frac{1}{N} \sum_{j=1}^{N} v_j.$$

The minimizing functional we considered is

$$\mathcal{J}(u; v^0) := \int_0^T \frac{1}{N} \sum_{i=1}^{N} \left(\|\bar{v} - v_i\|_2^2 + \nu \|u_i\|_2^2 + \beta \|u_i\|_1 \right) \mathrm{d}t, \tag{4.91}$$

where the scalars ν, β are weights representing how much expensive is the control. As you can see in Eq. (4.91), the consensus is penalised along a quadratic control and a non-smooth, sparsity-promoting term. In this way we address the problem of enforcing sparsity on an optimal consensus strategy, by adding the ℓ_1-norm $\|\cdot\|_1$ in the minimisation problem, as done in (11, 35, 50, 124). While existence of a minimiser u^* of (4.90) follows from the smoothness and convexity properties of the system dynamics and the cost, the Pontryagin Minimum Principle Pontryagin et al. (1962) yields first-order necessary conditions for the optimal control. However, the choice of a non-differentiable control

cost, gives raise to the non-smooth cost functional $\mathcal{J}$ of Eq. (4.91), for this reason we must resort to subdifferntial theory (31).
In order to find u, we start exploiting the Pontryagin maximum principle. For the sake of simplicity, in the following computations we consider $M = +\infty$, hence we don't have to take into account the projection of the control u inside the set C. To begin with, let $(p_i(t), q_i(t)) \in \mathbb{R}^d \times \mathbb{R}^d$ be adjoint variables associated to (x_i, v_i) and consider the Hamiltonian

$$\begin{aligned}\mathcal{H}(x, v, u, p, q) :=& \frac{1}{N}\sum_{i=1}^{N}\left(\|\bar{v} - v_i\|_2^2 + \nu\|u_i\|_2^2 + \beta\|u_i\|_1\right) + \frac{1}{N}\sum_{i=1}^{N}\langle p_i, v_i\rangle \\ &+ \frac{1}{N}\sum_{i=1}^{N}\langle q_i, \frac{1}{N}\sum_{j=1}^{N}P(x_i, x_j)(v_j - v_i) + u_i\rangle.\end{aligned} \tag{4.92}$$

We can compute the following adjoint equations, componentwise for every $i \in \{1, 2, \dots, N\}$

$$\begin{aligned}-\dot{p}_i &= \nabla_{x_i}\mathcal{H} = \frac{1}{N}\sum_{j=1}^{N}P'(\|x_i - x_j\|_2)\langle q_j - q_i, v_j - v_i\rangle(x_j - x_i), \\ -\dot{q}_i &= \nabla_{v_i}\mathcal{H} = p_i + \frac{1}{N}\sum_{j=1}^{N}P(\|x_i - x_j\|_2)(q_j - q_i) - 2(v_i - \bar{v}),\end{aligned} \tag{4.93}$$

with final conditions $p_i(T) = 0$ and $q_i(T) = 0$. We now need to compute $\nabla_{u_i}\mathcal{H}$ in order to find the optimality conditions

$$0 = \nabla_{u_i}\mathcal{H} = -q_i + 2\nu u_i + \beta\mathcal{D}(\|\cdot\|_1)(u_i), \tag{4.94}$$

since the ℓ_1-norm is non differentiable in zero, we have to look for the subdifferential $\mathcal{D}$, computed at zero, of the ℓ_1-norm.
The subdifferential of $\|u\|_1$ for agent i and component j in (4.94) turns out to be

$$\Big(\mathcal{D}(\|\cdot\|_1)(u_i)\Big)_j = \begin{cases}-1 & \text{if } u_{ij} < 0, \\ [-1, 1] & \text{if } u_{ij} = 0, \\ 1 & \text{if } u_{ij} > 0,\end{cases} \tag{4.95}$$

with $j = 1, \dots, d$, and $i = 1, \dots, N$. We prove this result with the following Lemma 4.1.

Lemma 4.1 (Subdifferential of ℓ_1-norm at 0)**.** *Given $\|\cdot\|_1 : \mathbb{R}^d \to \mathbb{R}$ the ℓ_1-norm on $\mathbb{R}^d$, the subdifferential of $\|\cdot\|_1$ at 0 is the dual norm unit ball*

$$\mathcal{D}(\|\cdot\|_1)(0) = \mathbf{B}_{\|\cdot\|_\infty}[0, 1].$$

Proof. By definition of subdifferential we have

$$\mathcal{D}(\|\cdot\|_1)(0) \equiv \{g \in \mathbb{R}^d : \|y\|_1 \geq \langle g, y - 0\rangle \text{ for all } y \in \mathbb{R}^d\}.$$

The latter holds true if and only if $\|g\|_\infty \leq 1$. Indeed, if $\|g\|_\infty \leq 1$, then by the generalized Cauchy-Schwarz inequality

$$\langle g, y\rangle \leq \|g\|_\infty \|y\|_1 \leq \|y\|_1 \quad \text{for any } y \in \mathbb{R}^d,$$

implying

$$\|y\|_1 \geq \langle g, y\rangle \quad \text{for all } y \in \mathbb{R}^d. \tag{4.96}$$

In the reverse direction, assume that (4.96) holds. Taking the maximum of both sides of (4.96) over all y satisfying $\|y\|_1 \leq 1$, we get

$$\|g\|_\infty = \max_{y:\|y\|_1\leq 1} \langle g, y\rangle \leq \max_{y:\|y\|_1\leq 1} \|y\|_1 = 1.$$

We have thus proved that the subdifferential of the ℓ_1-norm at zero is the dual norm unit ball

$$\mathcal{D}(\|\cdot\|_1)(0) = \mathbf{B}_{\|\cdot\|_\infty}[0,1] = \{g \in \mathbb{R}^d : \|g\|_\infty \geq 1\rangle = [-1,1]^d.$$

In particular, when $d = 1$, then $\|\cdot\|_1 = |\cdot|$, and we have $\mathcal{D}(|\cdot|)(0) = [-1,1]$. □

Remark 14 (Graphic representation in one dimensional case)**.** *Take into account a one dimensional physical space $d = 1$, we can minimize componentwise the Hamiltonian $\mathcal{H}$ in* (4.92) *with respect to u, and this corresponds to finding the minimum of the sum of the two functions*

$$y(u) = \nu u^2 - qu, \qquad z(u) = \beta\,|u|\,.$$

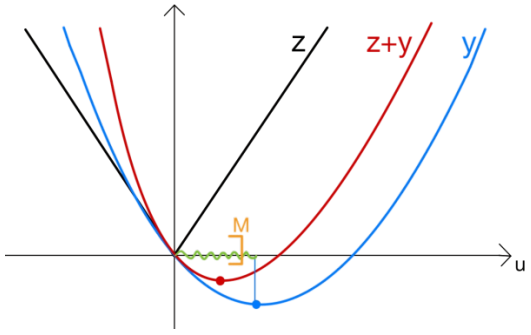

Figure 4.21: Graphic representation of y, z and $y + z$ in function of u for a positive Lagrange multiplier q.

In Figure 4.21, we depict the functions y, z and the sum $z + y$ in the case of a positive Lagrange multiplier q, for $q < 0$ we have the symmetric case. Depending on the different values of the parameters ν, β, q the minimum u^* will be a value between 0 and the the vertex of the parabola $y(u)$, but taking into account the projection over the set C, i.e., $|u^*| < M$.
In particular, computing $(z + y)'(u) = 0$, we can find a componentwise relation between the optimal control u^* and the Lagrange multiplier q^*

$$u^* = \begin{cases} \frac{q^*-\beta}{2\nu} & \text{if } u > 0 \text{ and } q^* > \beta, \\ \frac{q^*+\beta}{2\nu} & \text{if } u < 0 \text{ and } q^* < -\beta, \\ 0 & \text{if } u = 0 \text{ and } |q^*| \leq \beta. \end{cases}$$

4.2.1 A multi-population interacting system

We can consider a more general framework than system (4.89), in particular suppose we are dealing with a N-particles swarm whose positions are $x_1, x_2, \ldots, x_N$ and velocities are $v_1, v_2, \ldots, v_N$, with $x_i, v_i \in \mathbb{R}^d$, $i = 1, 2, \ldots, N$. Suppose further that we can control only $N_J < N$ agents, say those whose indexes are collected in the set J. Then we consider a collection of sets of indexes I_k, $k = 1, \ldots, K$, and every set corresponds to a population with N_{I_k} agents that interact according a particular interaction rule, that can be different for every set. For $i = 1, 2, \ldots, N$, and initial conditions

$$x_i(0) = x_i^0, \qquad v_i(0) = v_i^0,$$

the dynamic ruling this system of particles takes the form

$$\begin{aligned} \frac{\mathrm{d}x_i}{\mathrm{d}t} &= v_i, \\ \frac{\mathrm{d}v_i}{\mathrm{d}t} &= \sum_{j \in I_k,\ j=1}^{N_{I_k}} m_j P_k(x_i, x_j)(v_j - v_i) + \sum_{j \in J,\ j=1}^{N_J} m_j Q(x_i, x_j)(v_j - v_i) + \chi_J(i) u_i, \end{aligned} \tag{4.97}$$

where Q and P_k are some interaction kernels and, for any given set of indexes A, the function $\chi_A(i)$ returns 1 if $i \in A$, 0 otherwise. The scalars m_j instead, are weights such that $m_1 + m_2 + \ldots + m_N = 1$ and $m_j \geq 0$.

Example 1 (Leader-Follower model)**.** *As an example of Eq.* (4.97) *we look at a leader-follower model with*

$$P(x_i, x_j) = P(\|x_i - x_j\|_2) := \frac{1}{(1 + \|x_i - x_j\|_2^2)^\gamma}, \quad \gamma \geq 0. \tag{4.98}$$

For simplicity we consider $Q = P_k = P$, hence only two different populations, a set J of leader that we can control, and a set I of follower that have to reach the consensus

$$\bar{v} := \sum_{j=1}^{N} \frac{\chi_I(j)}{|I|} v_j$$

where $|I|$ is the number of indexes belonging to the set I. Notice that in this case the sets of indexes I and J have empty intersection and $|I| + |J| = N$.
We enforce consensus by means of the following functional

$$\mathcal{J}(u; v^0) := \int_0^T \sum_{i=1}^{N} \Big(\chi_I(i) \|\bar{v} - v_i\|_2^2 + \chi_J(i) \left(\nu_i \|u_i\|_2^2 + \beta_i \|u_i\|_1 \right) \Big) \mathrm{d}t,$$

where the scalars ν_i represent how expensive it is to control the i-th particle, if that is controllable. The adjoint equations for this case turn out to be

$$-\dot{p}_i = (\nabla_x \mathcal{H})_i = -\sum_{j=1}^{N} \langle q_i m_j - q_j m_i, v_i - v_j \rangle P'(x_i, x_j)(x_i - x_j)$$

$$-\dot{q}_i = (\nabla_v \mathcal{H})_i = p_i + \sum_{j=1}^{N} (q_j m_i - q_i m_j) P(x_i, x_j) - 2\chi_I(i)(v_i - \bar{v})$$

$$0 = (\nabla_u \mathcal{H})_i = -q_i \chi_J(i) + \chi_J(i) \left(2\nu_i u_i + \beta_i \mathcal{D}(\|\cdot\|_1)(u_i)\right).$$

The last set of equalities gives an explicit definition of our desired control u*, with* $\mathcal{D}(\|\cdot\|_1)(u_i)$ *as in Eq.* (4.95).
Clearly, the functions $p(t) = (p_1(t), p_2(t), \ldots, p_N(t))$ *and* $q(t) = (q_1(t), q_2(t), \ldots, q_N(t))$ *are to be determined first. It is evident that performing this optimization process is computationally very demanding. This paper also aim to deal with this in the numerical realisation of the models.*

4.3 Proximal gradient method

Since usually a controller act differently on every agent at every instant, we asked for a more parsimonious control design and we address the finite horizon control problem with a non-smooth, sparsity-promoting control penalisation. As shown in the previous section, this choice gives rise to a non-smooth cost functional $\mathcal{J}$, for which gradient-based numerical solvers are not directly suitable. To circumvent the non-smoothness of $\mathcal{J}$, we consider the class of iterative proximal gradient algorithms, which can be viewed as an extension of the classical gradient method.
Consider the minimization problem of the function F:

$$\min_{u \in C} \{F(u) \equiv h_1(u) + h_2(u)\}, \tag{4.99}$$

wheree $C = [-M, M]^{N \times d}$, and h_2 is a possibly nonsmooth function. For the model in Section 4.2, we have $F : \mathbb{R}^{N \times d} \to \mathbb{R}$ with

$$h_1(u) = \int_0^T \frac{1}{N} \sum_{i=1}^{N} \left(\nu \|u_i\|_2^2 - q_i u_i\right) \mathrm{d}t, \qquad h_2(u) = \int_0^T \frac{1}{N} \sum_{i=1}^{N} \beta \|u_i\|_1 \, \mathrm{d}t.$$

A method for numerically solving the minimization problem (4.99) is the projected sub-gradient algorithm which generates a sequence $\{u^{(k)}\}$ via

$$u^{(0)} \in \mathbb{R}^{N \times d}, \quad u^{(k)} = P_C \left(u^{(k-1)} - \alpha_k \nabla F(u^{(k-1)})\right),$$

where $\alpha_k > 0$ is a suitable stepsize. This gradient iteration can be viewed as a proximal regularization of the linearized function h_1 at $u^{(k-1)}$

$$u_k = \arg\min_{u \in C} \left\{ h_1(u^{(k-1)}) + \langle u - u^{(k-1)}, \nabla h_1(u^{(k-1)}) \rangle + \frac{1}{2\alpha_k} \left\|u - u^{(k-1)}\right\|_2^2 + \beta \|u\|_1 \right\},$$

we compute some simple algebraic manipulation and cancellation of constant terms

$$\begin{aligned}
&h_1(u^{(k-1)}) + \langle u - u^{(k-1)}, \nabla h_1(u^{(k-1)})\rangle + \frac{1}{2\alpha_k}\left\|u - u^{(k-1)}\right\|_2^2 \\
&= h_1(u^{(k-1)}) + \langle u, \nabla h_1(u^{(k-1)})\rangle - \langle u^{(k-1)}, \nabla h_1(u^{(k-1)})\rangle + \frac{1}{2\alpha_k}\langle u, u\rangle + \\
&\qquad - \frac{1}{\alpha_k}\langle u, u^{(k-1)}\rangle + \frac{1}{2\alpha_k}\langle u^{(k-1)}, u^{(k-1)}\rangle \\
&= \frac{1}{2\alpha_k}\langle u, u\rangle - \frac{1}{\alpha_k}\langle u, u^{(k-1)}\rangle + \langle u, \nabla h_1(u^{(k-1)})\rangle + \frac{1}{2\alpha_k}\langle u^{(k-1)}, u^{(k-1)}\rangle + \\
&\qquad - \langle u^{(k-1)}, \nabla h_1(u^{(k-1)})\rangle + \frac{\alpha_k}{2}\langle \nabla h_1(u^{(k-1)}), \nabla h_1(u^{(k-1)})\rangle,
\end{aligned}$$

and we obtain

$$u_k = \arg\min_{u\in C}\left\{\frac{1}{2\alpha_k}\left\|u - \left(u^{(k-1)} - \alpha_k \nabla h_1(u^{(k-1)})\right)\right\|_2^2 + \beta\left\|u\right\|_1\right\}. \tag{4.100}$$

We recall the definition of proximal operator

Definition 4.1 (proximal mapping)**.** *Given a function $f : \mathbb{A} \to \mathbb{B}$, the proximal mapping of f is the operator given by*

$$prox_f(x) = \arg\min_{y\in\mathbb{A}}\left\{\frac{1}{2}\left\|y - x\right\|_2^2 + f(y)\right\} \quad for\ any\ x \in \mathbb{A},$$

the proximal mapping takes a vector $x \in \mathbb{A}$ and maps it into a subset of $\mathbb{B}$ of $\mathbb{A}$, which might be empty, a singleton, or a set with multiple vectors.

Multiplying (4.100) by α_k and using definition 4.1, we obtain

$$u_k = \mathrm{prox}_{\beta\alpha_k\|u\|_1}\left(u^{(k-1)} - \alpha_k\nabla h_1(u^{(k-1)})\right).$$

In order to underline the dependence on parameters α_k, β, and M we identify the notations $\mathrm{prox}_{\beta\alpha_k,M} \equiv \mathrm{prox}_{\beta\alpha_k\|u\|_1}$. This method is known as the *proximal gradient method* (31), and it consists of a gradient step followed by a proximal mapping, where numerically we have

$$\mathrm{prox}_{a,b} : \mathbb{R}^{N\times d} \to \mathbb{R}^{N\times d}, \qquad (\mathrm{prox}_{a,b}(\mathbf{x}))_{ij} = \min\{\max\{|x_{ij}| - a, 0\}, b\}\mathrm{sgn}(x_{ij}).$$

This particular proximal map is called the iterative shrinkage-thresholding algorithm (ISTA) in the literature, since at each iteration a soft-thresholding operation (also known as "shrinkage") is performed.
The gradient iteriation is presented in Algorithm 3. After having chosen an initial guess, each iteration consists in the integration of the forward-backward optimality system given by the differential equations (4.89) and (4.93), followed by a step of the proximal gradient method. In the numerical tests we will chose the step α_k as in the Barzilai-Borwein method (see (29))

$$\alpha_k = \frac{\langle u^{(k)} - u^{(k-1)}, \nabla h_1(u^{(k)}) - \nabla h_1(u^{(k-1)})\rangle}{\|\nabla h_1(u^{(k)}) - \nabla h_1(u^{(k-1)})\|_2^2}, \tag{4.101}$$

where

$$\nabla h_1(u^{(k-1)}) = -q^{(k-1)} + 2\nu u^{(k-1)}. \tag{4.102}$$

Algorithm 3 [Proximal Gradient Descent]

0. Set $tol > 0$, $k_{\max}$, $u^{(0)}$, $u^{(-1)}$ and $k = 0$
while $\left\|\nabla h_1(u^{(k)})\right\|_2 > tol$ & $k < k_{\max}$ **do**
i. Obtain $(x^{(k)}, v^{(k)})$ from (4.89) with $u^{(k)}$
ii. Obtain $(p^{(k)}, q^{(k)})$ from (4.93) with $(x^{(k)}, v^{(k)})$
iii. Evaluate the gradient $\nabla h_1(u^{(k)})$ as in (4.102)
iv. Compute the step α_k as in (4.101)
v. Update $u^{(k+1)} = \text{prox}_{\beta\alpha_k, M}\Big(u^{(k)} - \alpha_k \nabla h_1(u^{(k)})\Big)$
vi. $k := k + 1$
end while

4.3.1 Asymptotic Monte Carlo algorithm

We present now a mean-field modelling approach for the control problem when the number of agents is sufficiently large. We start taking into account the continuous control problem that results in the limit of the discrete problem from Section 4.2 as $N \to \infty$. Formally, the second order dynamics (4.89) can be written as a Vlasov-type transport equation

$$\partial_t f + v \cdot \nabla_x f = -\nabla_v \cdot \left[f \left(\mathcal{P}[f] + u \right) \right], \qquad f(0, x, v) = f^0(x, v), \tag{4.103}$$

where $\mathcal{P}[f]$ denotes the nonlocal integral operator

$$\mathcal{P}[f](t, x, v) = \int_{\mathbb{R}^{2d}} P(x, x_*)(v_* - v) f(t, x_*, v_*) dx_* dv_*,$$

$f : [0, T] \times \mathbb{R}^d \times \mathbb{R}^d \to \mathbb{R}$ is the probability density for the state and $u : [0, T] \to \mathbb{R}^d$ is a forcing term. We can pose an equivalent minimization problem with respect to the discrete functional (4.91):

$$\min_u \mathcal{J}(u; f^0) := \int_0^T \int_{\mathbb{R}^{2d}} \left(\left\| \int_{\mathbb{R}^{2d}} w \, \mathrm{d}f(y, w) - v \right\|_2^2 + \nu \left\| u(t) \right\|_2^2 + \beta \left\| u(t) \right\|_1 \right) \mathrm{d}f(x, v) \, \mathrm{d}t.$$

We know that the solutions of the discrete control problem converge to that of the continuous problem, as discussed in (97, 8).
For the numerical solution of the mean-field model we employ the mean-field Monte-Carlo methods (MFMCs). These methods fall in the class of fast algorithms developed for interacting particle systems such as direct simulation Monte-Carlo methods (DSMCs). We consider N_s particles $v^0 \equiv \{v_i^0\}_i$ sampled from the initial distribution $f^0(x, v)$, and we introduce the following approximation for the mean-field dynamics

$$v_i^{n+1} = (1 - \Delta t \hat{P}_i^n) v_i^n + \Delta t \hat{P}_i^n \hat{V}_i^n + \Delta t u_i^n, \tag{4.104}$$

for $n \geq 0$ and where the quantities $\hat{P}_i^n$ and $\hat{V}_i^n$ are computed from a sub-sample of M_s particles randomly selected from the whole ensemble of N_s particles as follows

$$\hat{P}_i^n = \frac{1}{M_s} \sum_{k=1}^{M_s} P(x_i^n, x_{i_k}^n), \qquad \hat{V}_i^n = \frac{1}{M_s} \sum_{k=1}^{M_s} \frac{P(x_i^n, x_{i_k}^n)}{\hat{P}_i^n} v_{i_k}^n, \qquad i = 1, \ldots, N_s.$$

In order to treat the transport term in the dynamics (4.103), we use a splitting method to perform the free transport step. We compare the performance of the control laws through the discretized cost

$$J_{\Delta t,N_s}(u,g^0) := \frac{\Delta t}{N_s}\sum_{n=0}^{N_T}\sum_{j=1}^{N_s}(\left\|\bar{v}-v_j^n\right\|_2^2+\nu\left\|u_j^n\right\|_2^2+\beta\left\|u_j^n\right\|_1),$$

with time step Δt and N_s Monte Carlo samples.
For the numerical realization of the meanfield limit of the adjoint equations in (4.93), we still use the Monte-Carlo method and we end up with the following approximation

$$\begin{aligned} p_i^{n+1} &= p_i^n - \frac{\Delta t}{M_s}\sum_{k=1}^{M_s} P'(x_i^n,x_{i_k}^n)\langle q_{i_k}^n-q_i^n, v_{i_k}^n-v_i^n\rangle(x_{i_k}^n-x_i^n),\\ q_i^{n+1} &= q_i^n - \Delta t(p_i^n-2(v_i^n-\bar{v})) - \frac{\Delta t}{M_s}\sum_{k=1}^{M_s} P(x_i^n,x_{i_k}^n)(q_{i_k}^n-q_i^n). \end{aligned} \tag{4.105}$$

For details on meanfield derivation of the adjoint system we refer to (8, 118, 44).
We summarize in Algorithm 4 the steps to find the control $u(t)$ using the proximal gradient method described in Section 4.3, in the meanfield case. By using this Monte Carlo algorithm we can reduce the computational cost due to the computation of the interaction terms from the original $\mathcal{O}\left({N_s}^2\right)$ to $\mathcal{O}\left(M_sN_s\right)$.

Algorithm 4 [Prox. Grad. Descent for the Monte-Carlo Meanfield Approximation]

0. Set $tol>0$, $k_{\max}$, $u^{(0)}$, $u^{(-1)}$ and $k=0$
1. Given N_s particles $v^0=\{v_i^0\}_i$, with $i=1,\dots,N_s$, sampled from the initial distribution $f^0(x,v)$, and $M_s\le N_s$
while $\left\|\nabla h_1(u^{(k)})\right\|_2 > tol$ & $k<k_{\max}$ **do**
  for $n=(0:1:n_{tot})$ **do**
    i. Sample M_s particles uniformly without repetition among all N_s particles
    ii. Obtain $v^{n(k)}$ according to (4.104) with $u^{n(k)}$
    iii. Compute $x^{n(k)}$ with a forward Euler step given $v^{n(k)}$
    iv. Obtain $(p^{n(k)},q^{n(k)})$ from (4.105) with $(x^{n(k)},v^{n(k)})$
  end for
  i. Evaluate the gradient $\nabla h_1(u^{(k)})$ as in (4.102)
  ii. Compute the step α_k as in (4.101)
  iii. Update $u^{(k+1)}=\mathrm{prox}_{\beta\alpha_k,M}\Big(u^{(k)}-\alpha_k\nabla h_1(u^{(k)})\Big)$
  vi. $k:=k+1$
end while

4.4 Numerical tests

In this section we focus on the numerical realisation of the model, and we propose some numerical tests to show a comparison between controls with different levels of sparsity.

It is evident that whenever the dimension of the control space is very large, that is, either d, N or the number of timesteps n_{tot} are large, the optimization process is computationally very demanding, and the problem suffers from the curse of dimensionality. To mitigate this difficulty, we start with the use of a compact formulation in order to deal with the high dimensional control problem.

4.4.1 Efficient implementation and comptuational cost

We take $x(t), v(t), p(t), q(t)$, and $u(t)$ as elements of $\mathbb{R}^{N\times d}$, and we consider the implementation of the dynamics (4.89) and adjoint equations (4.93) described in Section 4.2. Let $\mathbf{P}$ be the matrix such that

$$\mathbf{P}_{ij} := P(\|x_i - x_j\|_2)$$

and $\mathbf{dP}$ be the matrix such that

$$\mathbf{dP}_{ij} := P'(\|x_i - x_j\|_2).$$

Now, we can write (4.89) more compactly as

$$\begin{aligned}
\frac{\mathrm{d}x}{\mathrm{d}t} &= v,\\
\frac{\mathrm{d}v_i}{\mathrm{d}t} &= \frac{1}{N}\sum_{j=1}^{N}\mathbf{P}_{ij}(v_j - v_i) + u, \quad i = 1, 2, \ldots, N
\end{aligned}$$

which is

$$\begin{aligned}
\frac{\mathrm{d}x}{\mathrm{d}t} &= v,\\
\frac{\mathrm{d}v}{\mathrm{d}t} &= \frac{1}{N}(\mathbf{P}v - v\cdot\mathbf{P}\mathbb{1}_{N\times d}) + u
\end{aligned}$$

where $\mathbb{1}_{N\times d}$ is the element of $\mathbb{R}^{N\times d}$ of only ones and $\cdot$ is the componentwise scalar product. In a totally analogous manner, we rewrite the equations $0 = \nabla_{v_i}\mathcal{H}$ appearing in (4.93):

$$\frac{\mathrm{d}q}{\mathrm{d}t} = -p - \frac{1}{N}(\mathbf{P}q - q\cdot\mathbf{P}\mathbb{1}_{N\times d}) + 2(v - \bar{v}).$$

The tricky part now is in the equations $0 = \nabla_{x_i}\mathcal{H}$ from (4.93). Let us begin by calling

$$\mathbf{Q}_{ij} := \langle q_j - q_i, v_j - v_i\rangle \mathbf{dP}_{ij}.$$

Then we have that

$$\frac{\mathrm{d}p}{\mathrm{d}t} = -\frac{1}{N}(\mathbf{Q}x - x\cdot\mathbf{Q}\mathbb{1}_{N\times d}).$$

Now, one can write as

$$\mathbf{Q} = \sum_{k=1}^{d}((qe_k)\,\mathbb{1}_{1\times N} - \mathbb{1}_{N\times 1}\,(qe_k)^T)\cdot((ve_k)\,\mathbb{1}_{1\times N} - \mathbb{1}_{N\times 1}\,(ve_k)^T)\cdot\mathbf{dP}$$

where e_k is the k-th canonical vector of $\mathbb{R}^N$ and, we stress, $\cdot$ is the componentwise multiplication.
What we did is actually rewrite the operations in order to exploit the power of BLAS (Basic Linear Algebra Subroutines), used to perform massive operations such as matrix-matrix or matrix-vector products. We exploited the fact that a rank 1 matrix has the advantage that it can be written as the product of a column vector by a row vector. This makes it possible to reduce the space allocated to store these matrices from N^2 to $2N$ and the computational complexity of the matrix-vector product from $\mathcal{O}(N^2)$ to $\mathcal{O}(N)$.
Using this compact implementation we are able to reach the computation CPU time shown in Table 4.4.1, which also indicates the evolution of the number of optimisation iterations, i.e. loops on Algorithm 3. We used the same data and parameters as in (24), a Runge-Kutta 4th order scheme was used to integrate the differential equations for the state and the adjoint with final time $T = 10$, time step $\Delta t = 0.1$, and a stopping tolerance for the gradient norm of $tol = 10^{-3}$. As a result, the time required to evolve and control a system of 1550 agents, was reduced from 49 hours (in (24)) to 10 minutes. This allowed not only to consider larger scale problems but also to implement a more satisfactory mean field approach.

Agents (N)	50	100	1550	5000
Iterations (I)	25	25	28	28
Time (T)	0.0004	0.0008	0.2013	2.0585

Table 4.8: Number of iterations (I) and CPU time (T) in hours for N agents for the discrete optimisation problem.

4.4.2 Controls' comparison between different sparsity levels

Now we present different numerical tests on microscopic and mean-field dynamics, in order to compare the sparse ($\beta \neq 0$) and classical ($\beta = 0$) controls. We consider first the model of Section 4.2 and then the leader-follower model in Example 1.
For all the tests we take the Cucker-Smale interaction kernel

$$P(r) := \frac{1}{(1+r^2)^\gamma}, \quad \gamma = 1,$$

and the initial distribution of particles (x_0, v_0) is chosen such that consensus towards the target $\bar{v}$ would not be reached without control action, i.e.

$$x_0 \sim \mathcal{N}\left(\begin{bmatrix}0\\0\end{bmatrix}, \begin{bmatrix}0.16 & 0\\ 0 & 0.16\end{bmatrix}\right), \qquad v_0 \sim \mathcal{N}\left(\begin{bmatrix}4\\-1\end{bmatrix}, \begin{bmatrix}1.44 & 0\\ 0 & 1.44\end{bmatrix}\right).$$

We use a Runge-Kutta 4th order scheme with fixed time step $\Delta t = 0.1$ to integrate the differential equations for the state and the adjoint until the final time $T = 5$. In Algorithm 3 we consider a stopping tolerance $tol = 10^{-3}$ for the gradient norm. In the microscopic model we take $N = 50$ agents, while in the meanfield case, the Monte Carlo method is employed for the approximation of the distribution function $f(t, x, v)$ in the phase space using a sample of $N_s = 10^4$ agents and a sub-sample of $M_s = 10^2$ agents for the approximation of the non-local integral operator.

Test 1: Micro and meso uncontrolled and controlled dynamics. Figure 4.22 shows a comparison of the free two-dimensional state x on the left and the positions under an approximation to the optimal control u found with the gradient descent algorithm, on the right. The evolution of the particles states in time is depicted with a blue line, while in red we indicate the final positions at time T. On the right, the classical control with a penalization factor $\nu = 0.1$ is shown, the control is forced to be bounded in a set $C = [-M, M]^{N\times d}$ with a constant $M = 0.5$, and alignment is reached rapidly as expected.

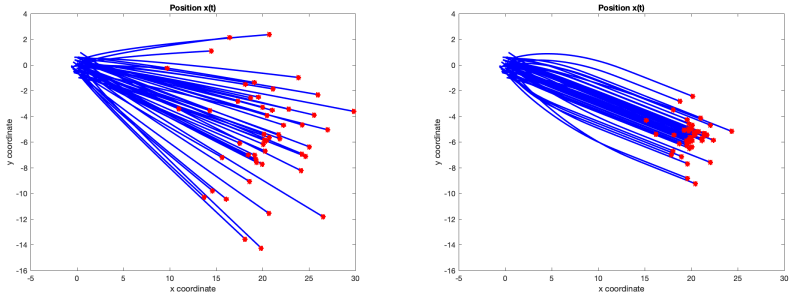

Figure 4.22: *Test 1.* Position of particles over time in the microscopic framework ($N = 50$). On the left the uncontrolled dynamics, on the right the controlled ($\nu = 0.1, \beta = 0, M = 0.5$) ones.

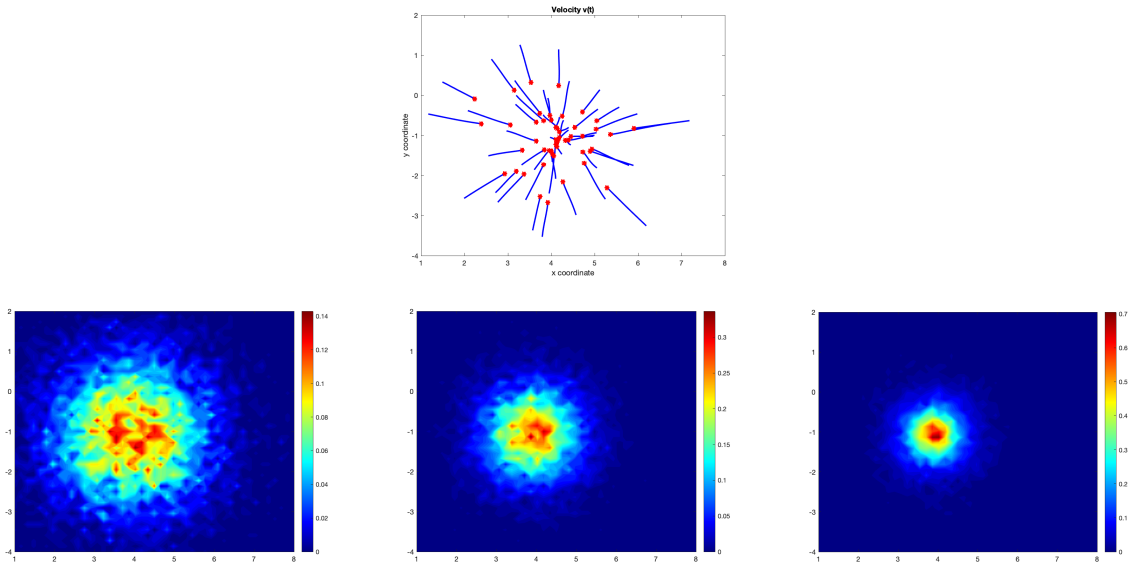

Figure 4.23: *Test 1.* Velocity of particles over time in the uncontrolled case. On the top the microscopic dynamics ($N = 50$), on the bottom the mesoscopic ($N_s = 10^4, M_s = 10^2$) ones for three time frames $t = 0, \frac{T}{2}, T$.

Figures 4.23, 4.24, and 4.25 show the two-dimensional velocities v in the no control, classical control, and sparse control case, respectively. In the first row of every figures

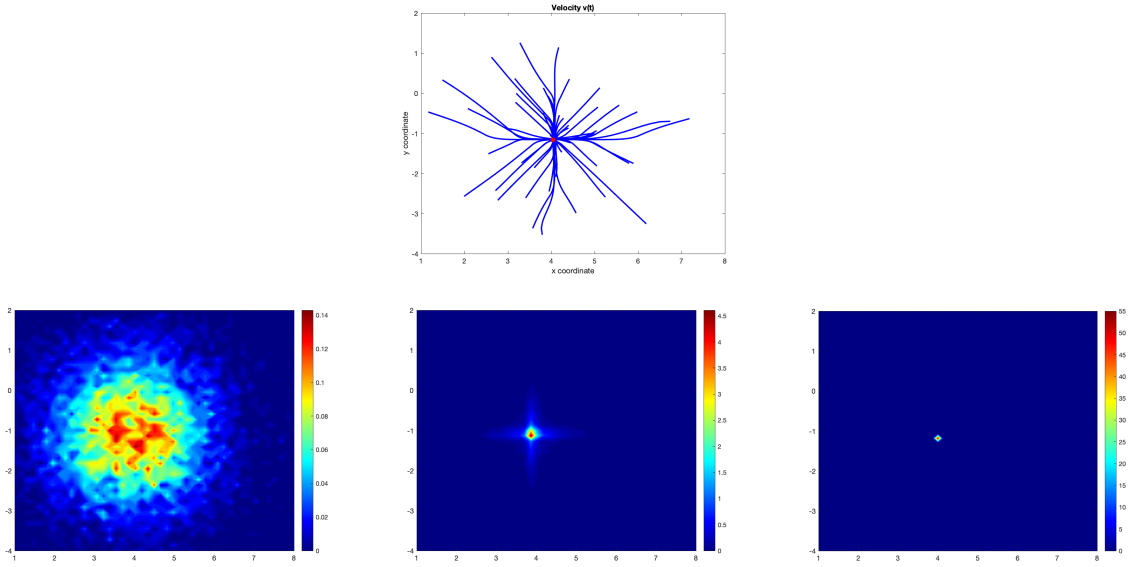

Figure 4.24: *Test 1.* Velocity of particles over time in the controlled case ($\nu = 0.1, \beta = 0, M = 0.5$). On the top the microscopic dynamics ($N = 50$), on the bottom the mesoscopic ($N_s = 10^4, M_s = 10^2$) ones for three time frames $t = 0, \frac{T}{2}, T$.

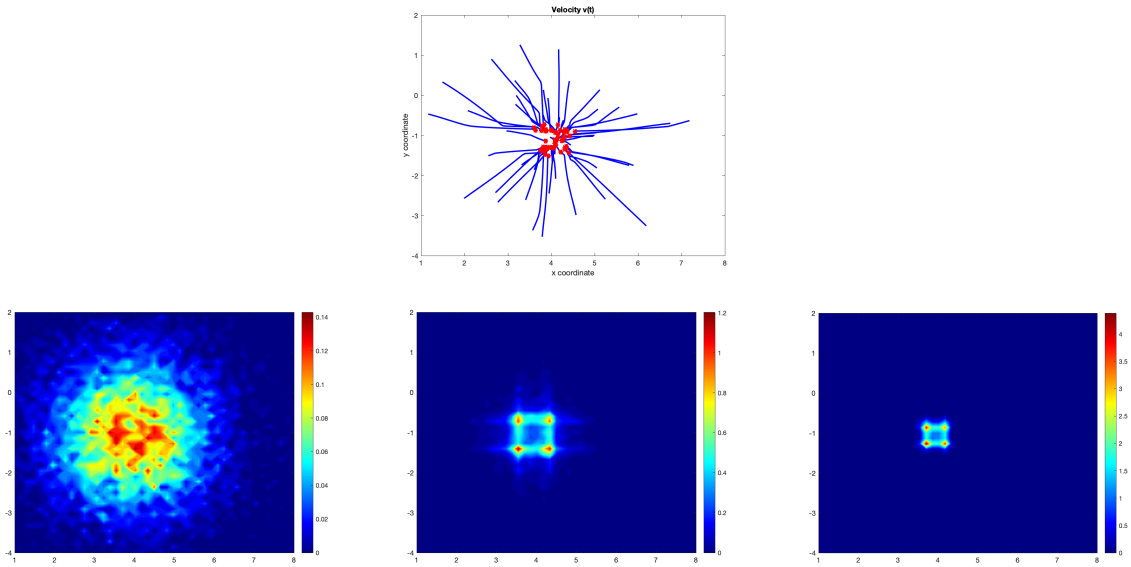

Figure 4.25: *Test 1.* Velocity of particles over time in the controlled case ($\nu = 0.1, M = 0.5$) with the additional non-smooth terms $\beta \|u_i\|_1$, $\beta = 2$. On the top the microscopic dynamics ($N = 50$), on the bottom the mesoscopic ($N_s = 10^4, M_s = 10^2$) ones for three time frames $t = 0, \frac{T}{2}, T$.

the microscopic velocities over time are presented, while in the second row there are three snapshots of the meanfield velocities taken at times $t = 0, \frac{T}{2}, T$.

We can observe that in the uncontrolled case the particles cannot reach the desired mean velocity $\bar{v}$. The other two controlled cases show that both controls are capable to drive the velocities to the desired target, in particular when we add the non-smooth term $\beta \|u_i\|_1$, $\beta = 0.5$, the velocities reach a square shape, due to the fact that we are cutting the smallest controls using the proximal operator. The cross shape in figures 4.24 and 4.25 is caused by the projection of the control over the set C.

Test 2: Different levels of sparsity. We compare different levels of sparsity, i.e. different values of β, with a penalization factor $\nu = 0.01$ in Figure 4.26, and $\nu = 0.0001$ in Figure 4.27.

	$\beta = 0$	$\beta = 0.5$	$\beta = 1.5$
$V(T)$	1.339e-8	0.009	0.059

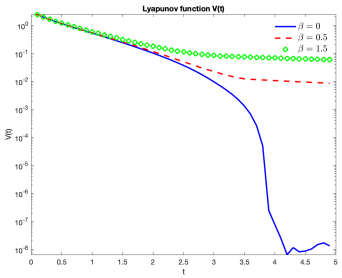

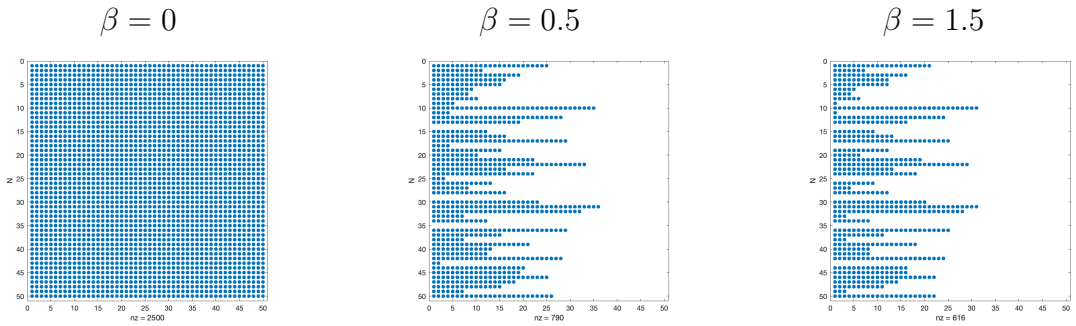

Figure 4.26: *Test 2.* Comparison of the microscopic control action ($\nu = 0.01, M = 0.5$) for different values of β. On the top a table with the values of the Lyapunov functional $V(t)$ at final time T and a figure with the decays of $V(t)$. On the bottom the on-off control actions in time for each agent in terms of ℓ_1 norm.

In both figures, on the top we show a table with the values of the Lyapunov functional $V(t)$ at final time T and a figure with the decays of $V(t)$, where

$$V(t) = \frac{1}{2N^2} \sum_{i,j=1}^{N} \|v_i - v_j\|_2^2 ,$$

while on the bottom the on-off control actions are depicted for each agent i and for each timestep t_n, in terms of the ℓ_1 norm $\|u_i(t_n)\|_1$. In the x-axis label, the number of non-zero components are specified. We can observe that, as expected, the value of the Lyapunov functional and the number of non-zero controls components decrease as β increases. This leads to a more parsimonious but still suitable control.

	$\beta = 0.05$	$\beta = 0.1$	$\beta = 0.5$
$V(T)$	8.053e-5	3.557e-4	0.008

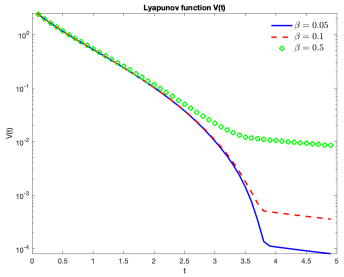

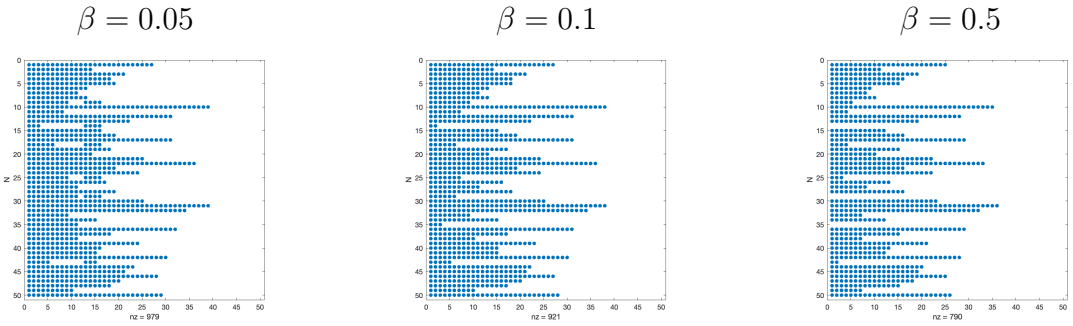

Figure 4.27: *Test 2.* Comparison of the microscopic control action ($\nu = 0.0001, M = 0.5$) for different values of β. On the top a table with the values of the Lyapunov functional $V(t)$ at final time T and a figure with the decays of $V(t)$. On the bottom the on-off control actions in time for each agent in terms of ℓ_1 norm.

Test 3: Comparison with a leader-follower model. We end the numerical section with a test using the leader-follower model in Example 1. In particular we take $|I| = 37$ leaders, $|J| = 13$ followers, and the parameters m_j equal $\frac{1}{N}$ for every agent j. We want to manually add sparsity controlling only the leaders. The result is in Figure 4.28, and in this test the value of the Lyapunov functional $V(t)$ at final time T is $V(T) = 0.1886$. This proves the fact that sparsity obtained with the non-smooth control penalisation is better, since it allows to reach a lower value of $V(T)$ even with more zero control components.

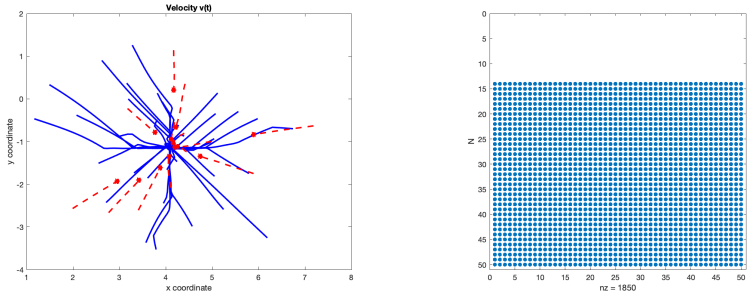

Figure 4.28: *Test 3.* Leader-follower dynamics. Velocity of particles over time and on-off control actions in the microscopic controlled case ($\nu = 0.0001, \beta = 0, M = 0.5$). The control is not applied to 13 agents over a total number of $N = 50$ agents. On the left, the uncontrolled velocities are depicted with dashed red lines.

4.5 Conclusions

In optimal control for multiagent systems, the question of a more parsimonious control is of paramount importance especially when the number of agents is very large. Efficient controls strategies should target only few individuals of the population, instead of wasting resources on the entire group at once. We concentrated in this chapter with control problems for second-order, nonlinear, multiagent systems and we focused on the design of control laws enforcing consensus emergence. As an extension of the proposed classical control, we addressed the finite horizon optimal control problem with a non-smooth, sparsity-promoting control penalisation, obtained with an ℓ_1-norm term in the control cost. To circumvent the resulting lack of smoothness in the cost functional we relied theoretically on sub-differential theory and we proposed a numerical realisation of the control synthesis via proximal gradient method. To reduce the computational complexity for an increasing number of agents, we discussed the approximation of the problem by following a mean-field modelling approach. We presented different numerical tests to show a substantial reduction of the computational costs and a comparison between classical and sparse controls both at microscopic and meanfield level.

5 Optimized leaders strategies for crowd evacuation in unknown environments with multiple exits

5.1 Introduction

Control methodologies for crowd motion are of paramount importance in real-life applications for the design of safety measures and risk mitigation. The creation of virtual models of a large ensemble of pedestrians is a first step for reliable predictions, otherwise not easily reproducible with real-life experiments.

Pedestrians have been properly modeled by means of different agent-based dynamics such as lattice models (58, 104), social force models (111, 142), or cellular automata models (1, 151). A different level of description is obtained using mesoscopic models (3, 7, 92) where the quantities of study are densities of agents; at a larger scale macroscopic models (54, 78, 60) describe the evolution of moments such as mass and momentum. Multiscale models have been also considered, to account for situations where different scales coexist, we refer in particular to (65, 67). Such a hierarchy of models is able to capture coherent global behaviors emerging from local interactions among pedestrians. These phenomena are strongly influenced by the social rules, the *rationality* of the crowd, and the knowledge of the surrounding environment. In the case of egressing pedestrians in an unknown environment with limited visibility we expect people to follow basically an instinctive behavior (54, 58, 104, 26), whereas a perfectly rational pedestrian will compute an optimal trajectory towards a specific target (the exit), forecasting exactly the behavior of other pedestrians (1, 127).

In this manuscript, we focus on the evacuation problem in an unknown environment with multiple exits. We aim at influencing their behavior towards the desired target with minimal intervention. Starting from the seminal work (7) we consider a bottom-up approach where few informed agents are acting minimizing verbal directives to individuals and preserving as much as possible their natural behavior. This approach is expected to be efficient in situations where direct communication is impossible, for example in the case of very large groups, emergencies, violent crowds reluctant to follow directions; or in panic situations where rational behavior is overtaken by instinctive decisions. Furthermore, we consider few additional agents, who are informed about the position of some exit and acting as unaware leaders. Hence, their dynamics will influence the global behavior of the crowd, introducing inertia that may constitute an additional difficulty in the optimization problem, for example increasing congestions next to the exits or increasing the level of uncertainty.

The control problem associated to the evacuation of a crowd falls in the larger research field aimed at investigating the control of *self-organizing agents*. From the mathematical view point, this type of problem is challenging due to the presence of non-local interaction terms and their high dimensionality. Control of alignment-type dynamics, such as the Cucker-Smale model (70), have risen a lot of interest in the mathematical community, where several strategies have been explored to enforce the emergence of consensus, see for example (25, 37, 9, 115). At the same time, to cope with the high dimensionality of such optimal control problems, reduced approaches have been explored (50, 98, 96, 38), promoting sparsity of the control acting only on few agents. In biological models, it has been shown that a small percentage of individuals can influence the whole group

towards a desired target, see (62). Similarly, leaders in crowd can act as control signals to enforce alignment towards a desired direction as recognizable leaders (5, 18, 39, 86, 137), or moving undercover (7, 62, 84, 106, 107), or even in a repulsive way (46). These strategies heavily rely on the power of the *social influence* (or herding effect), namely the natural tendency of people to follow other mates in situations of emergency or doubt. Alternative control methodologies consist in optimal design of the surrounding enviroment such as obstacles (64, 63, 10), or evacuation signage (156, 153), or exit locations (151).
The manuscript is organized as follows in Section 5.2 we introduce the mathematical framework for the microscopic dynamics of leader-follower type and we formulate different scenarios for the optimal control problem to be solved. In particular, we will distinguish between minimum time of evacuation, total mass evacuated, and optimal mass splitting among the multiple exits. In this work the word mass denotes the total amount of pedestrians. Section 5.3 is devoted to the description of the mesoscopic scale, first we introduce the mean-field type model, second we sketch an efficient Monte Carlo algorithm for its simulation. In Section 5.4 we focus on the numerical realization of the optimized strategies. We start introducing the algorithmic procedure used for the solution of the large-scale optimization problem, and we compare microscopic and mean-field dynamics in several scenarios and with different target functionals. Finally in Section 5.7 we outline possible extensions and further perspectives.

5.2 Control of pedestrian dynamics through leaders

In this section, we focus first on the mathematical description of pedestrian dynamics in complex environments. We consider an ensemble of agents, *followers*, in an unknown environment trying to reach exit locations, at the same time the crowd population includes few informed agents, *leaders*, acting as controllers but not distinguishable from followers. In particular, we account for a mixed approach where leaders are either aware of their role, then responding to an optimal force as the result of an offline optimization procedure, *optimized leaders*, or unaware of their role and moving with a greedy strategy towards a target exit position, *selfish leaders*. The main mechanisms ruling the behaviors among the followers are isotropic interactions with other agents based on metrical short-range repulsion, induced by social distancing and collisional avoidance, and topological long-range alignment dynamics. Leaders instead consider only short-range repulsion. Additionally, for followers, we account self-driving forces describing the exploration phase, preferential direction, and desired speed. The overall dynamics will be influenced by the surrounding environment when the exits are visible or close to obstacles.
In the following sections, we describe first the microscopic dynamics of the follower-leader system and later different control tasks for different applications.

5.2.1 Microscopic model with leaders and multiple exits

Following the approach proposed in (7, 10) we model leaders by a first-order model and followers by a second-order one, where both positions and velocities are state variables. We denote by d the dimension of the space in which the motion takes place (typically $d = 2$), by N^{F} the number of followers and by $N^{\mathrm{L}} \ll N^{\mathrm{F}}$ the number of leaders. We also

denote by $\Omega \equiv \mathbb{R}^d$ the walking area, and we identify the different exits by $x_e^\tau \in \Omega$ with $e = 1, \dots, N_e$.
To define each target's visibility area, we consider the set Σ_e, with $x_e^\tau \in \Sigma_e \subset \Omega$, and we assume that the target is completely visible from any point belonging to Σ_e and completely invisible from any point belonging to $\Omega \backslash \Sigma_e$, namely we also assume that visibility areas are disjoint sets, i.e $\Sigma_{e_i} \cap \Sigma_{e_j} = \varnothing$ for all $e_i, e_j \in \{1, .., N_e\}$.
For every $i = 1, \dots, N^{\mathrm{F}}$, let $(x_i(t), v_i(t)) \in \mathbb{R}^{2d}$ denote position and velocity of the agents belonging to the population of followers at time $t \geq 0$ and, for every $k = 1, \dots, N^{\mathrm{L}}$, let $(y_k(t), w_k(t)) \in \mathbb{R}^{2d}$ denote position and velocity of the agents among the population of leaders at time $t \geq 0$. Let us also define $\mathbf{x} := (x_1, \dots, x_{N^{\mathrm{F}}})$ and $\mathbf{y} := (y_1, \dots, y_{N^{\mathrm{L}}})$.
The microscopic dynamics described by the two populations is given by the following set of ODEs for $i = 1, \dots, N^{\mathrm{F}}$ and $k = 1, \dots, N^{\mathrm{L}}$,

$$\begin{cases} \dot{x}_i = v_i, \\ \dot{v}_i = S(x_i, v_i) + \sum_{j=1}^{N^{\mathrm{F}}} m_j^F H^{\mathrm{F}}(x_i, v_i, x_j, v_j; \mathbf{x}, \mathbf{y}) + \sum_{\ell=1}^{N^{\mathrm{L}}} m_\ell^L H^{\mathrm{L}}(x_i, v_i, y_\ell, w_\ell; \mathbf{x}, \mathbf{y}), \\ \dot{y}_k = w_k = \sum_{j=1}^{N^{\mathrm{F}}} m_j^F K^{\mathrm{F}}(y_k, x_j) + \sum_{\ell=1}^{N^{\mathrm{L}}} m_\ell^L K^{\mathrm{L}}(y_k, y_\ell) + \xi_k u_k^{\mathrm{opt}} + (1 - \xi_k) u_k^{\mathrm{self}}, \end{cases} \tag{5.106}$$

with initial data for followers $(x_i(0), v_i(0)) = (x_i^0, v_i^0)$ and leaders $(y_k(0), w_k(0)) = (y_k^0, w_k^0)$.
The quantities m_i^F, m_k^L weight the interaction of followers and leaders, in what follows we will assume that $m_1^F = \ldots = m_{N^{\mathrm{F}}}^F = m_1^L = \cdots = m_{N^{\mathrm{L}}}^L$ and the following mass constraint holds

$$m_i^F = \frac{\rho^F}{N^{\mathrm{F}}}, \qquad m_k^L = \frac{\rho^L}{N^{\mathrm{L}}}, \qquad \rho^F + \rho^L = 1, \tag{5.107}$$

for ρ^F, ρ^L positive quantities.

1. S is a self-propulsion term, given by the relaxation toward a random direction or the relaxation toward a unit vector pointing to the target (the choice depends on the position), plus a term which translates the tendency to reach a given characteristic speed $s \geq 0$ (modulus of the velocity), i.e.,

$$S(x, v) := C_s(s^2 - |v|^2)v + \sum_{e=1}^{N_e} \psi_e(x) C_\tau \left(\frac{x_e^\tau - x}{|x_e^\tau - x|} - v \right), \tag{5.108}$$

   where $\psi_e : \mathbb{R}^d \to [0, 1]$ is the characteristic function of Σ_e, and C_τ, C_s are positive constants.

2. The interactions follower-follower and follower-leader account a repulsion and an alignment component, as follows

$$\begin{aligned} H^{\mathrm{F}}(x, v, x', v'; \mathbf{x}, \mathbf{y}) &:= -C_r^{\mathrm{F}} R_{\gamma,r}(x, x')(x' - x) + (1 - \psi(x)) C_{al}^{\mathrm{F}} A(x, x'; \mathbf{x}, \mathbf{y}) (v' - v), \\ H^{\mathrm{L}}(x, v, y, w; \mathbf{x}, \mathbf{y}) &:= -C_r^{\mathrm{L}} R_{\gamma,r}(x, y)(y - x) + (1 - \psi(x)) C_{al}^{\mathrm{L}} A(x, y; \mathbf{x}, \mathbf{y}) (w - v), \end{aligned} \tag{5.109}$$

   for given positive constants $C_r^{\mathrm{F}}, C_{al}^{\mathrm{F}}, C_{al}^{\mathrm{L}}, C_{at}, r, \gamma$, and where $1 - \psi(x)$ is the characteristic function of the unknown environment $\Omega \backslash \cup_e \Sigma_e$, such that

$$\psi(x) := \sum_{e=1}^{N_e} \psi_e(x).$$

The first term on the right hand side of (5.109) represents the metrical repulsion force, where the intensity is modulated by the function $R_{\gamma,r}$ defined as

$$R_{\gamma,r}(x,y) = \begin{cases} \frac{e^{-|y-x|^\gamma}}{|y-x|} & \text{if } y \in B_r(x)\backslash\{x\}, \\ 0 & \text{otherwise,} \end{cases} \tag{5.110}$$

where $B_r(x)$ is the ball of radius $r > 0$ centered at $x \in \Omega$. The second term accounts for the (topological) alignment force, which vanishes inside the visibility regions, and where

$$A(x, y; \mathbf{x}, \mathbf{y}) := \chi_{\mathcal{B}_\mathcal{N}(x;\mathbf{x},\mathbf{y})}(y), \tag{5.111}$$

and by $\mathcal{B}_\mathcal{N}(x; \mathbf{x}, \mathbf{y})$ the *minimal* ball centered at x encompassing at least $\mathcal{N}$ agents.

3. The interactions leader-follower and leader-leader reduce to a mere (metrical) repulsion, i.e., $K^{\text{F}} = K^{\text{L}} = -C_r^{\text{L}} R_{\zeta,r}$, where $C_r^{\text{L}} > 0$ and $\zeta > 0$ are in general different from C_r^{F} and γ, respectively.

4. $u_k^{\text{opt}}, u_k^{\text{self}} : \mathbb{R}^+ \to \mathbb{R}^{dN^{\text{L}}}$ characterize the strategies of the leaders and are chosen in a set of admissible control functions. The parameter $\xi_k \in \{0, 1\}$ identifies for $\xi_k = 1$ leaders aware of their role, whose movements are the result of an optimization process, and alternatively for $\xi_k = 0$ leaders moving "selfishly" towards a specific exit. A specific description of leaders' strategy will be discussed in Section 5.4. Hence we account for situations where a small part of the mass is informed about exit positions, but policymakers have no control over them.

Remark 15.

- *Differently from the model proposed in (7, 10) the dynamics do not include random effects. However, we consider this uncertainty by assuming that the initial velocity directions of followers are distributed according to a prescribed density* $v_i^0 \sim p_v(\mathbb{R}^d)$*, for example, a uniform distribution over the unitary sphere* $\mathbb{S}_{d-1}$ *.*

- *The choice* $C_{al}^{\text{F}} = C_{al}^{\text{L}}$ *leads to* $H^{\text{F}} \equiv H^{\text{L}}$ *and, therefore, the leaders are not recognized by the followers as special. This feature opens a wide range of new applications, including the control of crowds not prone to follow authority's directives.*

- *The pedestrian microscopic model* (5.106) *allows agent movements in space without any constriction. However, in real applications, dynamics are constrained by walls or other kinds of obstacles. There are several ways of dealing with this feature in agent-based mode and we refer to (63, Sect. 2) for a review of obstacles handling techniques such as repulsive obstacle, rational turnaround, velocity cut-off. The choice for obstacle handling will be discussed in Section 5.4.*

5.2.2 Control framework for pedestrian dynamics

In order to define the strategies of optimized leaders, we formulate an optimal control problem to exploit the tendency of people to follow group mates in situations of emergency or doubt. The choice of a proper functional to be minimized constitutes a modeling

difficulty, and it is typically a trade-off between a realistic task and a viable realization of its minimization. In general we will set up the following constrained optimal control problem

$$\begin{aligned} &\min_{\mathbf{u}^{\mathrm{opt}}(\cdot)\in U_{adm}} \mathcal{J}(\mathbf{u}^{\mathrm{opt}}), \\ &\text{s.t.} \qquad (5.106), \end{aligned} \tag{5.112}$$

where $\mathbf{u}^{\mathrm{opt}} = (u_k^{opt}(\cdot))$ is the control vector associated to the optimized leaders, given a set of admissible controls U_{adm}. In what follows we will specify different functionals for different type of applications. For later convenience we introduced the empirical distributions defined as follows

$$f^{N^{\mathrm{F}}}(\cdot, x, v) = \sum_{i=1}^{N^{\mathrm{F}}} m_i^F \delta(x - x_i(\cdot))\delta(v - v_i(\cdot)), \tag{5.113}$$

$$g^{N^{\mathrm{L}}}(\cdot, x, v) = \sum_{j=1}^{N^{\mathrm{L}}} m_j^L \delta(x - y_j(\cdot))\delta(v - w_j(\cdot)). \tag{5.114}$$

- *Evacuation time.* In a situation where egressing pedestrians are in an unknown enviroment the most natural functional is the evacuation time, that we may define as follows

$$\mathcal{J}(\mathbf{x}, \mathbf{y}, \mathbf{u}^{\mathrm{opt}}) = \left\{ t > 0 \mid (x_i(t), y_j(t)) \notin \Omega \ \forall i = 1, \dots N^F, \forall j = 1, \dots, N^{\mathrm{L}} \right\}, \tag{5.115}$$

  where we explicit the dependency on the states vector of follower positions $\mathbf{x} \in \mathbb{R}^{dN^{\mathrm{F}}}$. This cost functional is extremely irregular, therefore the search of minima is particularly difficult, additionally the evacuation of the total mass in some situations can not be completely reached.

- *Total mass with multiple exits.* Instead of minimizing the total evacuation, we fix a final time $T > 0$ and we aim to minimize the total mass inside the computational domain $\Omega \setminus \cup_e \Sigma_e$, which coincides with maximizing the mass inside the visibility areas. The functional reads

$$\mathcal{J}(\mathbf{x}, \mathbf{y}, \mathbf{u}^{\mathrm{opt}}) = \int_{\mathbb{R}^d} \int_{\Omega \setminus \cup_e \Sigma_e} (f^{N^{\mathrm{F}}}(T, x, v) + g^{N^{\mathrm{L}}}(T, x, v)) dx dv. \tag{5.116}$$

- *Optimal mass splitting over multiple exits.* In complex environments, it may happen that total mass does not distribute in an optimal way between the target exits. This may lead to problems of heavy congestions and overcrowding around the exits that, in real-life situations, can cause injuries due to overcompression and suffocation. Hence we ask to distribute the total evacuated mass at final time T among the exits according to a given desired distribution. To this end we set

$$\mathcal{J}(\mathbf{x}, \mathbf{y}, \mathbf{u}^{\mathrm{opt}}) = \sum_{e=1}^{N_e} \left| \mathcal{M}_e^F(T) - \mathcal{M}_e^{\mathrm{des}} \right|^2, \tag{5.117}$$

  where $\mathcal{M}_e^{\mathrm{des}}$ is the desired mass to be reached in the visibility area Σ_e and $\mathcal{M}_e^F(T)$ is the total mass of followers and leaders who reached exit x_e^τ up to final time T.

5.3 Mean-field approximation of follower-leader system

Mean-field scale limit for large number of interacting individuals has been investigated in several directions for single and multiple population dynamics, see for example (53, 77), and it is a fundamental step to tame the curse of dimensionality arising for coupled systems of ODEs.
In the current setting, we want to give a statistical description of the followers-leaders dynamics considering a continuous density for followers and maintaining leaders microscopic. Hence, we introduce the non-negative distribution function of followers $f = f(t,x,v)$ with $x \in \mathbb{R}^d, v \in \mathbb{R}^d$ at time $t \geq 0$, the meso-micro system corresponding to (5.106) reads as follows

$$\begin{aligned} &\partial_t f + v \cdot \nabla_x f = -\nabla_v \cdot \left(f \left(S(x,v) + \mathcal{H}^F[f, g^{N^{\text{L}}}] + \mathcal{H}^L[f, g^{N^{\text{L}}}] \right) \right), \\ &\dot{y}_k = w_k = \int_{\mathbb{R}^{2d}} K^{\text{F}}(y_k, x) f(t,x,v)\ dx\ dv + \sum_{\ell=1}^{N^{\text{L}}} m_\ell^L K^{\text{L}}(y_k, y_\ell) \\ &\qquad\qquad + \xi_k u_k^{\text{opt}} + (1-\xi_k) u_k^{\text{self}}, \end{aligned} \tag{5.118}$$

where the followers dynamics is described by a kinetic equation of Vlasov-type, and where we use the corresponding empirical distribution for leaders $g^{N^{\text{L}}}$. Furthermore we assume that the follower and leader densities are such that their number densities are

$$\varrho^F = \int_{\mathbb{R}^{2d}} f(t,x,v)\ dx\ dv, \qquad \varrho^L = \int_{\mathbb{R}^{2d}} g^{N^{\text{L}}}(t,x,v)\ dx\ dv.$$

We observe that the terms $S(\cdot), K^{\text{F}}(\cdot)$ and $K^{\text{L}}(\cdot)$ are defined respectively as in the microscopic setting, whereas the non-local operators $\mathcal{H}^F, \mathcal{H}^L$ correspond to the following integrals

$$\begin{aligned} \mathcal{H}^F[f, g^{N^{\text{L}}}](t,x,v) &= -C_r^{\text{F}} \int_{\mathbb{R}^d} \int_{B_r(x)} R_{\gamma,r}(x,x')(x'-x) f(t,x',v')\ dx'dv' \\ &+ C_{al}^{\text{F}} (1-\psi(x)) \int_{\mathbb{R}^d} \int_{\mathcal{B}_{r_*}(t,x)} (v'-v) f(t,x',v')\ dx'dv', \end{aligned} \tag{5.119}$$

$$\begin{aligned} \mathcal{H}^L[f, g^{N^{\text{L}}}](t,x,v) &= -C_r^{\text{L}} \int_{\mathbb{R}^d} \int_{B_r(x)} R_{\gamma,r}(x,x')(x'-x) g^{N^{\text{L}}}(t,x',v')\ dx'dv' \\ &+ C_{al}^{\text{L}} (1-\psi(x)) \int_{\mathbb{R}^d} \int_{\mathcal{B}_{r_*}(t,x)} (v'-v) g^{N^{\text{L}}}(t,x',v')\ dx'dv', \end{aligned} \tag{5.120}$$

where the first term corresponds to the metrical repulsion as in (5.110), and the second part accounts the topological ball $\mathcal{B}_{r_*}(t,x) \equiv \mathcal{B}_{r^*}(t,x; f, g^{N^{\text{L}}})$ whose radius is defined for a fixed $t \geq 0$ by the following variational problem

$$r^*(t,x) = \arg\min_{\alpha>0} \left\{ \int_{\mathbb{R}^d} \int_{B_\alpha(x)} \left(f(t,x,v) + g^{N^{\text{L}}}(t,x,v) \right)\ dx\ dv \geq \varrho_{\text{top}} \right\}, \tag{5.121}$$

where $\varrho_{\text{top}} > 0$ is the target topological mass.

Remark 16.

- *Rigorous derivation of the mean-field limit* (5.118) *from* (5.106) *is a challenging task due to the strong irregularities induced by the behavior of topological-type interactions. We refer to (109) for possible regularization in the case of Cucker-Smale type dynamics, and to (33, 76) for alignment driven by jump-type processes.*

- *Alternative derivation of mesoscopic models in presence of diffusion has been obtained in (7), where the authors derived a Fokker-Planck equation of the original microscopic system via quasi-invariant scaling of binary Boltzmann interactions. This technique, analogous to the so-called grazing collision limit in plasma physics, has been thoroughly studied in (150) and allows to pass from a Boltzmann description to the mean-field limit, see for example (141).*

- *For optimal control of large interacting agent systems, the derivation of a mean-field approximation involves the convergence of minimizers from microscopic to mesoscopic scale. This problem has been addressed from different directions, and we refer to (98, 38).*

Remark 17. *In order to obtain a closed hydrodynamic system for* (5.118) *a standard assumption is to assume the velocity distribution to be mono-kinetic, i.e.* $f(t,x,v) = \rho(t,x)\delta(v - V(t,x))$*, and the fluctuations to be negligible. Hence, computing the moments of* (5.118) *leads to the following macroscopic system for the density* ρ *and the bulk velocity* V*,*

$$\begin{cases} \partial_t \rho + \nabla_x \cdot (\rho V) = 0, \\ \partial_t (\rho V) + \nabla_x \cdot (\rho V \otimes V) = \mathcal{G}_m \left[\rho, \rho^{\text{L}}, V, V^{\text{L}}\right] \rho, \\ \dot{y}_k = w_k = \displaystyle\int_{\mathbb{R}^d} K^{\text{F}}(y_k, x)\rho(t,x)\, dx + \sum_{\ell=1}^{N^{\text{L}}} K^{\text{L}}(y_k, y_\ell) \\ \qquad\qquad + \xi_k u_k^{opt} + (1-\xi_k) u_k^{self}, \end{cases} \tag{5.122}$$

where $\rho^{\text{L}}(x,t), V^{\text{L}}(x,t)$ *represent the leaders macroscopic density and bulk velocity, respectively, and* $\mathcal{G}_m$ *the macroscopic interaction operator associated to the followers, we refere to (16, 53) for further details.*

5.3.1 MFMC algorithms

For the numerical solution of the mean-field followers dynamics in (5.118) we employ mean-field Monte-Carlo methods (MFMCs) generalizing the approaches proposed in (15, 141). These methods fall in the class of fast algorithms developed for interacting particle systems such as direct simulation Monte-Carlo methods (DSMCs), and they are strictly related to more recent class of algorithms named Random Batch Methods (RBMs) (122). In order to approximate the evolution of the followers density, first we sample N_s^F particles from the initial distribution $f^0(x,v)$ in the phase space, i.e. $\{(x_i^0, v_i^0)\}_{i=1}^{N_s^F}$. Furthermore we consider a subsample of M particles, $j_1, \dots, j_M$ uniformly without repetition such that $1 \le M \le N_s^F$. In order to approximate the non-local terms $\mathcal{H}^F, \mathcal{H}^L$ we evaluate the interactions with a subsample of size M at every time step. Hence we define the

discretization step as

$$v_i^{n+1} = v_i^n + \Delta t S(x_i^n, v_i^n) - \Delta t \left[\hat{R}_i^{F,n}(\hat{X}_i^n - x_i^n) + \hat{R}_i^{L,n}(\hat{Y}_i^n - x_i^n) \right] + \Delta t(1 - \psi(x_i^n)) \left[\hat{A}_i^{F,n}(\hat{V}_i^n - v_i^n) + \hat{A}_i^{L,n}(\hat{W}_i^n - v_i^n) \right], \tag{5.123}$$

where we defined the following auxiliary variables for the repulsion term (5.110),

$$\begin{aligned} \hat{R}_i^{F,n} &= \frac{C_r^{\mathrm{F}} \varrho^F}{M} \sum_{k=1}^{M} R_{\gamma,r}(x_i^n, x_{j_k}^n), \quad \hat{X}_i^n = \frac{C_r^{\mathrm{F}} \varrho^F}{M} \sum_{k=1}^{M} \frac{R_{\gamma,r}(x_i^n, x_{j_k}^n)}{\hat{R}_i^{F,n}} x_{j_k}^n, \\ \hat{R}_i^{L,n} &= \frac{C_r^{\mathrm{L}} \varrho^L}{N^{\mathrm{L}}} \sum_{\ell=1}^{N^{\mathrm{L}}} R_{\gamma,r}(x_i^n, y_\ell^n), \quad \hat{Y}_i^n = \frac{C_r^{\mathrm{L}} \varrho^L}{N^{\mathrm{L}}} \sum_{k=1}^{N^{\mathrm{L}}} \frac{R_{\gamma,r}(x_i^n, y_\ell^n)}{\hat{R}_i^{L,n}} y_\ell^n. \end{aligned} \tag{5.124}$$

For the topological alignment we have

$$\begin{aligned} \hat{A}_i^{F,n} &= \frac{C_{al}^{\mathrm{F}} \varrho^F}{M} \sum_{k=1}^{M} \chi_{\mathcal{B}_{r_M^*}(x_i;\mathbf{x},\mathbf{y})}(x_{j_k}), \quad \hat{V}_i^n = \frac{C_{al}^{\mathrm{F}} \varrho^F}{M} \sum_{k=1}^{M} \frac{\chi_{\mathcal{B}_{r_M^*}(x_i;\mathbf{x},\mathbf{y})}(x_{j_k})}{\hat{A}_i^{F,n}} v_{j_k}^n, \\ \hat{A}_i^{L,n} &= \frac{C_{al}^{\mathrm{L}} \varrho^L}{N^{\mathrm{L}}} \sum_{\ell=1}^{N^{\mathrm{L}}} \chi_{\mathcal{B}_{r_M^*}(x_i;\mathbf{x},\mathbf{y})}(x_{j_k}), \quad \hat{W}_i^n = \frac{C_{al}^{\mathrm{L}} \varrho^L}{N^{\mathrm{L}}} \sum_{k=1}^{N^{\mathrm{L}}} \frac{\chi_{\mathcal{B}_{r_M^*}(x_i;\mathbf{x},\mathbf{y})}(x_{j_k})}{\hat{A}_i^{L,n}} w_\ell^n, \end{aligned} \tag{5.125}$$

where, the topological ball $\mathcal{B}_{r_M^*}(x)$ is the topological ball defined over the subsample of M agents, with radius such that

$$r_M^*(t, x_i) = \arg\min_{\alpha>0} \left\{ \frac{\varrho^F}{M} \sum_{k=1}^{M} \chi_{B_\alpha(x_i)}(x_{j_k}) + \frac{\varrho^L}{N^{\mathrm{L}}} \sum_{\ell=1}^{N^{\mathrm{L}}} \chi_{B_\alpha(x_i)}(y_\ell) \geq \varrho_{\mathrm{top}} \right\}. \tag{5.126}$$

From the above considerations we obtain the following Algorithm in the time interval $[0, T]$.

Algorithm 1 (MFMC follower-leader)**.**

1. *Given N_s^F samples v_i^0, with $i = 1, \ldots, N_s^F$ computed from the initial distribution $f(x, v)$ and $M \leq N_s^F$;*
2. **for** $n = 0$ **to** n_{tot}
   (a) **for** $i = 1$ **to** N_s^F
      i. *sample M particles $j_1, \ldots, j_M$ uniformly without repetition among all particles;*
      ii. *compute the quantities $\hat{R}_i^{L,n}, \hat{R}_i^{F,n}, \hat{X}_i^n$ and $\hat{Y}_i^n$ from (5.124);*
      iii. *compute the quantities $\hat{A}_i^{L,n}, \hat{A}_i^{F,n}, \hat{V}_i^n$ and $\hat{W}_i^n$ from (5.125);*
      iv. *compute the velocity change v_i^{n+1} according to (5.123);*
      v. *compute the position change*

$$x_i^{n+1} = x_i^n + \Delta t v_i^{n+1}.$$

end for

end for

Remark 18.

- *By using this Monte Carlo algorithm we can reduce the computational cost due to the computation of the interaction term from the original* $\mathcal{O}\left(N_s^{F\,2}\right)$ *to* $\mathcal{O}\left(MN_s^F\right)$. *For* $M = N_s^F$ *we obtain the explicit Euler scheme for the original* N_s^F *particle system.*

5.4 Numerical optimization of leaders strategies

In this section we focus on the numerical realization of the general optimal control problem of type

$$\min_{\mathbf{u}^{\mathrm{opt}}(\cdot)\in U_{adm}} \mathcal{J}(\mathbf{u}^{\mathrm{opt}}), \tag{5.127}$$

constrained to the evolution of microscopic (5.106) or mean-field system (5.118). We observe that the minimization task for evacuation time or total mass can be extremly difficult, due to the strong irregularity and the presence of many local minima.
In order to optimize (5.127) we propose instead an alternative suboptimal, but computationally efficient strategy, named modified Compass Search (CS). This method falls in the class of metaheuristic algorithms, it ensures the convergences towards local minima, without requiring any regularity of the cost functional (20).
We use the CS method in order to optimize the trajectory of the *aware* leaders. The idea is to start from an initial guess $u_k^{\mathrm{opt},(0)}$ which produces an admissible trajectory toward a target exit, for example as follows

$$u_k^{\mathrm{opt},(0)}(t) = \beta\frac{\Xi_k(t) - y_k(t)}{\|\Xi_k(t) - y_k(t)\|} + (1-\beta)(m_F(t) - y_k(t)), \tag{5.128}$$

where $\Xi_k(t)$ is the target position at time t, depending on the environment and such that $\Xi_k(t) = x_e^\tau$ for $t > t_*$. The parameter $\beta \in [0,1]$ measures the tendency of leaders to move toward the target $\Xi_k(t)$ or staying close to followers center of mass $m_F(t)$.
We will refer to (5.128) as "go-to-target" strategy. Then CS method iteratively modifies the current best control strategy found so far computing small random piecewise constant variation of points on the trajectories. Then, if the cost functional decreases, the variation is kept, otherwise it is discarded. We consider piecewise constant trajectories, introducing suitable switching times for the leaders controls.
We summurize this procedure in the following algorithm.

Algorithm 2 (Modified Compass Search)**.**

1. *Select a discrete set of sample times* $S_M = \{t_1, t_2, \ldots, t_M\}$, *the parameters* $j = 0$, j_{max} *and* J_E.

2. *Select an initial strategy* u^* *piecewise constant over the set* S_M, *e.g. constant direction and velocity speed towards a fixed target* $\Xi_k(t)$, $k = 1, \ldots, N^L$, *see Equation* (5.128). *Compute the functional* $\mathcal{J}(\boldsymbol{x}, \boldsymbol{u}^*)$.

3. *Perform a perturbation of the trajectories over a fixed set of points $P^*(t)$ on current optimized leader trajectories with small random variations over the time-set S_M,*

$$P^{(j)}(t_m) = P^*(t_m) + B_m, \quad m = 1, \dots, M, \tag{$\mathcal{P}$}$$

where $B_m \sim Unif([-1,1]^d)$ is a random perturbation and set for $m = 1, \dots, M$,

$$u^{opt,(j)}(t) = \frac{P^*(t_{m+1}) - P^*(t_m)}{\|P^*(t_{m+1}) - P^*(t_m)\|}, \quad t \in [t_m, t_{m+1}].$$

Finally compute $\mathcal{J}(\boldsymbol{x}, \boldsymbol{u}^{(j)})$.

4. `while` $j < j_{max}$ *AND* $\mathcal{J}(\boldsymbol{x}, \boldsymbol{u}^*) < \mathcal{J}_E$

   (a) *Update $j \leftarrow j + 1$.*

   (b) *Perform the perturbation $(\mathcal{P})$ and compute $\mathcal{J}(\boldsymbol{x}, \boldsymbol{u}^{(j)})$.*

   (c) `If` $\mathcal{J}(\boldsymbol{x}, \boldsymbol{u}^{(j)}) \leq \mathcal{J}(\boldsymbol{x}, \boldsymbol{u}^*)$
   set $u^* \leftarrow u^{(j)}$ and $\mathcal{J}(\boldsymbol{x}, \boldsymbol{u}^*) \leftarrow \mathcal{J}(\boldsymbol{x}, \boldsymbol{u}^{(j)})$.

   `repeat`

Remark 19.

- *Compass search does not guarantee the convergence to a global minimizer, on the other hand it offers a good compromise in terms of computational efficiency.*
- *Alternative metaheuristic schemes can be emploied to enanche leader trajectories and improbing the convergence towards the global minimizer, among several possibilities we refer to genetic algorithms, and particle swarm based optimizations.*
- *The synthesis of control strategies via compass search for the microscopic and the mean-field dynamics can produce different results, due to the strong non-linearities of the interactions, and the non-convexity of the functional considered, such as the evacuation time. However, in any case, the solutions retrived by this approach statisfy a local optimality criteria by construction.*

5.5 Numerical experiments

We present three different numerical experiments at microscopic and mesoscopic levels, corresponding to the minimization of cost functionals presented in Section 5.2.2.
Numerical discretization. The dynamics at microscopic level is discretized by a forward Euler scheme with a time step $\Delta t = 0.1$, whereas the evolution of the mean-field dynamics is approximated by MFMCs algorithms. We choose a sample of $\mathcal{O}(10^3)$ particles for the approximation of the density and we reconstruct their evolution in the phase space by kernel density estimator with a multivariate standard normal density function with bandwidth $h = 0.4$. Table 5.5 reports the parameters of the model for the various scenarios unchanged for every test. The number of leaders instead changes and it will be specified later.

Table 5.9: Model parameters for the different scenarios.

N^F	$\mathcal{N}$	C_r^F	C_r^L	C_a^L	C_a^F	C_τ	C_s	s^2	$r \equiv \zeta$	γ
150	20	2	1.5	3	3	1	0.5	0.4	1	1

Obstacles handling. In order to deal with obstacles we use a *cut-off velocity* approach, namely we compute the velocity field first neglecting the presence of the obstacles, then nullifying the component of the velocity vector which points inside the obstacle. This method is used in, e.g., (7, 65, 68) and requires additional conditions to avoid situations where pedestrians stop walking completely because both components of the velocity vector vanish, e.g. in presence of corners, or when obstacles are very close to each other. We refer to (63) for more sophisticated approaches of obstacles handling.

5.5.1 Test 1: Minimum time evacuation with multiple exits

In this first test, leaders aim to minimize the time of evacuation (5.115), hence trying to enforce crowd towards the exit avoiding congestion and ease the outflux of the pedestrian. We assume that leaders informed about exits position follow 'go-to-target' strategy defined as in (5.128), where the target is defined by the different exits and will be specified for each leader. In what follows we account for two different settings comparing microscopic and mesoscopic dynamics.

Setting a) Three exits We consider the case of a room with no obstacles and three exits located at $x_1^\tau = (35, 10)$, $x_2^\tau = (16, 20)$, $x_3^\tau = (10, 10)$ with visibility areas $\Sigma_e = \{x \in \mathbb{R}^2 : |x - x_e^\tau| < 5\}$. We consider two different types of leaders, we call selfish leaders y^{self} the agents who do not care about followers and follow the direction that connects their positions to the exits. While the optimized leaders y^{opt} are aware of their role and they move with the aim to reach the exits and to maintain contact with the crowd, only the trajectories of this type of leaders will be optimized. The admissible leaders trajectories are defined as in Equation (5.128), we choose $\beta = 1$ for selfish leaders, $\beta = 0.6$ for optimized leaders and the target position as $\Xi_k(t) = x_e^\tau \ \forall t$ and for every leader k. At initial time leaders and followers are uniformly distributed in the domain $[17, 29] \times [6.5, 13.5]$ where followers velocities are sampled from a normal distribution with average -0.5 and variance 0.1, hence biased towards the wrong direction. We report in Figure 5.29 the initial configuration for both microscopic and mesoscopic dynamics.
Microscopic case. We consider $N^L = 9$ leaders, three optimized and six unaware leaders. Each leader is associated with an exit: unaware leaders move towards the nearest exit, whereas each optimized leader is assigned to a different exit.
Figure 5.30 shows the evolution of the agents with the go-to-target strategy on the left and with the optimal strategy obtained by the compass search algorithm on the right. As it can be seen in Figure 5.30 with the go-to-target strategy the whole crowd reaches the exit, after 850 time steps. We distinguish optimized leaders y^{opt} with a dashed black line. Optimized movements for leaders are retrived by means of Algorithm 2, with initial guess go-to-target strategy, we report in Figure 5.31 the decrease of the performance function (5.115) as a function of the iterations of compass search. Eventually optimized

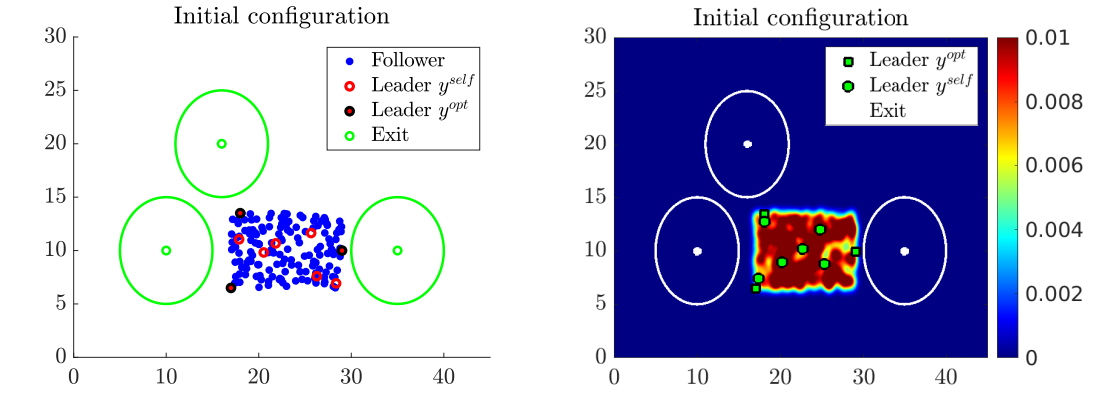

Figure 5.29: *Test 1a.* Minimum time evacuation with multiple exits, initial configuration.

Table 5.10: *Test 1a.* Performance of leader strategies over microscopic dynamics.

	uncontrolled	go-to-target	CS (50 it)
Evacuation time (time steps)	> 1000	850	748
Evacuated mass (percentage)	46%	100%	100%

leaders influence the crowds for a larger amount of time and the total mass is evacuated after 748 time steps, as shown in Table 5.10. Figure 5.32 compares the evacuated mass

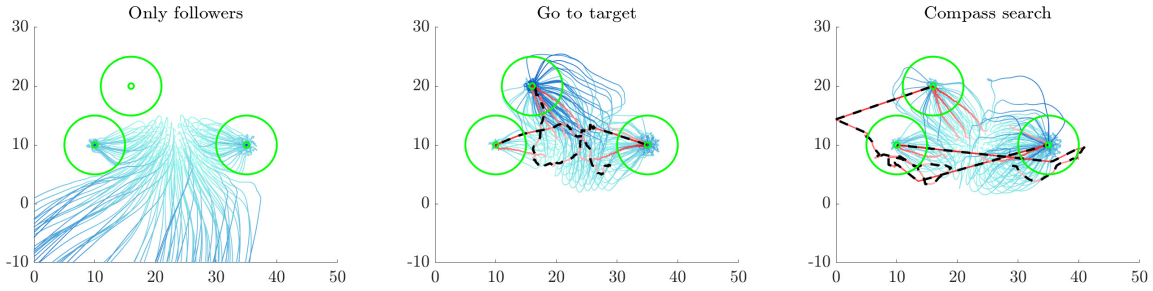

Figure 5.30: *Test 1a.* Microscopic case: minimum time evacuation with multiple exits. On the left the uncontrolled case, in the centre the go-to-target and on the right the optimal compass search strategy.

and the occupancy of the exits visibility zone as a function of time for the uncontrolled case, the go-to-target strategy and the optimal compass search strategy. Dashed lines indicate times of total mass evacuation.

Mesoscopic case. We consider now a continuous density of followers, in the same setting of the previous microscopic case: we account for $N^L = 9$ microscopic leaders moving in a room with no obstacles and three exits. Hence we compare uncontrolled dynamics, go-to-target strategies, and optimized strategies with compass search. In Table 5.11 we show that without any control followers are unable to reach the total evacuation reaching 84% of total mass evacuated. Go-to-target strategy improves total mass evacuated, however, a small part of the mass spreads around the domain and is not able to reach the target exit. Eventually, with optimized strategies, we reach the evacuation of the total mass in

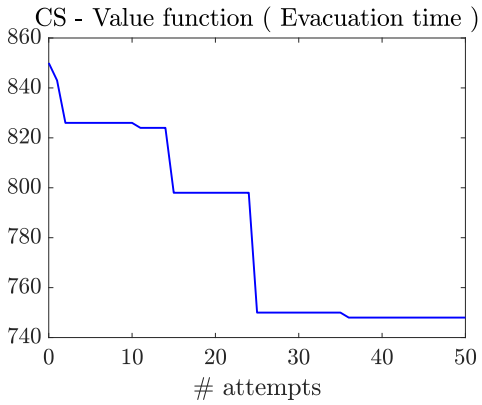

Figure 5.31: *Test 1a.* Microscopic case: decrease of the value function (5.115) as a function of compass search iteration.

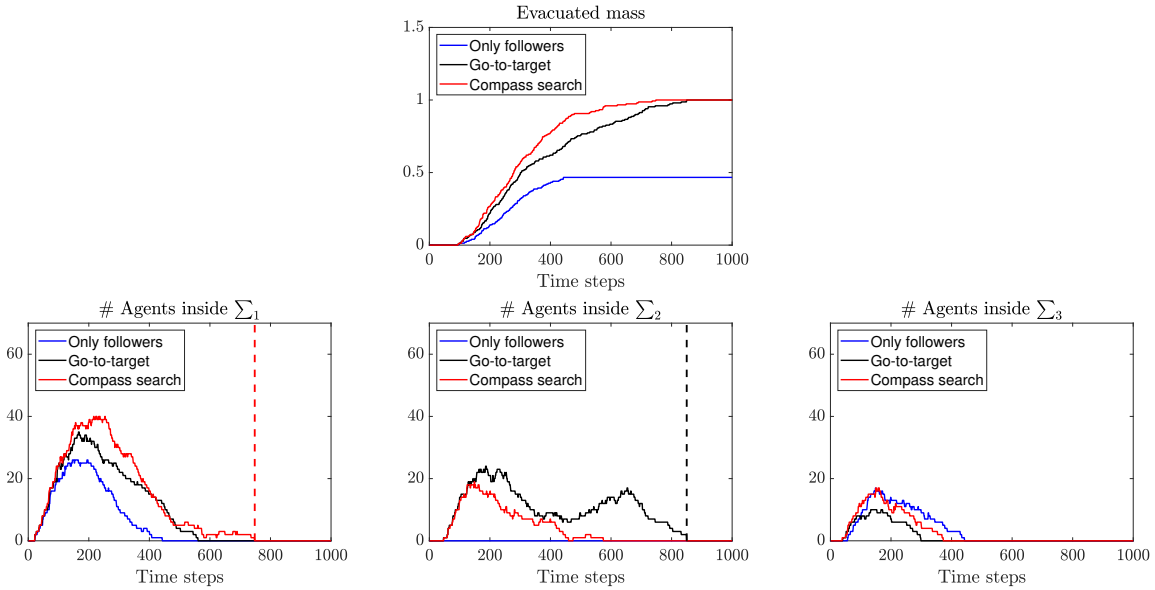

Figure 5.32: *Test 1a.* Microscopic case: minimum time evacuation with multiple exits. Evacuated mass (first row), occupancy of the visibility area Σ_1 (second row, left), Σ_2 (second row, centre) and Σ_3 (second row, right) as a function of time for uncontrolled, go-to-target and optimal compass search strategies. The dot line denotes the time step in which the whole mass is evacuated, the line is black for the go-to-target and red for the optimal compass search strategy.

897 simulation steps. The better performance of the optimized strategy can be observed directly from Figure 5.33, where functional (5.115) is evaluated at subsequent iterations of Algorithm 2. In Figure 5.34 we show three snapshots of the followers density comparing leaders with different strategies and the uncontrolled case. In the upper row, we report the evolution without any control. The middle row shows leaders driven by a go-to-target strategy promoting evacuation of followers density. At time $t = 50$ leaders are moving to influence the followers towards the three exits. At time $t = 100$, the followers mass splits and starts to reach the exits. At time $t = 1000$, complete evacuation is almost reached.

Table 5.11: *Test 1a.* Performance of leader strategies over mesoscopic dynamics.

	uncontrolled	go-to-target	CS (50 it)
Evacuation time (time steps)	> 1000	> 1000	897
Evacuated mass (percentage)	84%	99%	100%

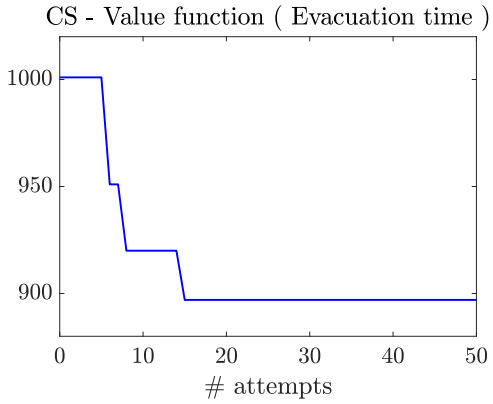

Figure 5.33: *Test 1a.* Mesoscopic case: minimum time evacuation with multiple exits. Decrease of the value function (5.115) as a function of attempts.

The bottom row depicts improved strategies of leaders, where total mass is evacuated at time step 912.
Finally in Figure 5.35 we summarize the results showing the evacuated mass as the cumulative distribution of agents who reached the exit, and the occupancy of the visibility areas in terms of total mass percentage for the various exits. Dashed red line indicates time of complete evacuation.

Setting b) Two exits in a closed environment. Assume now to have a room with walls that contains two exits, $x_1^\tau = (50, 0)$ and $x_2^\tau = (30, 50)$. Followers are uniformely distributed in $[0, 10] \times [0, 10]$. Assume that initially two unaware leaders y^{self} move towards exit x_1^τ with selfish strategy, i.e. $\beta = 0$ in (5.128). Hence the goal is to minimize the total evacuation time as reported in (5.115) introducing two additional leaders y^{opt} moving towards exit x_2^τ, for this two leaders we choose the parameter $\beta = 0.6$ in (5.128). The target position is $\Xi_k(t) = x_e^\tau \ \forall t$ and for every leader k. Figure 5.36 shows the initial configuration in the microscopic and mesoscopic case, and with an initial position of $N^L = 4$ unaware and aware leaders.
Microscopic case. In Figure 5.37 we report the crowd's evolution in various scenarios: left plot shows the trajectories where only unaware leaders are present, in this case, the whole crowd reaches the exit x_1^τ; central and right plots show the influence of two aware leaders moving to x_2^τ respectively with fixed and optimized strategies. Unaware leaders influence the whole crowd to move towards the exit, however generating overcrowding at x_1^τ and leaving some agents getting lost. Introducing two aware leaders with fixed strategies the whole mass is evacuated in 1966 time steps, with optimized strategies evacuation time is further reduced to 1199 time steps. In these last cases, the mass is split between the two exits and hence overcrowding phenomena are reduced. In Table 5.12 the total evacuation time and the corresponding evacuated mass for the three scenarios

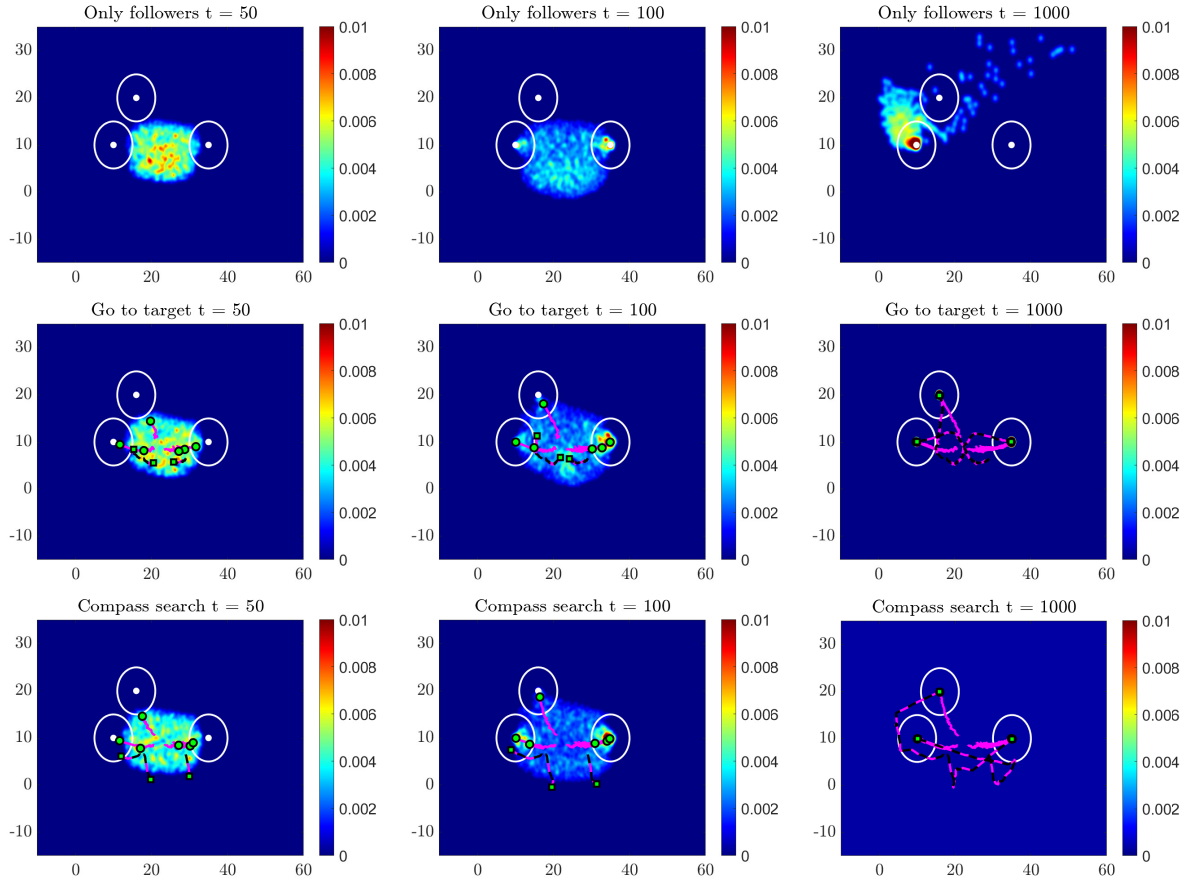

Figure 5.34: *Test 1a.* Three snapshots taken at time $t = 50$, $t = 100$, $t = 1000$ of the mesoscopic densities for the minimum time evacuation with multiple exits. In the upper row the uncontrolled case, in the central row the three aware leaders follows a go-to-target strategy, whereas in the bottom row their trajectories are optimized according to CS algorithm.

are reported, where we indicate that optimized strategy is obtained after 50 iterations of compass search. Finally, in Figure 5.38 we report the occupancy of the visibility areas and the cumulative distribution of the mass evacuate as a function of time for the various scenarios.

Mesoscopic case. We consider now the mean-field approximation of the microscopic setting. We report in Figure 5.39 three snapshots of followers density and trajectories of leaders, for each scenerio. In this case, unaware leaders moving selfishly towards exit x_1^τ are able to influence followers and evacuate 81% at final time, whereas the rest of the mass is congested around the exit. Introducing two aware leaders with a fixed strategy toward x_2^τ is not sufficient to reach total evacuation at final time which is and at final time 95% of the mass is evacuated. The bottom row depicts the case with optimized leaders strategies, in this case, the total mass is evacuated at time step 1750. We summarize the performances of the results in Table 5.13, and in Figure 5.40 we report the occupancy of the visibility areas and the cumulative distribution of mass evacuated as a function of time.

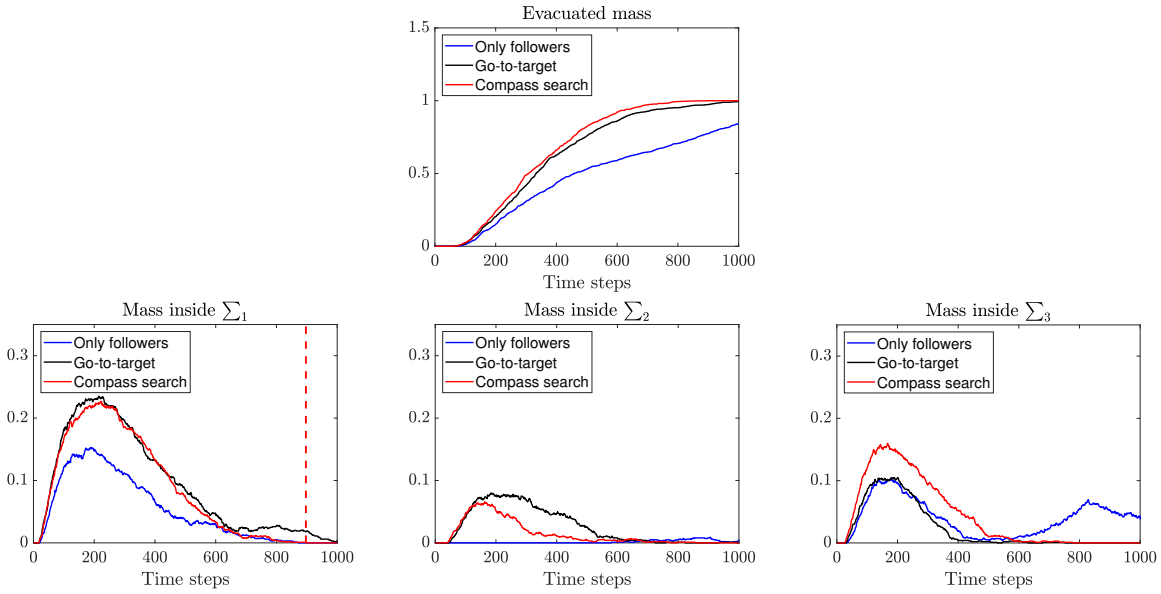

Figure 5.35: *Test 1a.* Mesoscopic case: minimum time evacuation with multiple exits. Evacuated mass (first row), occupancy of the visibility area Σ_1 (second row, left), Σ_2 (second row, centre) and Σ_3 (second row, right) as a function of time for go-to-target and optimal compass search strategies. The dot line denotes the time step in which the whole mass is evacuated with the optimal compass search strategy.

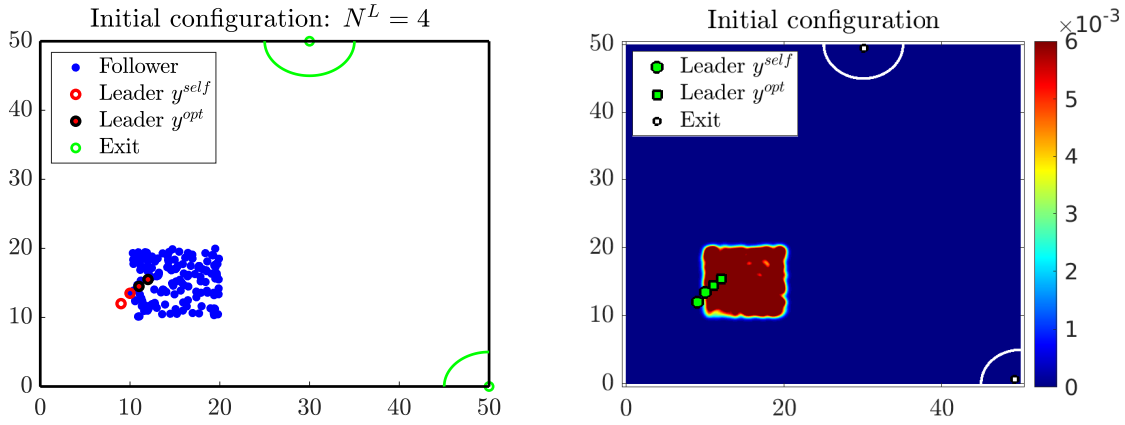

Figure 5.36: *Test 1b.* Minimum time evacuation with multiple exits and obstacles, initial configuration for microscopic and mesoscopic case.

5.5.2 Test 2 : Mass evacuation in presence of obstacles

We consider two rooms, one inside the other, where the internal room is limited by three walls while the external one is bounded by four walls. We assume that walls are nonvisible obstacles, i.e. people can perceive them only by physical contact. This corresponds to an evacuation in case of null visibility (but for the exit points which are still visible from within Σ_1 and Σ_2). Consider the case of two exits, $x_1^\tau = (2, 78)$ and $x_2^\tau = (45, 2)$ positioned in the external room. Figure 5.41 provides a description of the

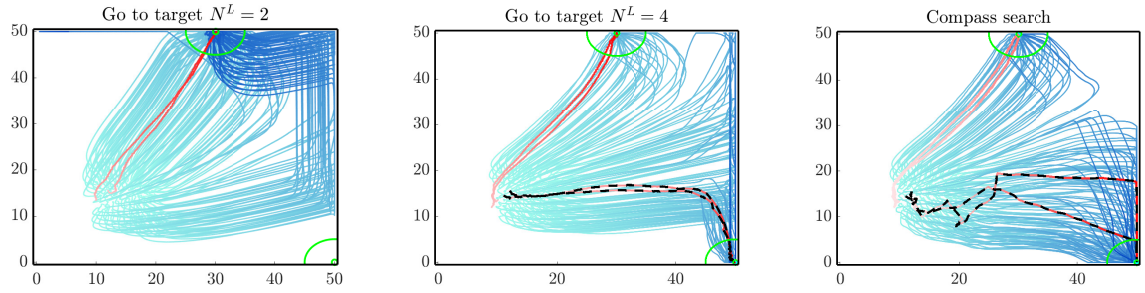

Figure 5.37: *Test 1b.* Microscopic case: minimum time evacuation with multiple exits and obstacles. Go-to-target $N^L = 2$ (left), go-to-target $N^L = 4$ (centre), optimal compass search (right).

Table 5.12: *Test 1b.* Performance of leader strategies over microscopic dynamics.

	go-to-target $N^L = 2$	go-to-target $N^L = 4$	CS (50 it)
Evacuation time (time steps)	>2000	1966	1199
Evacuated mass (percentage)	99%	100%	100%

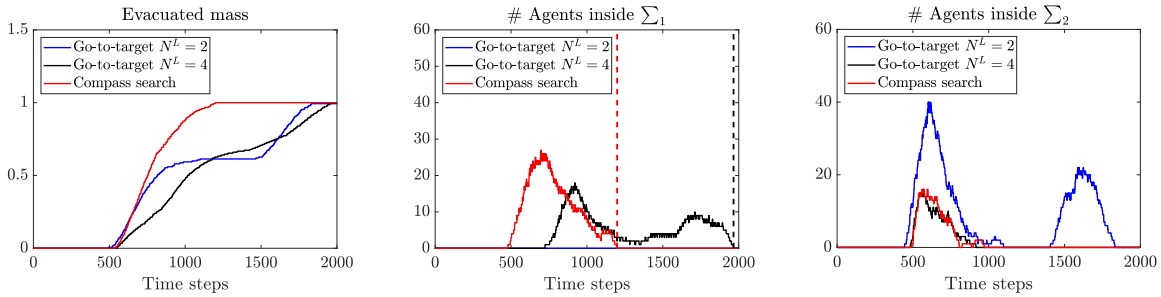

Figure 5.38: *Test 1b.* Microscopic case: minimum time evacuation with multiple exits and obstacles. Evacuated mass (left), occupancy of the visibility area Σ_1 (centre) and Σ_2 (right) as a function of time for go-to-target and optimal compass search strategies. The black and red dot lines denote the time step in which the whole mass is evacuated with the go-to-target ($N^L = 4$) and optimal compass search strategy, respectively.

initial configuration. Note that in order to evacuate, people must first leave the inner room, in which they are initially confined, and then search for exits. Evacuation in presence of obstacles is not always feasible. Instead of minimizing the total evacuation time as in section 5.5.1, we aim to minimize the total mass inside the domain as reported in (5.116) and hence to maximize the total evacuated mass.

Each leader will move toward one of the exits following a go-to-target, similar to (5.128), and such that it is admissible for the configuration of the obstacles. We choose $\beta = 1$ for every leader. The target position is $\Xi_k(t) = x_e^\tau$ for $t > t_*$, while for $t < t_*$ we consider one intermediate point in order to let the leaders to evacuate the inner room.

Microscopic case. We consider $N^L = 6$ leaders, with two aware leaders. Initially, followers have zero velocity. Three leaders, only one aware, will move towards exit x_1^τ, and the

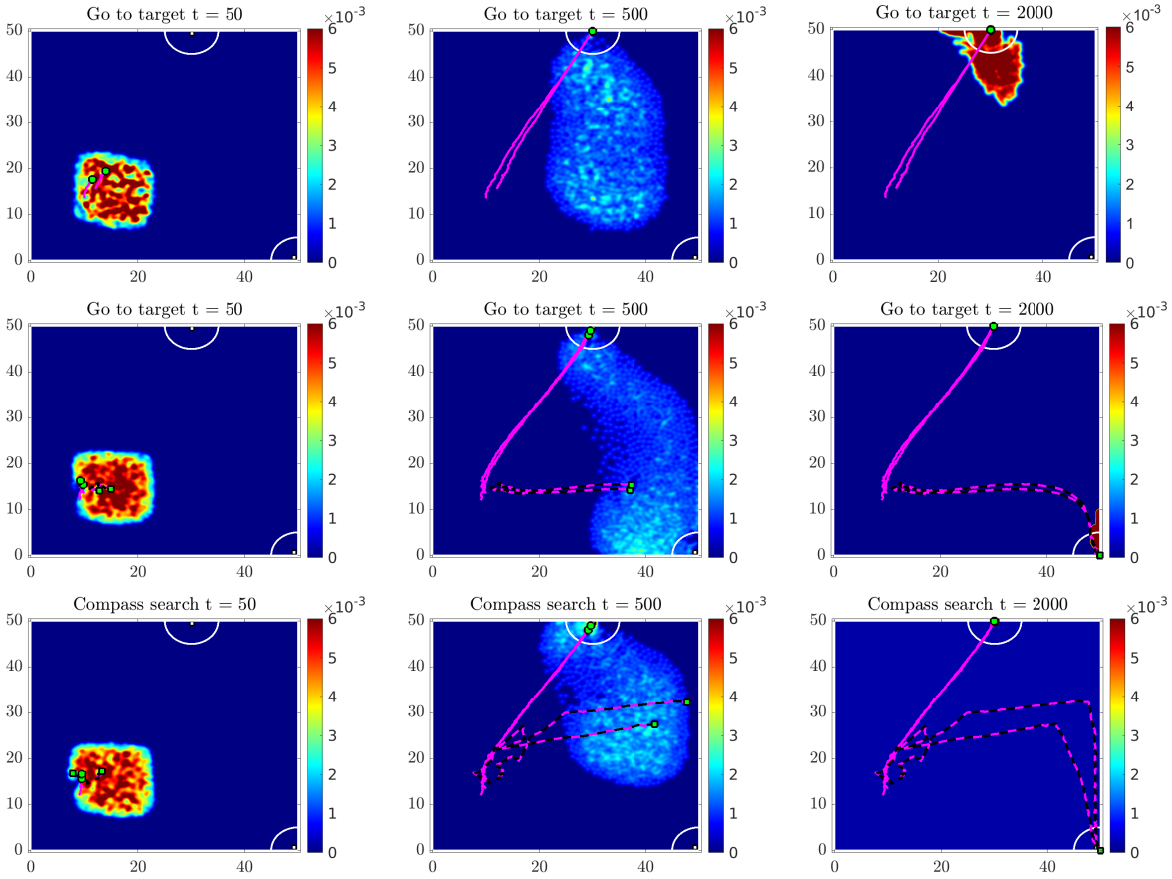

Figure 5.39: *Test 1b.* Mesoscopic case: minimum time evacuation with multiple exits and obstacles. Three snapshots taken at time $t = 50$, $t = 500$, $t = 2000$ with the go-to-target strategy in the case $N^L = 2$ (upper row), $N^L = 4$ (central row) and with the optimized compass-search strategy (lower row).

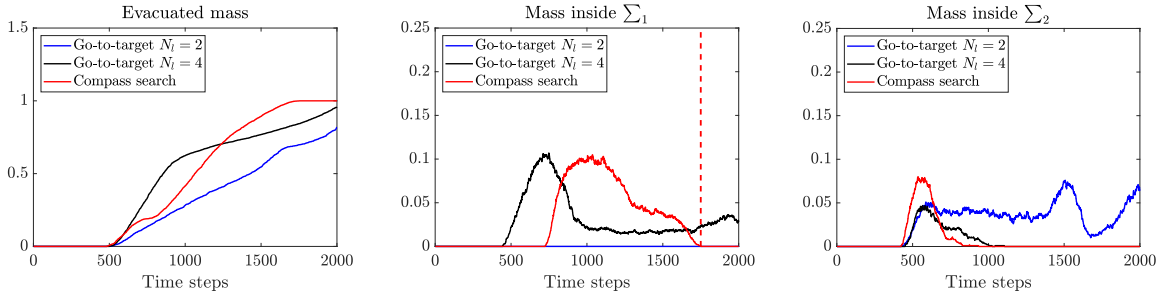

Figure 5.40: *Test 1b.* Mesoscopic case: minimum time evacuation with multiple exits and obstacles. Evacuated mass (left), occupancy of the visibility area Σ_1 (centre) and Σ_2 (right) as a function of time for go-to-target and optimal compass search strategies. The red dot line denotes the time step in which the whole mass is evacuated with the optimal compass search strategy.

Table 5.13: *Test 1b.* Performance of leader strategies over mesoscopic dynamics.

	go-to-target $N^L = 2$	go-to-target $N^L = 4$	CS(50 it)
Evacuation time (time steps)	>2000	>2000	1750
Evacuated mass	81%	95%	100%

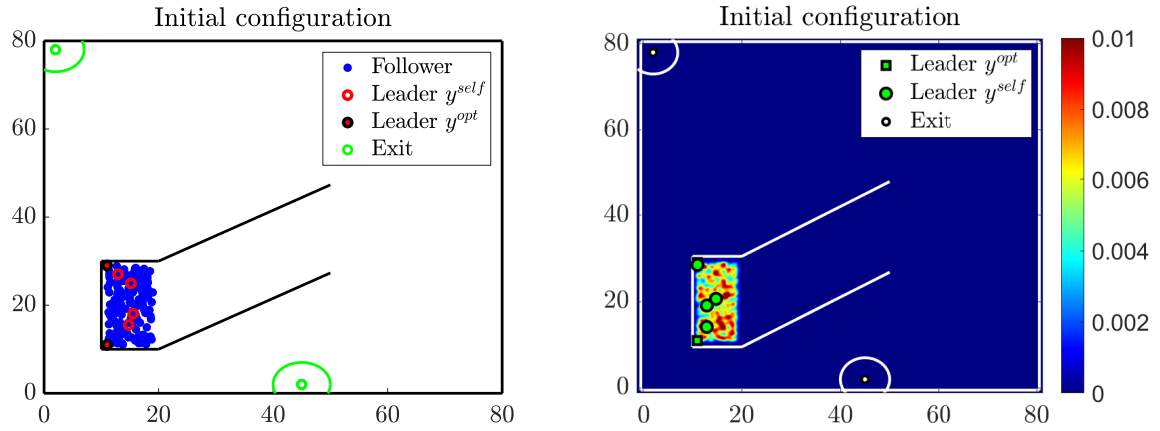

Figure 5.41: *Test 2.* Maximization of mass evacuated in presence of obstacles, initial configuration.

remaining towards exit x_2^τ. We report in Figure 5.42 the evolution with the go-to-target strategy on the left, and with optimized strategies for the two aware leaders on the right. With go-to-target strategy leaders first leave the room and then move towards the exits. Since leaders move rapidly towards the exits, their influence over followers vanishes after a certain time. Indeed, part of the followers hits the right boundary wall and does not reach the exits. Instead, with optimized strategies, leaders are slowed down, as consequence followers are influenced by leaders for a larger amount of time. Table 5.14 reports the comparison between two strategies in terms of evacuated mass, where with only three iterations of the optimization method total evacuation is accomplished. In Figure 5.43 we compare the cumulative distribution of evacuated mass and the occupancy of the exits visibility areas as a function of time for go-to-target strategy and optimized strategy. We remark that with minimal change of the fixed strategy we reach evacuation of the total mass.

Mesoscopic case. Consider now the case of continuous mass of followers, and the equivalent setting as in the microscopic case. Initial configuration is reported in Figure 5.41. We report the evolution of the two scenarios in Figure 5.44, where in the upper row we

Table 5.14: *Test 2.* Performance of various strategies for obstacle case with two exits in the microscopic case.

	go-to-target	CS (3 it)
Evacuation time (time steps)	>3000	2948
Evacuated mass (percentage)	42%	100%

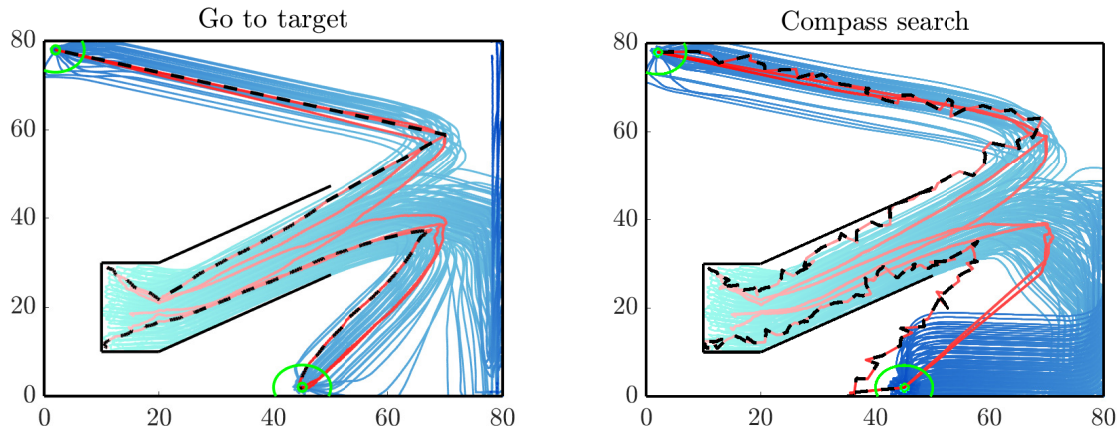

Figure 5.42: *Test 2.* Microscopic case: mass maximization in presence of obstacles. On the left, go-to-target. On the right, optimal compass search.

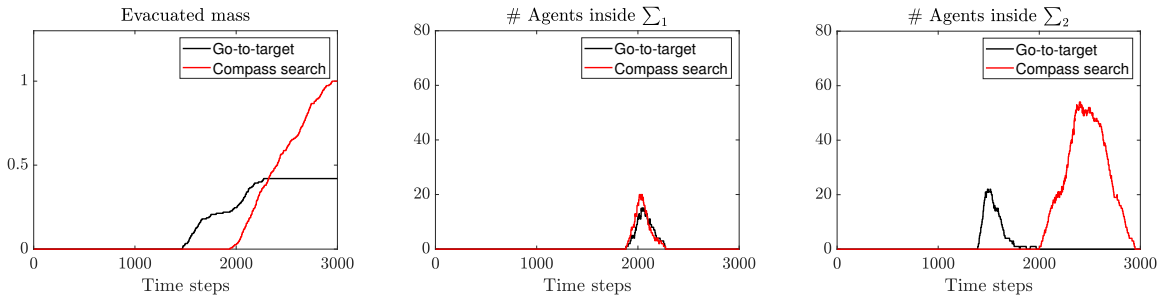

Figure 5.43: *Test 2.* Microscopic case: mass maximization in presence of obstacles. Evacuated mass (left), occupancy of the visibility area Σ_1 (centre) and Σ_2 (right) as a function of time for go-to-target and optimal compass search strategies.

depict three different time frames of the dynamics obtained with go-to-target strategy. Once leaders have moved outside the inner room, at time $t = 1400$, followers mass splits into two parts. However, only leaders moving towards the lower exit x_2^τ are able of steering the followers towards the target, the rest of the followers moving upwards get lost and at final time $t = 3000$ is located close to the left wall. Hence, partial evacuation of followers is achieved, as shown in Table 5.15 we retrieve 78.8% of total mass evacuated. Only one exit is used, this may cause problems of heavy congestion around the exits. Bottom row of Figure 5.44 shows the situation with optimized leaders strategy. Differently from the previous case at time $t = 2380$ the whole mass has been evacuated, part of the followers mass reaches the lower exits and the remaining mass reaches x_1^τ after a while. In Table 5.15 we reported the performances of the two approaches. In Figure 5.45 we compare the evacuated mass and the occupancy of the exits visibility zone as a function of time for go-to-target strategy and opitmized strategy after 5 iterations of compass search method.

Table 5.15: *Test 2.* Performances of total mass evacuation problems in the mesoscopic case.

	go-to-target	CS (5 it)
Evacuation time (time steps)	>3000	2380
Evacuated mass (percentage)	78,8 %	100 %

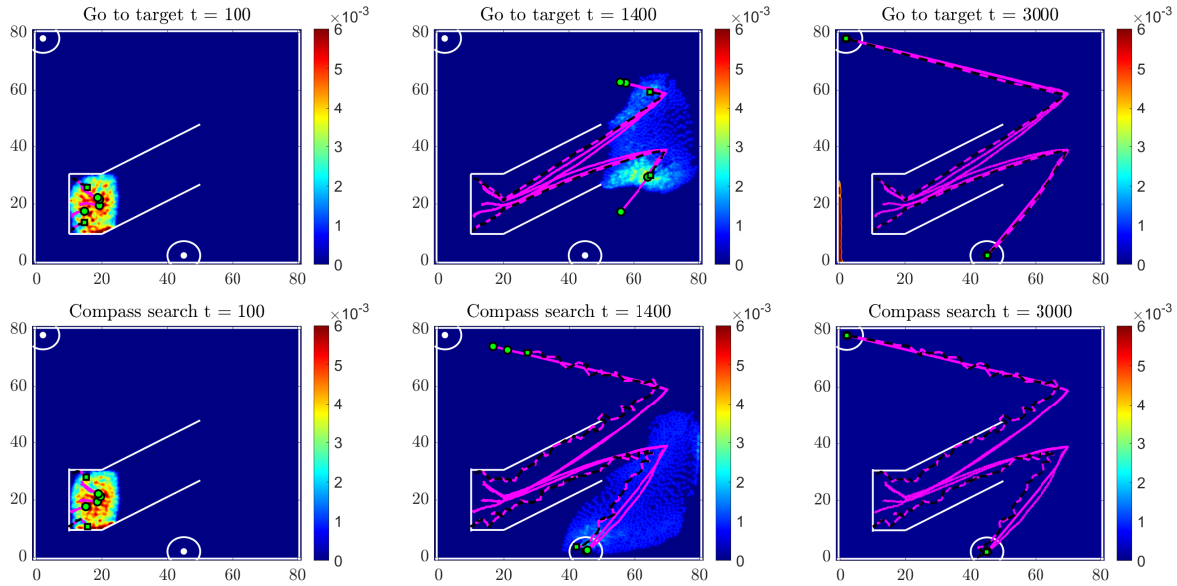

Figure 5.44: *Test 2.* Mesoscopic case: mass maximization in presence of obstacles. Upper row: three snapshots taken at time $t = 100$, $t = 1400$, $t = 3000$ with the go-to-target strategy. Lower row: three snapshots taken at time $t = 100$, $t = 1400$, $t = 3000$ with the optimized compass search strategy.

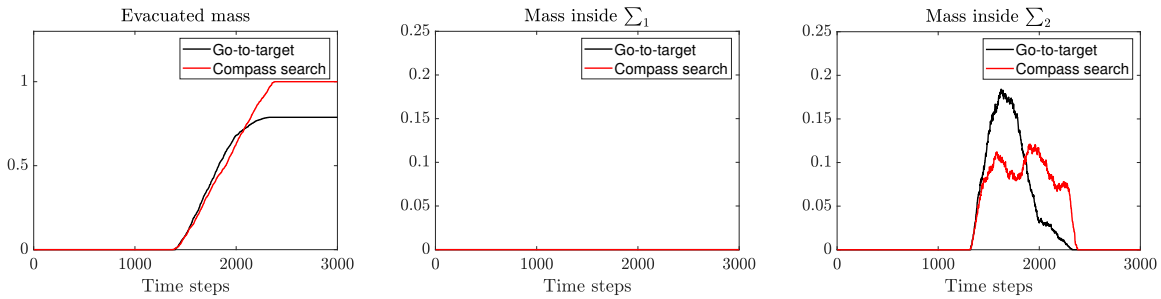

Figure 5.45: *Test 2.* Mesoscopic case: mass maximization in presence of obstacles. Evacuated mass (left), occupancy of the visibility area Σ_1 (centre) and Σ_2 (right) as a function of time for go-to-target and optimal compass search strategies.

5.5.3 Test 3: Optimal mass splitting over multiple exits

Problems of heavy congestions and overcrowding around the exits arise naturally in evacuation and, in real-life situations, they can cause injuries due to over-compression

Table 5.16: *Test 3a.* Performances of mass splitting in the microscopic case.

	go-to-target	CS (50 it)
Evacuation time (time steps)	> 3000	2704
Mass evacuated from E_1	0%	45%
Mass evacuated from x_2^τ	72%	55%
Total mass evacuated	72%	100%

and suffocation. Instead of maximizing the total evacuated mass or the minimum time, we ask to distribute the total evacuated mass at final time T between all the exits as reported in (5.117). The choice of mass redistribution among the different exits can be done according to the specific application and environment. In what follows we consider two different examples, both with two exits, and we will require that mass splits uniformly between the two targets.

Setting 1) Two exits in a close enviroment. As first example we consider the same setting of Test 2, where complete evacuation was achieved, but all followers were directed toward a single exit. In this case we aim to optimize leaders strategies in order to equidistribute the total mass of follower among the two exits.
Microscopic case. In Figure 5.46 we depict the scenario for the fixed strategy and the optimized one. We observe that again with go-to-target strategy the complete evacuation is not achieved. Moreover, since the vast majority of followers reach the lower exit x_2^τ, heavy congestion is formed in the visibility area Σ_2. On the other hand with an optimized strategy two aware leaders slow down their motion spending more time inside the inner room. In this way, followers are split between the two exits, and the entire mass is evacuated at final time. In Table 5.16 we report the performances of the two strategies, where for optimized strategy we have 45% of mass in x_1^τ and 55% in x_2^τ. In Figure 5.47

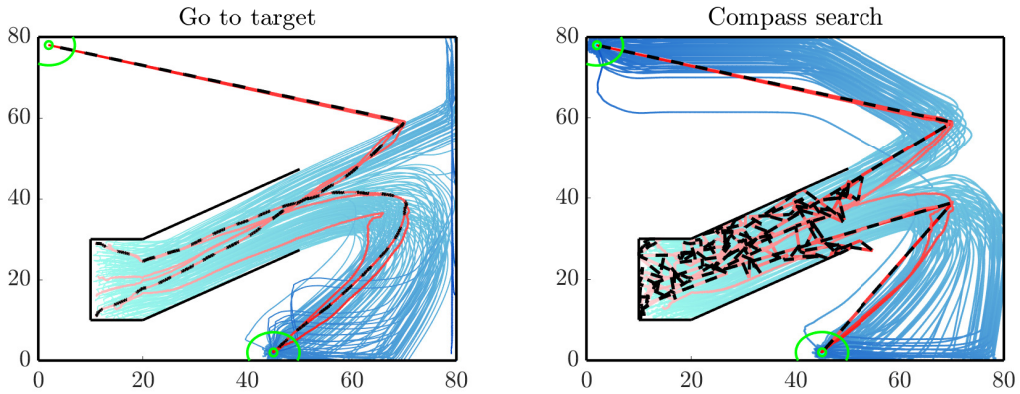

Figure 5.46: *Test 3a.* Microscopic case: mass splitting in presence of obstacles. On the left, go-to-target. On the right, optimal compass search.

we report the evacuated mass and the occupancy of the exits visibility zone as a function of time for go-to-target strategy and optimal compass search strategy. Note that, with the compass search strategy, the whole mass is split between the two exits reducing the overcrowding in the visibility region.

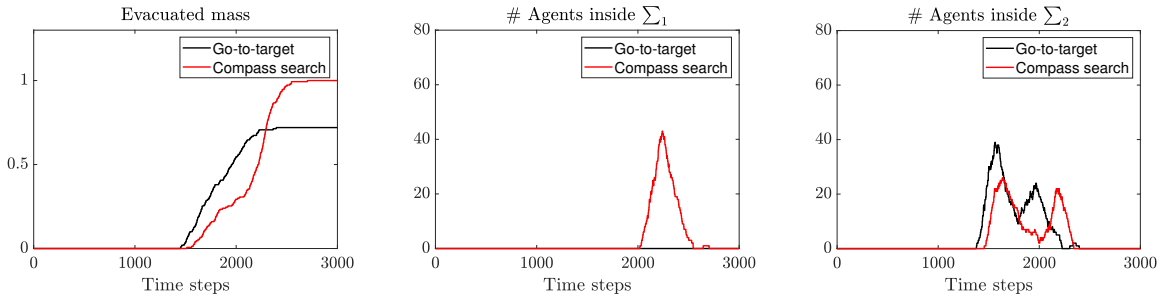

Figure 5.47: *Test 3a.* Microscopic case: mass splitting in presence of obstacles. Evacuated mass (left), occupancy of the visibility area Σ_1 (centre) and Σ_2 (right) as a function of time for go-to-target and optimal compass search strategies.

Table 5.17: *Test 3a.* Performances of mass splitting in the mesoscopic case.

	go-to-target	CS (50 it)
Evacuation time (time steps)	> 3000	> 3000
Mass evacuated from x_1^τ	0%	49%
Mass evacuated from x_2^τ	$78,8\%$	50%
Total mass evacuated	78,8%	99%

Mesoscopic case. We report now the case of a continuum density of followers. For the go-to-target strategy, we consider the same dynamics of the previous test, in this case the mass of followers does not split between the two exits, as shown in Figure 5.44, and the $78,8\%$ reaches exit x_2^τ. In Figure 5.48, three snapshots were taken at three different times with the compass search strategy. At time $t = 100$, leaders move to evacuate the followers mass out of the inner room. At time $t = 1400$, the followers mass splits in two masses, one moving towards the upper and the other towards the lower exits. At time $t = 3000$, almost all the followers mass is evacuated. The mass is split between the two exits as shown in Table 5.17. In Figure 5.45 we compare the evacuated mass and the

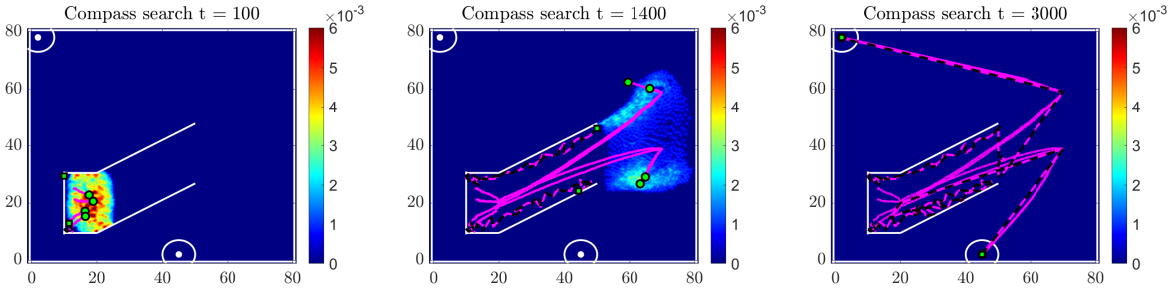

Figure 5.48: *Test 3a.* Mesoscopic case: mass splitting in presence of obstacles. Three snapshots taken at time $t = 100$, $t = 1400$, $t = 3000$ with the optimal compass search strategy. For the go-to-target case we refer to the first row of Figure 5.44.

occupancy of the exits visibility zone as a function of time for go-to-target strategy and optimal compass search strategy. With the compass search technique the occupation of

the visibility areas is reduced since the splitting of the total mass between the two exits is optimized. Hence, the risk of injuries due to overcrowding in real-life situations should be reduced.

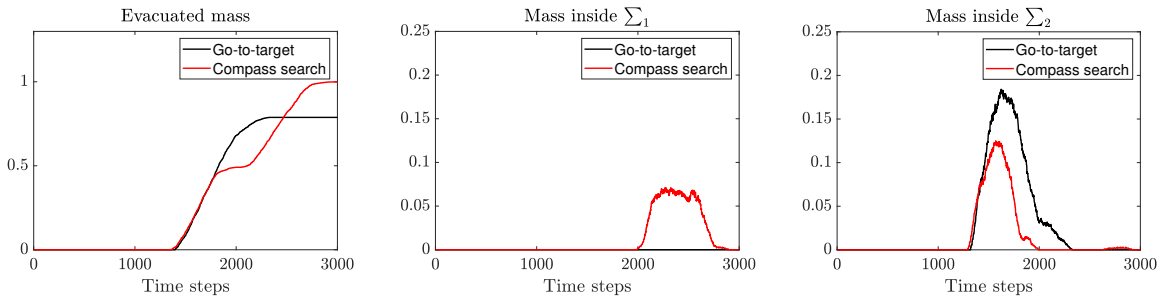

Figure 5.49: *Test 3a.* Mesoscopic case: mass splitting in presence of obstacles. Evacuated mass (left), occupancy of the visibility area Σ_1 (centre) and Σ_2 (right) as a function of time for go-to-target and optimal compass search strategies.

Setting b) Two exits with staircases. Consider two rooms and two exits, limited by walls, positioned at different floors, and connected by a staircase. Each room has an exit located in the bottom right corner. We assume followers and leaders to be uniformly distributed in a square inside the first room. Similar to the previous case, we assume that the model includes eight unaware and two aware leaders in total $N^L = 10$. The admissible leaders trajectories are defined as in Equation (5.128), we choose $\beta = 1$ for every leaders. The target position is $\Xi_k(t) = x_1^\tau \ \forall t$ for the leaders moving towards the exit in the first room. While for the others is $\Xi_k(t) = x_2^\tau$ for $t > t_*$ and for $t < t_*$ we select two intermediate points in such a way that first leaders reach the staircases and then the second room. Indeed, to evacuate, agents must either reach the exit in the first room, called exit x_1^τ, or move towards the staircase, reach the second room and then search for the other exit, called exit x_2^τ. The initial configuration is shown in Figure 5.50.

Microscopic case. Consider $N^L = 10$ leaders. Assume that two leaders are aware of their role while the remaining are selfish leaders. Exits for every leader are chosen at time $t = 0$ in such a way that five unaware leaders move toward exit x_1^τ and the remaining toward exit x_2^τ. Among them, one of the two aware leaders moves towards one exit and the other towards the other exit.

In the case of go-to-target strategy, leaders drive some followers to exit x_1^τ and some others to the staircase. The ones that reach the staircase move from the upper to the lower room and then are driven by leaders to exit x_2^τ. As shown in Figure 5.51 on the left, some followers are able to reach exit x_1^τ and some others to reach the second room. However, since the vast majority of leaders are unaware and move selfishly towards the exits, followers do not evacuate completely. Hence the only exit useful for evacuation is the one placed in the first room, exit x_1^τ, whose visibility area is overcrowded. On the right of Figure 5.51 leaders movement follows an optimized strategy allowing followers to split between the two exits. In this case, complete evacuation is achieved. Table 5.18 reports the performances of the two strategies. With the go-to-target strategy, all the

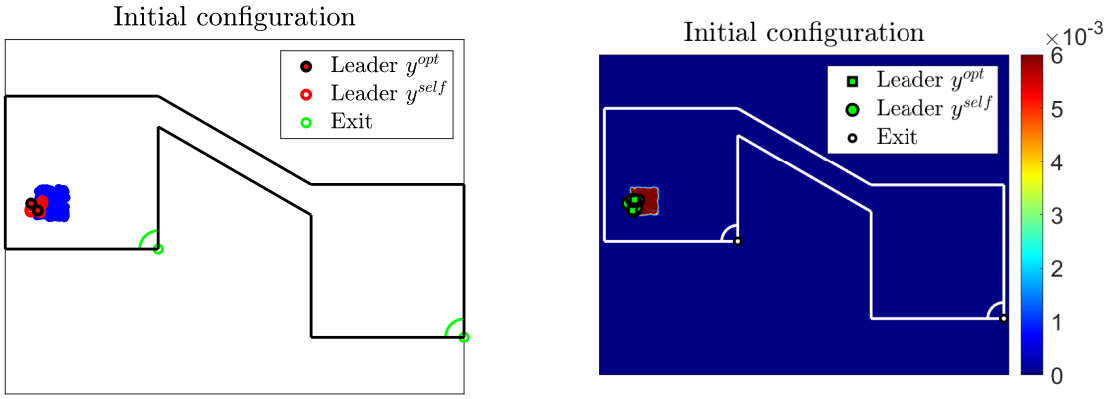

Figure 5.50: *Test 3b.* Mass splitting in presence of staircases, initial configuration.

Table 5.18: *Test 3b.* Performances of mass splitting in the microscopic case.

	go-to-target	CS (50 it)
Evacuation time (time steps)	> 3000	2627
Mass evacuated from x_1^τ	57%	62%
Mass evacuated from x_2^τ	0%	38%
Total mass evacuated	57%	100%

evacuated followers reach the visibility area Σ_1 and hence are evacuated from exit x_1^τ. With an optimized strategy instead, a larger amount of followers is evacuated and the overcrowding of the visibility areas is reduced.
In Figure 5.52 we compare the evacuated mass and the occupancy of the exits visibility zone as a function of time for go-to-target strategy and optimal compass search strategy. Note that, with the compass search strategy, the whole mass is split between the two exits while with the go-to-target strategy the evacuated mass reaches only exit x_1^τ.

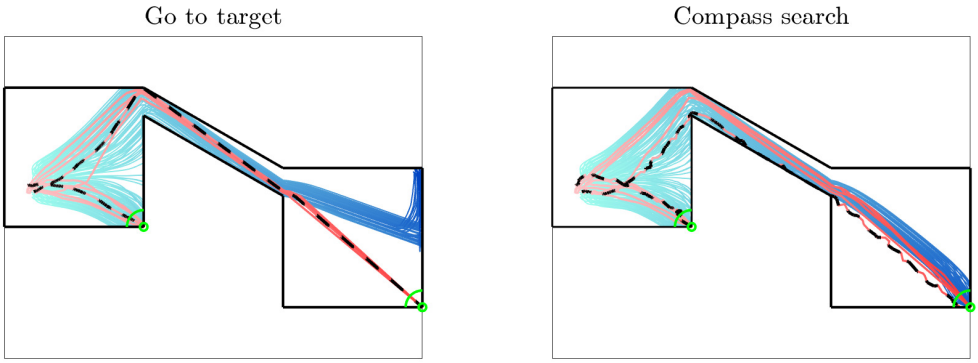

Figure 5.51: *Test 3b.* Microscopic case: mass splitting in presence of staircases. On the left, go-to-target. On the right, compass search.

Mesoscopic case. Consider the case of a continuous mass of followers. Similar to the

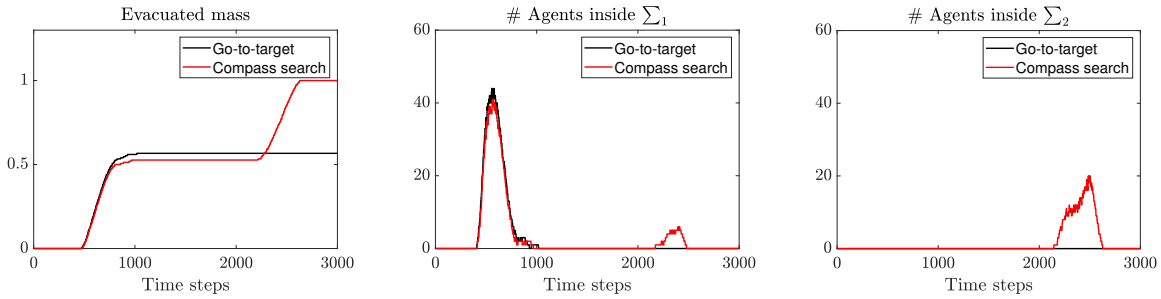

Figure 5.52: *Test 3b.* Microscopic case: mass splitting in presence of obstacles. Evacuated mass (left), occupancy of the visibility area Σ_1 (centre) and Σ_2 (right) as a function of time for go-to-target and compass search strategies.

Table 5.19: *Test 3b.* Performances of mass splitting in the mesoscopic case.

	go-to-target	CS (50 it)
Evacuation time (time steps)	> 3000	> 3000
Mass evacuated from x_1^τ	$46,6\%$	51%
Mass evacuated from x_2^τ	$1,2\%$	48%
Total mass evacuated	$47,8\%$	99%

microscopic case we observe in Figure 5.53 the evolution of the dynamics with fixed strategy and with the optimized one. The upper row shows that with the go-to-target strategy the total evacuated mass is not split between the two exits since just the $1,2\%$ of mass reaches exit x_2^τ. However, as shown in Table 5.19 a larger percentage of followers reaches exit x_1^τ and the remaining part spreads in the second room without evacuate.
The lower row of Figure 5.53 shows the dynamics obtained with the optimized compass search strategy. At the time $t = 500$ a larger follower mass is moving towards the staircase. At time $t = 3000$ almost all the mass is evacuated and split between the two exits. In Table 5.19 we compare the two strategies showing that with the compass search technique it is possible to improve the mass splitting.
In Figure 5.54 we compare the evacuated mass and the occupancy of the exits visibility zone as a function of time for go-to-target strategy and optimal compass search strategy. Note that, with the compass search strategy a larger percentage of mass reaches exit x_2^τ than with the go-to-target strategy.

5.6 Discussion and comparision

In the previous tests we have considered different scenarios to create more complex situations in relation to the functionals chosen, (157). In general, given a ceratin setting, it is difficult to choose the optimal number of leaders that guarantee evacuation, and a high number of leaders does not necessarily imply better evacuation efficiency, see for example (134). Another challenging aspect is to give an uniform measure of the performance of the different strategies in such different contexts. A viable option is to quantify the congestion around the exits to exclude dangerous situations. Following the

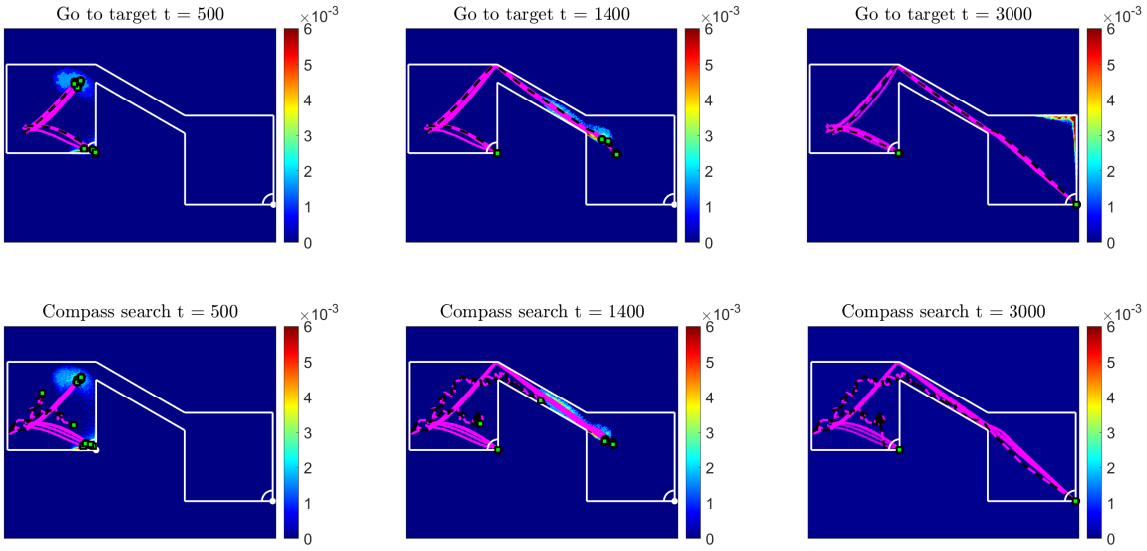

Figure 5.53: *Test 3b.* Mesoscopic case: mass splitting in presence of staircases. Upper row: three snapshots taken at time $t = 500$, $t = 1400$, $t = 3000$ with the go-to-target strategy. Lower row: three snapshots taken at time $t = 500$, $t = 1400$, $t = 3000$ with the optimized compass search strategy.

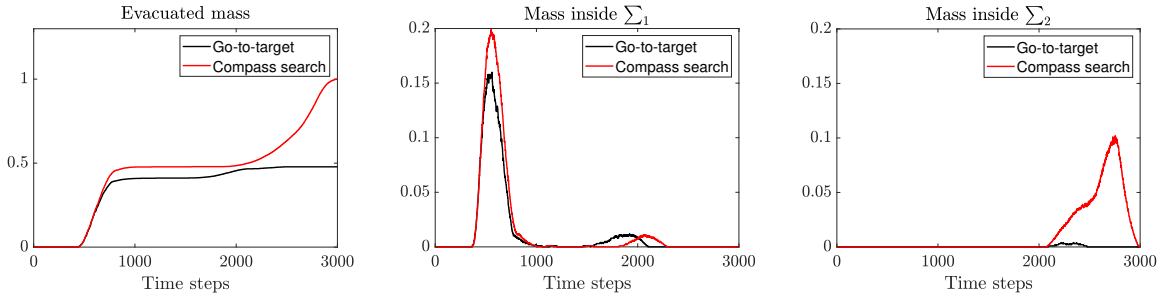

Figure 5.54: *Test 3b.* Mesoscopic case: mass splitting in presence of obstacles. Evacuated mass (left), occupancy of the visibility area Σ_1 (centre) and Σ_2 (right) as a function of time for go-to-target and optimal compass search strategies.

idea in (91) we consider the congestion value

$$cong_{\Sigma_i}(t) = \rho_{\Sigma_i}(t) var_{\Sigma_i}(v(t))$$

where $\rho_{\Sigma_i}(t)$ is the number of agents (mass) in the microscopic (mesoscopic) case inside Σ_i at time t and

$$var_{\Sigma_i}(v(t)) = \frac{1}{\rho_{\Sigma_i}(t)} \sum_{j \in \Sigma_i} \left(|v_j(t)| - s\right)^2 .$$

We consider also m_{Σ_i} the maximum number of pedestrians over time inside the visibility area Σ_i and l_{Σ_i} the percentage of time in which the visibility area Σ_i is not empty, finally we denote by M_{Σ_i} the percentage of mass inside Σ_i in the mesoscopic case.

In this way we can compare the congestion of the various exits for different settings, showing that the more desiderable situations are when $cong_{\Sigma_i}$ and m_{Σ_i} (M_{Σ_i}) are small and l_{Σ_i} is high.
We reported in Table 5.20 and Table 5.21 respectively the values for the microscopic and the mesoscopic setting.

Table 5.20: Comparison of the congestion in the visibility areas for the microscopic case. In red the maximum value of $cong_{\Sigma_i}$ among the visibility areas Σ_i.

	$cong_{\Sigma_1}$	$cong_{\Sigma_2}$	$cong_{\Sigma_3}$	m_{Σ_1}	m_{Σ_2}	m_{Σ_3}	l_{Σ_1}	l_{Σ_2}	l_{Σ_3}
Test 1a	0.039	0.011	0.012	40	19	17	0.73	0.51	0.33
Test 1b	0.013	0.009	-	27	16	-	0.36	0.22	-
Test 2	0.009	0.056	-	20	54	-	0.13	0.31	-
Test 3a	0.035	0.027	-	43	26	-	0.19	0.29	-
Test 3b	0.024	0.006	-	41	20	-	0.28	0.16	-

Table 5.21: Comparison of the congestion in the visibility areas for the mesoscopic case. In red the maximum value of $cong_{\Sigma_i}$ among the visibility areas Σ_i.

	$cong_{\Sigma_1}$	$cong_{\Sigma_2}$	$cong_{\Sigma_3}$	M_{Σ_1}	M_{Σ_2}	M_{Σ_3}	l_{Σ_1}	l_{Σ_2}	l_{Σ_3}
Test 1a	0.025	0.005	0.016	0.22	0.6	0.16	0.88	0.79	0.75
Test 1b	0.010	0.005	-	0.1	0.08	-	0.51	0.26	-
Test 2	0	0.009	-	0	0.12	-	0	0.36	-
Test 3a	0.005	0.011	-	0.07	0.12	-	0.3	0.32	-
Test 3b	0.013	0.004	-	0.2	0.1	-	0.41	0.3	-

Finally, Figures 5.55-5.56 show the mean velocity and the congestion level for the case of evacuation with three exits (*Test 1a*) in the microscopic and mesoscopic case respectively. These plots underline that if the congestion level is higher then the mean velocity is lower.

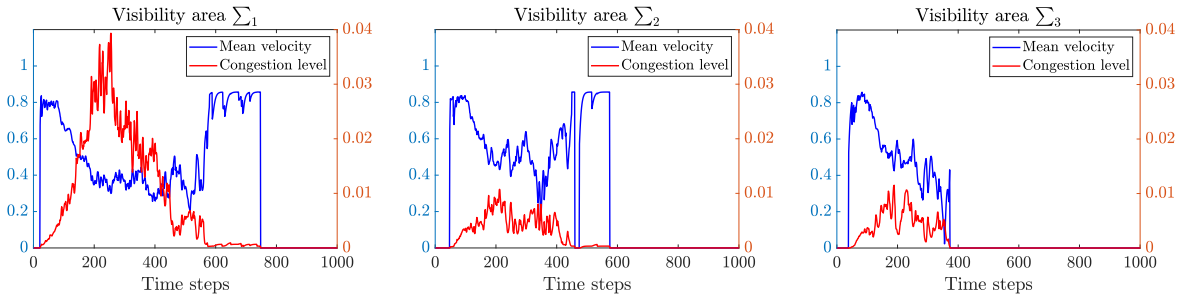

Figure 5.55: *Test 1a.* Microscopic case: number of agents and mean velocity of the visibility areas.

5.7 Conclusions

This work has been devoted to the study of optimized strategies for the control of egressing pedestrians in an unknown environment. In particular, we studied situations with

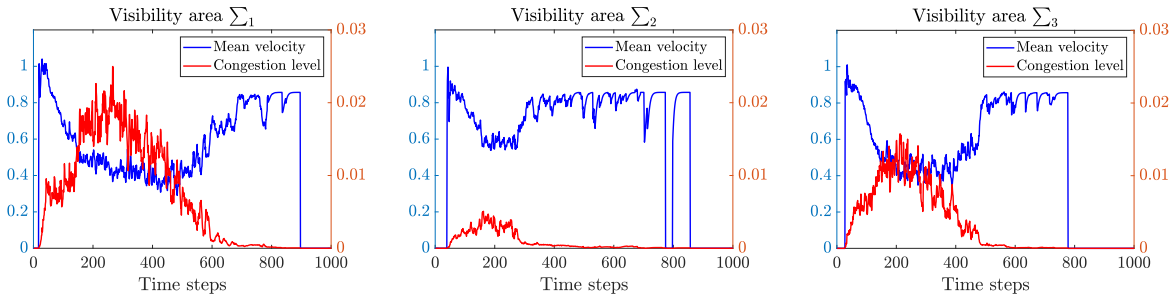

Figure 5.56: *Test 1a.* Mesoscopic case: mass of agents and mean velocity of the visibility areas.

complex environments where multiple exits and obstacles are present. Few informed agents act as controllers over the crowd, without being recognized as such. Indeed it has been shown that minimal intervention can change completely the behavior of a large crowd, and at the same time avoiding adversarial behaviors. On the other hand, we observed that if part of the informed agents moves without coordinated action, this may cause critical situations, such as congestion around the exit. Hence it is important to have a clear understanding of different strategies to enhance the safe evacuation of the crowd. To this end, we explored various optimization tasks such as minimum time evacuation, maximization of mass evacuated, and optimal mass distribution among exits. We investigated these dynamics at the various scales: from the microscopic scale of agent-based systems to the statistical description of the system given by mesoscopic scale. Numerically we proposed an efficient scheme for the simulation of the mean-field dynamics, whereas we use a meta-heuristic approach for the synthesis of optimized leaders strategies. The proposed numerical experiments suggest that the optimization of leaders movements is enough to de-escalate critical situations.
Different questions arise at the level of control through leaders with multiple exits and obstacles. In such a rich environment several research directions can be explored, such as optimal positioning and amount of leaders within the crowd, or different type of cooperative strategies among different groups of leaders to optimally distribute the followers crowd.

6 Acknowledgments

Inizio questi ringraziamenti dal mio supervisore Giacomo Albi, grazie per il supporto, la pazienza, gli insegnamenti e le spiegazioni che non mi hai mai fatto mancare in questi anni, grazie per il tuo equilibrio, per avere spinto nei momenti opportuni e avermi lasciato più spazio quando ne ho avuto bisogno. Grazie per avermi sempre permesso e consigliato di viaggiare, ampliando le mie conoscenze accademiche e personali, anche vedendo posti bellissimi e divertendomi. Grazie per avermi aiutata a mantenere il ritmo giusto anche durante il particolare periodo della pandemia. Questa tesi non sarebbe stata tale senza il tuo aiuto, è un onore essere stata la tua prima dottoranda. E grazie ancora per avermi dato la possibilità di conoscere e collaborare con importanti professori e colleghi, a questo riguardo ringrazio i Professori Dante Kalise e Michael Herty per il vostro aiuto e le vostre collaborazioni, in particolare Michael per l'ospitalità ricevuta ad Aachen durante le mie settimane di visita accademica e per avermi dimostrato una grande fiducia proponendomi la mia attuale posizione di ricerca.
Ringrazio i Professori Lorenzo Pareschi e Bertram Düring per avere accettato di revisionare la mia tesi, grazie per avermi dedicato il vostro tempo e per le vostre incoraggianti parole. Ringrazio i Professori del secondo piano di Ca Vignal 2, Marco e Nicola per essere stati presenti e comprensivi durante un periodo difficile, e il Professore Marigonda per l'infinita pazienza nell'ascoltarmi e le lunghe chiacchierate, per aiutarmi sempre a credere in me stessa.
Grazie ai colleghi con cui ho collaborato, Franco, Federica e Giuseppe, per avermi fatto scoprire quanto è più bella e stimolante la ricerca se fatta in compagnia.
Grazie a tutti i compagni d'ufficio che ho avuto in questi anni per avere alleggerito le giornate di lavoro e a tutti gli amici di Verona per le infinite serate del mercoledì.
Grazie in particolare a Fabio, perché in te sono sicura di avere trovato un vero amico.
Grazie a Rossana, per la tua spensieratezza e le divertenti serate passate insieme, ma anche per la tua sensibilità, per i racconti condivisi, i tuoi consigli e le parole al momento giusto, per supportarmi e sopportarmi anche e soprattutto nei momenti più difficili, so che su di te potrò sempre contare anche se dall'altra parte del mondo.
Grazie ai miei nuovi colleghi di Aachen per esservi mostrati gentili e disponibili fin dal primo giorno, in particolare a Elisa, per avermi permesso d'iniziare una nuova avventura potendo contare sulla vicinanza di un'amica.
Grazie ai colleghi e amici che ho conosciuto nei numerosi viaggi, per condividere sempre la passione, le aspettative, le paure, i continui alti e bassi del nostro lavoro, grazie per non farmi sentire sola anche quando sono lontana da casa.
Grazie ai miei più cari amici, ad Alessandro e Nicola e grazie a Giulia, Silvia, Pietro ed Eleonora, perché anche se ci vediamo poco, la nostra amicizia e pazzia è sempre la stessa che avevamo tra i banchi del liceo, grazie perché con voi rido sinceramente come con nessun altro faccio.
Un grazie infinito alle mie due amiche del cuore, Martina e Ilaria, per essere sempre i miei punti di riferimento, per la nostra amicizia sincera, per condividere tutto ciò che ci rende così simili e rispettare ciò che ci rende allo stesso tempo estremamente diverse. Grazie perché ci siete ogni giorno, nonostante la distanza, grazie per accettarmi sempre per quella che sono, e aiutarmi a scoprire passo dopo passo ciò che voglio diventare.
Grazie infine alla mia famiglia, per il calore che posso sentire solo a casa, grazie a Miriam,

Marco e Roberto, grazie in particolare a mio fratello e a mia sorella per avermi aiutata a diventare la donna che sono oggi e per avermi fatto il regalo più grande di essere zia di Nicolò, Diego e Nicole, grazie a voi ragazzi perché riuscite, con un semplice abbraccio, a ricordarmi sempre che ne vale la pena, questa tesi è dedicata a voi.
Grazie a mia mamma e a mio papà per il vostro supporto durante tutti i miei studi e per avermi dato da sempre massima fiducia, rispetto e libertà in tutte le mie scelte.
E grazie anche a me stessa, per avere avuto il coraggio d'intraprendere questo viaggio e avere avuto ancora più coraggio nel portarlo a termine. Grazie a chi ne ha fatto parte, perché il mio viaggio siete stati voi.

References

[1] A. Abdelghany, K. Abdelghany, H. Mahmassani, and W. Alhalabi. Modeling framework for optimal evacuation of large-scale crowded pedestrian facilities. *European J. Oper. Res.*, 237(3):1105–1118, 2014.

[2] M. Aduamoah, B. D. Goddard, J. W. Pearson, and J. C. Roden. PDE-Constrained optimization models and pseudospectral methods for multiscale particle dynamics. arXiv:2009.09850, 2020.

[3] J. P. Agnelli, F. Colasuonno, and D. Knopoff. A kinetic theory approach to the dynamic of crowd evacuation from bounded domains. *Math. Models Methods Appl. Sci.*, 25(1):109–129, 2015.

[4] G. Albi, N. Bellomo, L. Fermo, S.-Y. Ha, J. Kim, L. Pareschi, D. Poyato, and J. Soler. Vehicular traffic, crowds, and swarms: from kinetic theory and multiscale methods to applications and research perspectives. *Math. Models Methods Appl. Sci.*, 29(10):1901–2005, 2019.

[5] G. Albi, N. Bellomo, L. Fermo, S.-Y. Ha, J. Kim, L. Pareschi, D. Poyato, and J. Soler. Vehicular traffic, crowds, and swarms: from kinetic theory and multiscale methods to applications and research perspectives. *Math. Models Methods Appl. Sci.*, 29(10):1901–2005, 2019.

[6] G. Albi, M. Bongini, E. Cristiani, and D. Kalise. Invisible control of self-organizing agents leaving unknown environments. *SIAM J. Appl. Math.*, 76(4):1683–1710, 2016.

[7] G. Albi, M. Bongini, E. Cristiani, and D. Kalise. Invisible control of self-organizing agents leaving unknown environments. *SIAM J. Appl. Math.*, 76(4):1683–1710, 2016.

[8] G. Albi, Y.-P. Choi, M. Fornasier, and D. Kalise. Mean field control hierarchy. *Appl. Math. Optim.*, 76(1):93–135, 2017.

[9] G. Albi, Y.-P. Choi, M. Fornasier, and D. Kalise. Mean field control hierarchy. *Applied Mathematics & Optimization*, 76(1):93–135, 2017.

[10] G. Albi, E. Cristiani, L. Pareschi, and D. Peri. Mathematical models and methods for crowd dynamics control. In *Crowd Dynamics, Volume 2*, pages 159–197. Springer, 2020.

[11] G. Albi, M. Fornasier, and D. Kalise. A boltzmann approach to mean-field sparse feedback control. *IFAC-PapersOnLine*, 50(1):2898–2903, 2017.

[12] G. Albi, M. Herty, D. Kalise, and C. Segala. Moment-driven predictive control of mean-field collective dynamics, 2021.

[13] G. Albi, M. Herty, and L. Pareschi. Kinetic description of optimal control problems and applications to opinion consensus. *Commun. Math. Sci.*, 13(6):1407–1429, 2015.

[14] G. Albi and L. Pareschi. Binary interaction algorithms for the simulation of flocking and swarming dynamics. *Multiscale Model. Simul.*, 11(1):1–29, 2013.

[15] G. Albi and L. Pareschi. Binary interaction algorithms for the simulation of flocking and swarming dynamics. *Multiscale Modeling & Simulation*, 11(1):1–29, 2013.

[16] G. Albi and L. Pareschi. Modeling of self-organized systems interacting with a few individuals: from microscopic to macroscopic dynamics. *Appl. Math. Lett.*, 26:397–401, 2013.

[17] G. Albi, L. Pareschi, and M. Zanella. Boltzmann-type control of opinion consensus through leaders. *Philos. Trans. R. Soc. Lond. Ser. A Math. Phys. Eng. Sci.*, 372(2028):20140138, 18, 2014.

[18] G. Albi, L. Pareschi, and M. Zanella. Boltzmann-type control of opinion consensus through leaders. *Phil. Trans. R. Soc. A*, 372:20140138/1–18, 2014.

[19] G. Albi, L. Pareschi, and M. Zanella. Uncertainty quantification in control problems for flocking models. *Mathematical Problems in Engineering*, 2015, 04 2015.

[20] C. Audet, K.-C. Dang, and D. Orban. Optimization of algorithms with OPAL. *Math. Prog. Comp.*, 6(3):233–254, 2014.

[21] B. Azmi, D. Kalise, and K. Kunisch. Optimal feedback law recovery by gradient-augmented sparse polynomial regression. arXiv:2007.09753, 2020.

[22] B. Azmi and K. Kunisch. A hybrid finite-dimensional RHC for stabilization of time-varying parabolic equations. *SIAM J. Control Optim.*, 57(5):3496–3526, 2019.

[23] H. Babovsky and H. Neunzert. On a simulation scheme for the boltzmann equation. *Math. Methods Appl. Sci.*, 8(1):223–233, 1986.

[24] R. Bailo, M. Bongini, J. A. Carrillo, and D. Kalise. Optimal consensus control of the cucker-smale model. *IFAC-PapersOnLine*, 51(13):1 – 6, 2018.

[25] R. Bailo, M. Bongini, J. A. Carrillo, and D. Kalise. Optimal consensus control of the cucker-smale model. *IFAC-PapersOnLine*, 51(13):1–6, 2018.

[26] R. Bailo, J. A. Carrillo, and P. Degond. Pedestrian models based on rational behaviour. In *Crowd Dynamics, Volume 1*, pages 259–292. Springer, 2018.

[27] D. Balagué, J. A. Carrillo, T. Laurent, and G. Raoul. Nonlocal interactions by repulsive-attractive potentials: radial ins/stability. *Phys. D*, 260:5–25, 2013.

[28] M. Ballerini, N. Cabibbo, R. Candelier, A. Cavagna, E. Cisbani, I. Giardina, A. Orlandi, G. Parisi, A. Procaccini, M. Viale, et al. Empirical investigation of starling flocks: a benchmark study in collective animal behaviour. *Animal behaviour*, 76(1):201–215, 2008.

[29] J. Barzilai and J. M. Borwein. Two-point step size gradient methods. *IMA journal of numerical analysis*, 8(1):141–148, 1988.

[30] T. Başar and P. Bernhard. *H-infinity optimal control and related minimax design problems: a dynamic game approach*. Springer Science & Business Media, 2008.

[31] A. Beck. *First-order methods in optimization*. SIAM, 2017.

[32] N. Bellomo and J. Soler. On the mathematical theory of the dynamics of swarms viewed as complex systems. *Math. Models Methods Appl. Sci.*, 22(suppl. 1):1140006, 29, 2012.

[33] A. Blanchet and P. Degond. Kinetic models for topological nearest-neighbor interactions. *J. Stat. Phys.*, 169(5):929–950, 2017.

[34] A. Bobylev and K. Nanbu. Theory of collision algorithms for gases and plasmas based on the Boltzmann equation and the Landau-Fokker-Planck equation. *Phys. Rev. E*, 61(4):4576, 2000.

[35] M. Bongini and M. Fornasier. Sparse stabilization of dynamical systems driven by attraction and avoidance forces. *Networks & Heterogeneous Media*, 9(1):1, 2014.

[36] M. Bongini, M. Fornasier, M. Hansen, and M. Maggioni. Inferring interaction rules from observations of evolutive systems i: The variational approach. *Mathematical Models and Methods in Applied Sciences*, 27(05):909–951, 2017.

[37] M. Bongini, M. Fornasier, and D. Kalise. (Un)conditional consensus emergence under perturbed and decentralized feedback controls. *Discrete Contin. Dyn. Syst.*, 35(9):4071–4094, 2015.

[38] M. Bongini, M. Fornasier, F. Rossi, and F. Solombrino. Mean-field pontryagin maximum principle. *Journal of Optimization Theory and Applications*, 175(1):1–38, 2017.

[39] A. Borzì and S. Wongkaew. Modeling and control through leadership of a refined flocking system. *Math. Models Methods Appl. Sci.*, 25(2):255–282, 2015.

[40] L. Boudin and F. Salvarani. A kinetic approach to the study of opinion formation. *M2AN Math. Model. Numer. Anal.*, 43(3):507–522, 2009.

[41] S. Boyd, L. El Ghaoui, E. Feron, and V. Balakrishnan. *Linear matrix inequalities in system and control theory*. SIAM, 1994.

[42] A. Bressan and B. Piccoli. *Introduction to the mathematical theory of control*, volume 1. American institute of mathematical sciences Springfield, 2007.

[43] L. M. Briceño Arias, D. Kalise, and F. J. Silva. Proximal methods for stationary mean field games with local couplings. *SIAM J. Control Optim.*, 56(2):801–836, 2018.

[44] M. Burger, R. Pinnau, C. Totzeck, and O. Tse. Mean-field optimal control and optimality conditions in the space of probability measures. *SIAM Journal on Control and Optimization*, 59(2):977–1006, 2021.

[45] M. Burger, R. Pinnau, C. Totzeck, O. Tse, and A. Roth. Instantaneous control of interacting particle systems in the mean-field limit. *J. Comput. Phys.*, 405:109181, 20, 2020.

[46] M. Burger, R. Pinnau, C. Totzeck, O. Tse, and A. Roth. Instantaneous control of interacting particle systems in the mean-field limit. *Journal of Computational Physics*, 405:109181, 2020.

[47] E. F. Camacho and C. B. Alba. *Model predictive control*. Springer Science & Business Media, 2013.

[48] E. J. Candes, J. K. Romberg, and T. Tao. Stable signal recovery from incomplete and inaccurate measurements. *Communications on Pure and Applied Mathematics: A Journal Issued by the Courant Institute of Mathematical Sciences*, 59(8):1207–1223, 2006.

[49] J. A. Canizo, J. A. Carrillo, and J. Rosado. A well-posedness theory in measures for some kinetic models of collective motion. *Math. Models Methods Appl. Sci.*, 21(03):515–539, 2011.

[50] M. Caponigro, M. Fornasier, B. Piccoli, and E. Trélat. Sparse stabilization and optimal control of the Cucker-Smale model. *Math. Control Relat. Fields*, 3(4):447–466, 2013.

[51] M. Caponigro, M. Fornasier, B. Piccoli, and E. Trélat. Sparse stabilization and control of alignment models. *Math. Models Methods Appl. Sci.*, 25(3):521–564, 2015.

[52] J. A. Carrillo, Y.-P. Choi, and M. Hauray. The derivation of swarming models: mean-field limit and Wasserstein distances. In *Collective dynamics from bacteria to crowds*, pages 1–46. Springer, 2014.

[53] J. A. Carrillo, M. Fornasier, G. Toscani, and F. Vecil. Particle, kinetic, and hydrodynamic models of swarming. In *Mathematical modeling of collective behavior in socio-economic and life sciences*, pages 297–336. Springer, 2010.

[54] J. A. Carrillo, S. Martin, and M.-T. Wolfram. An improved version of the Hughes model for pedestrian flow. *Math. Models Methods Appl. Sci.*, 26(4):671–697, 2016.

[55] J. A. Carrillo, L. Pareschi, and M. Zanella. Particle based gPC methods for mean-field models of swarming with uncertainty. *Communications in Computational Physics*, 25(2):508–531, 2018.

[56] J. Cheng, B. Hofmann, M. Fornasier, H. Rauhut, J. Borwein, L. D. Russell, C. Byrne, P. Eggermont, M. Burger, B. Kaltenbacher, et al. Handbook of mathematical methods in imaging: Volume 1. 2015.

[57] Y.-P. Choi, D. Kalise, J. Peszek, and A. A. Peters. A collisionless singular Cucker-Smale model with decentralized formation control. *SIAM J. Appl. Dyn. Syst.*, 18(4):1954–1981, 2019.

[58] E. N. M. Cirillo and A. Muntean. Dynamics of pedestrians in regions with no visibility - A lattice model without exclusion. *Physica A*, 392:3578–3588, 2013.

[59] M. A. Cohen and S. Grossberg. Absolute stability of global pattern formation and parallel memory storage by competitive neural networks. *IEEE transactions on systems, man, and cybernetics*, (5):815–826, 1983.

[60] R. M. Colombo and M. Lécureux-Mercier. Nonlocal crowd dynamics models for several populations. *Acta Mathematica Scientia*, 32(1):177–196, 2012.

[61] S. Cordier, L. Pareschi, and G. Toscani. On a kinetic model for a simple market economy. *J. Stat. Phys.*, 120(1-2):253–277, 2005.

[62] I. D. Couzin, J. Krause, N. R. Franks, and S. A. Levin. Effective leadership and decision-making in animal groups on the move. *Nature*, 433:513–516, 2005.

[63] E. Cristiani and D. Peri. Handling obstacles in pedestrian simulations: Models and optimization. *Appl. Math. Model.*, 45:285–302, 2017.

[64] E. Cristiani and D. Peri. Robust design optimization for egressing pedestrians in unkwnown environments. *Appl. Math. Model.*, 72:553–568, 2019.

[65] E. Cristiani, B. Piccoli, and A. Tosin. Multiscale modeling of granular flows with application to crowd dynamics. *Multiscale Model. Simul.*, 9:155–182, 2011.

[66] E. Cristiani, B. Piccoli, and A. Tosin. *Multiscale modeling of pedestrian dynamics*, volume 12 of *MS&A. Model. Simul. Appl.* Springer, Cham, 2014.

[67] E. Cristiani, B. Piccoli, and A. Tosin. *Multiscale Modeling of Pedestrian Dynamics*. Modeling, Simulation & Applications. Springer, 2014.

[68] E. Cristiani, F. S. Priuli, and A. Tosin. Modeling rationality to control self-organization of crowds: An environmental approach. *SIAM J. Appl. Math.*, 75(2):605–629, 2015.

[69] F. Cucker and S. Smale. Emergent behavior in flocks. *IEEE Trans. Automat. Control*, 52(5):852–862, 2007.

[70] F. Cucker and S. Smale. Emergent behavior in flocks. *IEEE Trans. Autom. Contr.*, 52(5):852–862, 2007.

[71] F. Cucker and S. Smale. On the mathematics of emergence. *Japanese Journal of Mathematics*, 2(1):197–227, 2007.

[72] P. Degond, S. Göttlich, M. Herty, and A. Klar. A network model for supply chains with multiple policies. *Multiscale Model. Simul.*, 6(3):820–837, 2007.

[73] P. Degond, M. Herty, and J.-G. Liu. Flow on sweeping networks. *Multiscale Model. Simul.*, 12(2):538–565, 2014.

[74] P. Degond, J.-G. Liu, S. Motsch, and V. Panferov. Hydrodynamic models of self-organized dynamics: derivation and existence theory. *Methods Appl. Anal.*, 20(2):89–114, 2013.

[75] P. Degond and S. Motsch. Continuum limit of self-driven particles with orientation interaction. *Math. Models Methods Appl. Sci.*, 18(suppl.):1193–1215, 2008.

[76] P. Degond and M. Pulvirenti. Propagation of chaos for topological interactions. *Ann. Appl. Probab.*, 29(4):2594–2612, 2019.

[77] M. Di Francesco and S. Fagioli. Measure solutions for non-local interaction pdes with two species. *Nonlinearity*, 26(10):2777, 2013.

[78] M. Di Francesco, P. A. Markowich, J.-F. Pietschmann, and M.-T. Wolfram. On the hughes' model for pedestrian flow: The one-dimensional case. *Journal of Differential Equations*, 250(3):1334–1362, 2011.

[79] G. Dimarco, R. Caflisch, and L. Pareschi. Direct simulation Monte Carlo schemes for coulomb interactions in plasmas. *Commun. Appl. Ind. Math.*, 1(1):72–91, 2010.

[80] G. Dimarco, L. Pareschi, and M. Zanella. Uncertainty quantification for kinetic models in socio–economic and life sciences. In *Uncertainty quantification for hyperbolic and kinetic equations*, pages 151–191. Springer, 2017.

[81] S. Dolgov, D. Kalise, and K. Kunisch. Tensor decompositions for high-dimensional hamilton-jacobi-bellman equations. arXiv:1908.01533, 2019.

[82] D. L. Donoho. Compressed sensing. *IEEE Transactions on information theory*, 52(4):1289–1306, 2006.

[83] G.-R. Duan and H.-H. Yu. *LMIs in control systems: analysis, design and applications*. CRC press, 2013.

[84] H. Duan and C. Sun. Swarm intelligence inspired shills and the evolution of cooperation. *Sci. Rep.*, 4:5210, 2014.

[85] G. E. Dullerud and F. Paganini. *A course in robust control theory: a convex approach*, volume 36. Springer Science & Business Media, 2013.

[86] B. Düring, P. Markowich, J.-F. Pietschmann, and M.-T. Wolfram. Boltzmann and Fokker-Planck equations modelling opinion formation in the presence of strong leaders. *Proc. R. Soc. A*, 465:3687–3708, 2009.

[87] J. R. Dyer, A. Johansson, D. Helbing, I. D. Couzin, and J. Krause. Leadership, consensus decision making and collective behaviour in humans. *Philos. Trans. Roy. Soc. B*, 364(1518):781–789, 2009.

[88] M. R. D'Orsogna, Y.-L. Chuang, A. L. Bertozzi, and L. S. Chayes. Self-propelled particles with soft-core interactions: patterns, stability, and collapse. *Phys. Rev. Lett.*, 96(10):104302, 2006.

[89] A. Eqtami, D. V. Dimarogonas, and K. J. Kyriakopoulos. Event-based model predictive control for the cooperation of distributed agents. In *2012 Amer. Control Conf.*, pages 6473–6478, 2012.

[90] G. Estrada-Rodriguez and H. Gimperlein. Interacting particles with Lévy strategies: limits of transport equations for swarm robotic systems. *SIAM J. Appl. Math.*, 80(1):476–498, 2020.

[91] C. Feliciani and K. Nishinari. Measurement of congestion and intrinsic risk in pedestrian crowds. *Transportation research part C: emerging technologies*, 91:124–155, 2018.

[92] A. Festa, A. Tosin, and M.-T. Wolfram. Kinetic description of collision avoidance in pedestrian crowds by sidestepping. *Kinet. Relat. Models*, 11(3):491–520, 2018.

[93] M. Fornasier, J. Haskovec, and G. Toscani. Fluid dynamic description of flocking via the Povzner-Boltzmann equation. *Phys. D*, 240(1):21–31, 2011.

[94] M. Fornasier, S. Lisini, C. Orrieri, and G. Savaré. Mean-field optimal control as gamma-limit of finite agent controls. *European J. Appl. Math.*, 30(6):1153–1186, 2019.

[95] M. Fornasier, B. Piccoli, and F. Rossi. Mean-field sparse optimal control. *Philos. Trans. R. Soc. Lond. Ser. A Math. Phys. Eng. Sci.*, 372(2028):20130400, 21, 2014.

[96] M. Fornasier, B. Piccoli, and F. Rossi. Mean-field sparse optimal control. *Philosophical Transactions of the Royal Society A: Mathematical, Physical and Engineering Sciences*, 372(2028):20130400, 2014.

[97] M. Fornasier and F. Solombrino. Mean-field optimal control. *ESAIM Control Optim. Calc. Var.*, 20(4):1123–1152, 2014.

[98] M. Fornasier and F. Solombrino. Mean-field optimal control. *ESAIM Control Optim. Calc. Var.*, 20(4):1123–1152, 2014.

[99] G. F. Franklin, J. D. Powell, A. Emami-Naeini, and J. D. Powell. *Feedback control of dynamic systems*, volume 4. Prentice hall Upper Saddle River, 2002.

[100] G. Freudenthaler and T. Meurer. PDE-based multi-agent formation control using flatness and backstepping: analysis, design and robot experiments. *Automatica*, 115:108897, 13, 2020.

[101] J. Garnier, G. Papanicolaou, and T.-W. Yang. Consensus convergence with stochastic effects. *Vietnam J. Math.*, 45(1-2):51–75, 2017.

[102] J. Gómez-Serrano, C. Graham, and J.-Y. Le Boudec. The bounded confidence model of opinion dynamics. *Math. Models Methods Appl. Sci.*, 22(2):1150007, 46, 2012.

[103] L. Grüne and J. Pannek. Nonlinear model predictive control. In *Nonlinear model predictive control*, pages 45–69. Springer, 2017.

[104] R.-Y. Guo, H.-J. Huang, and S. C. Wong. Route choice in pedestrian evacuation under conditions of good and zero visibility: experimental and simulation results. *Transportation Res. B*, 46(6):669–686, 2012.

[105] S.-Y. Ha and E. Tadmor. From particle to kinetic and hydrodynamic descriptions of flocking. *Kinet. Relat. Models*, 1(3):415–435, 2008.

[106] J. Han, M. Li, and L. Guo. Soft control on collective behavior of a group of autonomous agents by a shill agent. *Jrl. Syst. Sci. & Complexity*, 19(1):54–62, 2006.

[107] J. Han and L. Wang. Nondestructive intervention to multi-agent systems through an intelligent agent. *PLoS ONE*, 8(5):e61542, 2013.

[108] Y. Han, A. Hegyi, Y. Yuan, S. Hoogendoorn, M. Papageorgiou, and C. Roncoli. Resolving freeway jam waves by discrete first-order model-based predictive control of variable speed limits. *Transportation Research Part C: Emerging Technologies*, 77:405–420, 2017.

[109] J. Haskovec. Flocking dynamics and mean-field limit in the Cucker-Smale-type model with topological interactions. *Phys. D*, 261:42–51, 2013.

[110] R. Hegselmann, U. Krause, et al. Opinion dynamics and bounded confidence models, analysis, and simulation. *Journal of artificial societies and social simul.*, 5(3), 2002.

[111] D. Helbing, I. Farkas, and T. Vicsek. Simulating dynamical features of escape panic. *Nature*, 407:487–490, 2000.

[112] M. Herty and D. Kalise. Suboptimal nonlinear feedback control laws for collective dynamics. In *2018 IEEE 14th Intern. Conf. on Control and Automat. (ICCA)*, pages 556–561, 2018.

[113] M. Herty and L. Pareschi. Fokker-Planck asymptotics for traffic flow models. *Kinet. Relat. Models*, 3(1):165–179, 2010.

[114] M. Herty, L. Pareschi, and S. Steffensen. Mean–field control and Riccati equations. *Netw. Heterog. Media*, 10(3):699, 2015.

[115] M. Herty, L. Pareschi, and S. Steffensen. Mean-field control and Riccati equations. *Netw. Heterog. Media*, 10(3):699–715, 2015.

[116] M. Herty and C. Ringhofer. Averaged kinetic models for flows on unstructured networks. *Kinet. Relat. Models*, 4(4):1081–1096, 2011.

[117] M. Herty and C. Ringhofer. Feedback controls for continuous priority models in supply chain management. *Comput. Methods Appl. Math.*, 11(2):206–213, 2011.

[118] M. Herty and C. Ringhofer. Consistent mean field optimality conditions for interacting agent systems. *Communications in Mathematical Sciences*, 17(4):1095–1108, 2019.

[119] M. Herty and M. Zanella. Performance bounds for the mean-field limit of constrained dynamics. *Discrete Contin. Dyn. Syst.*, 37(4):2023, 2017.

[120] J. Hu and S. Jin. Uncertainty quantification for kinetic equations. In *Uncertainty quantification for hyperbolic and kinetic equations*, pages 193–229. Springer, 2017.

[121] J. Hu, S. Jin, and D. Xiu. A stochastic galerkin method for hamilton–jacobi equations with uncertainty. *SIAM Journal on Scientific Computing*, 37(5):A2246–A2269, 2015.

[122] S. Jin, L. Li, and J.-G. Liu. Random Batch Methods (RBM) for interacting particle systems. *J. Comput. Phys.*, 400:108877, 2020.

[123] S. Jin, D. Xiu, and X. Zhu. A well-balanced stochastic galerkin method for scalar hyperbolic balance laws with random inputs. *Journal of Scientific Computing*, 67(3):1198–1218, 2016.

[124] D. Kalise, K. Kunisch, and Z. Rao. Infinite horizon sparse optimal control. *Journal of Optimization Theory and Applications*, 172(2):481–517, 2017.

[125] Y. Katz, K. Tunstrøm, C. C. Ioannou, C. Huepe, and I. D. Couzin. Inferring the structure and dynamics of interactions in schooling fish. *Proceedings of the National Academy of Sciences*, 108(46):18720–18725, 2011.

[126] I. Khalil, J. Doyle, and K. Glover. *Robust and optimal control*. prentice hall, new jersey, 1996.

[127] A. Lachapelle and M.-T. Wolfram. On a mean field game approach modeling congestion and aversion in pedestrian crowds. *Transportation research part B: methodological*, 45(10):1572–1589, 2011.

[128] O. Le Maître and O. M. Knio. *Spectral methods for uncertainty quantification: with applications to computational fluid dynamics*. Springer Science & Business Media, 2010.

[129] P. Lin and Y. Jia. Robust h-infinity consensus analysis of a class of second-order multi-agent systems with uncertainty. *IET control theory & applications*, 4(3):487–498, 2010.

[130] J. Liu, Y. Zhang, H. Liu, Y. Yu, and C. Sun. Robust event-triggered control of second-order disturbed leader-follower mass: A nonsingular finite-time consensus approach. *International Journal of Robust and Nonlinear Control*, 29(13):4298–4314, 2019.

[131] S. Liu, M. Jacobs, W. Li, L. Nurbekyan, and S. J. Osher. Computational methods for nonlocal mean field games with applications.

[132] Y. Liu and Y. Jia. Robust h-infinity consensus control of uncertain multi-agent systems with time delays. *International Journal of Control, Automation and Systems*, 9, 12 2011.

[133] Y. Luo and W. Zhu. Event-triggered h-infinity finite-time consensus control for nonlinear second-order multi-agent systems with disturbances. *Advances in Difference Equations*, 2021(1):1–19, 2021.

[134] Y. Ma, R. K. K. Yuen, and E. W. M. Lee. Effective leadership for crowd evacuation. *Physica A: Statistical Mechanics and its Applications*, 450:333–341, 2016.

[135] D. Q. Mayne, J. B. Rawlings, C. V. Rao, and P. O. Scokaert. Constrained model predictive control: Stability and optimality. *Automatica*, 36(6):789–814, 2000.

[136] L. P. Mo, H. Y. Zhang, and H. Y. Hu. Finite-time h-infinity consensus of multi-agent systems with a leader. In *Applied Mechanics and Materials*, volume 241, pages 1608–1613. Trans Tech Publ, 2013.

[137] S. Motsch and E. Tadmor. A new model for self-organized dynamics and its flocking behavior. *J. Stat. Phys.*, 144(5):923–947, 2011.

[138] S. Motsch and E. Tadmor. Heterophilious dynamics enhances consensus. *SIAM review*, 56(4):577–621, 2014.

[139] A. Narayan and T. Zhou. Stochastic collocation on unstructured multivariate meshes. *Communications in Computational Physics*, 18(1):1–36, 2015.

[140] K.-K. Oh, M.-C. Park, and H.-S. Ahn. A survey of multi-agent formation control. *Automatica*, 53:424–440, 2015.

[141] L. Pareschi and G. Toscani. *Interacting multi-agent systems. Kinetic equations & Monte Carlo methods*. Oxford University Press, USA, 2013.

[142] D. R. Parisi and C. O. Dorso. Microscopic dynamics of pedestrian evacuation. *Physica A*, 354:606–618, 2005.

[143] M. M. Peet. Lecture notes in lmi methods in optimal and robust control, 2020.

[144] A. A. Peters, R. H. Middleton, and O. Mason. Leader tracking in homogeneous vehicle platoons with broadcast delays. *Automatica*, 50(1):64–74, 2014.

[145] M. Petrovitch. Sur une manière d'étendre le théorème de la moyenne aux équations différentielles du premier ordre. *Mathematische Annalen*, 54:417–436, 1901.

[146] R. E. Stern, S. Cui, M. L. Delle Monache, R. Bhadani, M. Bunting, M. Churchill, N. Hamilton, H. Pohlmann, F. Wu, B. Piccoli, et al. Dissipation of stop-and-go waves via control of autonomous vehicles: Field experiments. *Transp. Research Part C: Emerging Techn.*, 89:205–221, 2018.

[147] G. Toscani. Kinetic models of opinion formation. *Commun. Math. Sci.*, 4(3):481–496, 2006.

[148] A. Tosin and M. Zanella. Kinetic-controlled hydrodynamics for traffic models with driver-assist vehicles. *Multiscale Model. Simul.*, 17(2):716–749, 2019.

[149] P. Varutti, B. Kern, T. Faulwasser, and R. Findeisen. Event-based model predictive control for networked control systems. In *Proc. of the 48h IEEE Conf. on Decision and Control (CDC) held jointly with 2009 28th Chinese Control Conf.*, pages 567–572, 2009.

[150] C. Villani. *Handbook of Mathematical Fluid Dynamics*, volume 1, chapter A review of mathematical topics in collisional kinetic theory. Elsevier, 2002.

[151] J. Wang, L. Zhang, Q. Shi, P. Yang, and X. Hu. Modeling and simulating for congestion pedestrian evacuation with panic. *Physica A*, 428:396–409, 2015.

[152] J. Willems. Least squares stationary optimal control and the algebraic riccati equation. *IEEE Transactions on automatic control*, 16(6):621–634, 1971.

[153] H. Xie, L. Filippidis, E. R. Galea, D. Blackshields, and P. J. Lawrence. Experimental analysis of the effectiveness of emergency signage and its implementation in evacuation simulation. *Fire and Materials*, 36(5-6):367–382, 2012.

[154] D. Xiu. *Numerical methods for stochastic computations*. Princeton university press, 2010.

[155] D. Xiu and J. S. Hesthaven. High-order collocation methods for differential equations with random inputs. *SIAM Journal on Scientific Computing*, 27(3):1118–1139, 2005.

[156] Z. Zhang, L. Jia, and Y. Qin. Optimal number and location planning of evacuation signage in public space. *Safety science*, 91:132–147, 2017.

[157] M. Zhou, H. Dong, Y. Zhao, Y. Zhang, and P. A. Ioannou. Optimal number and location planning of evacuation leader in subway stations. *IFAC-PapersOnLine*, 51(9):410–415, 2018.

Declaration of authorship

I hereby declare that the report submitted is my own unaided work. All direct or indirect sources used are acknowledged as references. I am aware that the Thesis in digital form can be examined for the use of unauthorized aid and in order to determine whether the report as a whole or parts incorporated in it may be deemed as plagiarism. For the comparison of my work with existing sources I agree that it shall be entered in a database where it shall also remain after examination, to enable comparison with future Theses submitted. Further rights of reproduction and usage, however, are not granted here. This paper was not previously presented to another examination board and has not been published.

Verona, 16th May 2022